Treball de Fi de Màster

Màster Universitari en Enginyeria Industrial

Interaction analysis of large-scale PV power plants considering the AC network

Autor: José Montero Cassinello

Director: Eduardo Prieto Araujo

Convocatòria: Setembre 2018

Escola Tècnica Superior

d'Enginyeria Industrial de Barcelona

Abstract

In this thesis, a detailed interaction analysis between the internal grid of a Photovoltaic (PV) power plant and the AC grid is performed. This study is approached obtaining the small-signal model of the PV power plant, including a specific model of the inverter control, the medium voltage cable layout, a Power Plant Controller (PPC) and the AC grid. This model includes the dynamics associated to the PPC as well as the detailed control of the PV inverters. Based on this model, the oscillation modes of the system are highlighted and a participation factor analysis is performed to identify which variables can be problematic. This analysis is carried out for different grid strength conditions and different cable impedance values. The derived linear model and the subsequent mathematical analysis results are validated through time domain simulations.

Index

Figure Index

Preface

Technological progress has become an essential component of human society since the dawn of time. The increased speed at which new technologies have been developed and implemented has completely redefined the rate at which mankind consumes energetic resources. Electrical engineering has always strived to provide long distance power transmission in a comfortable and cost-efficient way. For this reason, research in different electrical distribution techniques has been fundamental in the development of new solutions, based on the new challenges posed by evolving technology.

With the increase in global power consumption, the contamination and natural resource depletion of the power generation sector has become a priority issue to be addressed by the engineering community. For this reason, research in renewable power generation and its integration into the grid has been one of the most studied technical aspects of electrical engineering in recent times.

With higher renewable generation, the structure of the classic electrical grid structure which has been ubiquitous since the end of the 19th century is bound to change. Due to the stochastic nature of renewable power generation, decentralisation of the generation itself can aid in dampening its lack of consistence. Distributed generation is a growing trend in this field and must therefore be studied appropriately.

Photovoltaic generation enables the possibility of installing small power plants near urban areas, reducing the strain on conventional power supply systems in a sustainable way. This case is particularly strong in rural areas allocated within the southern European countries where the weather is optimal for these kind of systems. Even though photovoltaic power plants cannot achieve the same power density as other systems like the nuclear plants, they can act as an accessory power supply in the near future.

At CITCEA-UPC research group, renewable integration research and engineering projects of the sort are a big part of the company’s activity.

Introduction

Objectives

This project consists on the study of the system oscillations of the internal AC grid of a photovoltaic power plant. This sort of study has previously been performed on many different power conversion systems [1]-[2]. However, to the knowledge of the author, the literature does not include an in depth study of the interactions contained within the internal AC grid of the Photovoltaic Power Plant (PVPP) and its connection to the AC grid.

The main objective of this thesis consists on producing a small-signal model of the internal grid of the PVPP and to apply linear control analysis techniques in order to identify the factors which produce oscillatory behaviour in the system. This model will serve as an initial milestone in further interaction studies to be developed at the CITCEA-UPC research centre.

The project was developed in the following phases:

- The main working principles of a photovoltaic power plant PVPP and the inverter control are introduced in Chapter 1.
- The Voltage Source Converter's (VSC) basic principles and control are explained in detail in Chapter 2
- The case study and Non-linear model are detailed in chapter 3.
- The linearization process of the system and its small-signal model are detailed in chapter 4.
- The results are detailed in chapter 5, including the small-signal model validation, the participation factor computation for different AC grid conditions and a time domain simulation comparison of the different dynamics of the system.

Scope of the project

The scope of this project is to comprehend the influence the AC grid strength has on the dynamic behaviour of the internal grid of a photovoltaic power plant. In this thesis, the full linear and non-linear modelling of the system is detailed. The PVPP control system has been reduced to a PI fed power loop excluding frequency or voltage droop control designs as it is a future endeavour of the CITCEA research group. The influence internal control parameters produce on the oscillatory behaviour of the system has also been excluded for the sake of conciseness.

1 Photovoltaic Power Plant Basic Principles

1.1 Introduction

Phasing out non-renewable energy generation sources has become one of the main priorities in mankind's strive for sustainable development. According to the Intergovernmental Panel on Climate Change (IPCC), the energy supply sector is accountable for 35% of human activity produced greenhouse gas emissions [3].Considering that the electricity demand is expected to grow up to a 41% due to increasing industrial and domestic needs [4] , renewable integration is one of the main components of the future energy generation strategy as imposed by the European Commission [5].

The PV installed generation capacity as of late 2016 was of 303 GW according to [6] and is expected to grow further in the following years. Very high power photovoltaic power plants installed in places like Yanchi (1 GW), Rosamond (575 MW) and Riverside County (550 MW) among others.

These high power PV plants rely on very heavy investment as well as a very well planned electrical layout that requires intense research in control techniques for cost-effective system operation.

In this chapter, the main structure of a PVPP is explained, breaking the most ubiquitous layout options and designs.

1.2 Photovoltaic Panel

The power source of a PV power plant consists on a series of PV panels that are usually connected in series also known as strings. The number of panels that form a string determine the type of inverter used in the power conversion. However, inverter DC voltage can also be used to determine how many PV panels are connected in each of the strings. The inverter's rated power must be suitable for the number of PV strings connected in parallel [7].

The photovoltaic panel uses the photoelectric effect to convert incident solar radiation into a DC voltage. A solar panel is made up of smaller PV cells which are usually connected in series and grouped up into a solar panel. The peak power that can be supplied from a PV panel is usually around the 225 W mark.

The PV panel market has mostly consisted of crystalline silicon and multi- crystalline silicone with the highest efficiencies. However other materials are also used ranging from amorphous silicon designs.

The efficiency of a given solar panel varies with the material it is made of ranging from 12% to 20% peak efficiency [8] under optimal boundary conditions. Extensive research in material science is currently being undertaken in order to achieve more efficient solar panel designs [9] as well as the palliating the effect atmospheric conditions have on the panel power output[10], [11].

Taking into account that the power output of a single PV panel is quite low, in order to be able to supply power comparable to any other type of power plant, a PVPP requires thousands of panels. These panels are usually connected in series constituting PV strings. PV strings are sometimes connected in parallel to form PV arrays.

Therefore, in order to generate high amounts of power, PV power plants occupy vast amounts of terrain and requiring heavy investment in maintenance of the whole complex.

However, with the rapid growth of the PV panel manufacturing sector, the panel price has been decreasing over the years (see Figure 1.1) making this type of technology a very interesting future asset of the global energy generation sector.

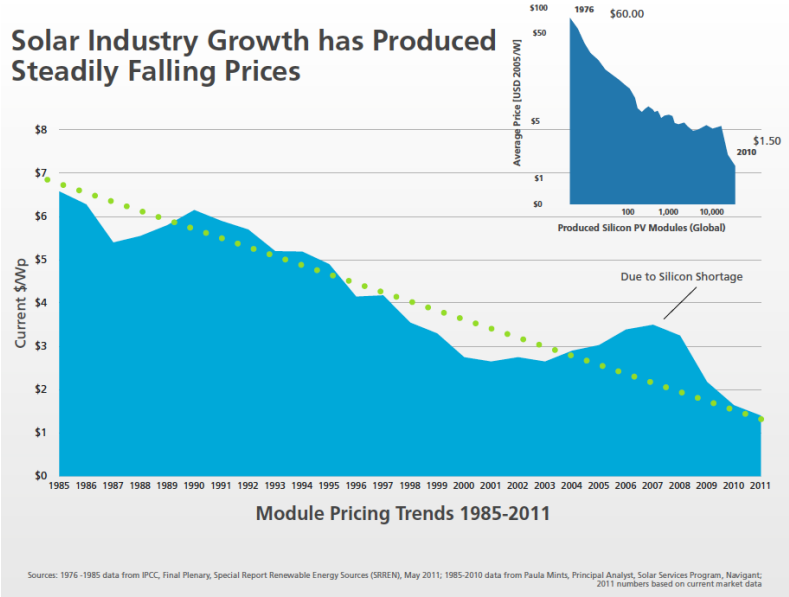

Figure 1.1 PV panel price-peak power ratio evolution

This is one of the reasons many countries are subsidising the construction of PV power plants, boosting the possibilities of the PV technology in a distributed generation application.

1.3 The Solar Inverter

The solar inverter converts the DC voltage generated by the PV panel strings into AC voltage, enabling connection to many different types of applications. In the case of PV power plants, the power generated from the PV panels is injected to the grid and therefore requires high rated power converters, different from the small household inverters for local PV installations [12]. These inverters belong to the static converter family which uses transistor commutation to control the output voltage.

The power conversion process can be done in either one or two stages. In the one stage power conversion, the PV panel strings are connected directly to the DC side of the inverter and power is directly converted to AC voltage. In two-stage power converter designs, a DC/DC converter is connected between the PV panels and the DC side of the converter [13]. Including a DC/DC converter in the power conversion process enables more flexible PV panel distributions and generally implies a higher efficiency of the DC/AC converter as it can ensure that the DC side of the inverter sees the optimal voltage. Another advantage of the two-stage power conversion is that the DC/DC converter can include a galvanic isolation system which prevents the flow of leakage current from the PV panels into the utility grid. However, the previously mentioned advantages come to the detriment of the system's cost, and high power DC/DC converters do not currently exceed the few kW range [14].

Considering that the inverter is responsible for converting the generated DC power into an AC power in an adequate form for the grid, the inverter must be capable of controlling the frequency and filtering any undesired harmonics of the output signal.

1.4 Solar Power Plant Topology

The different ways in which PV panels and PV inverters are connected to form a PV power plant can be broken into three main topologies:

- Central inverter topology (Figure 1.2): In the Central inverter topology, a series of parallel PV strings also known as PV arrays are connected to a single inverter. The rated power of the inverter must be quite high, considering that PV arrays can output very high peak power. This topology can encounter reliability problems as it uses less inverters, but can output the highest amount of power out of the 3 introduced topologies.

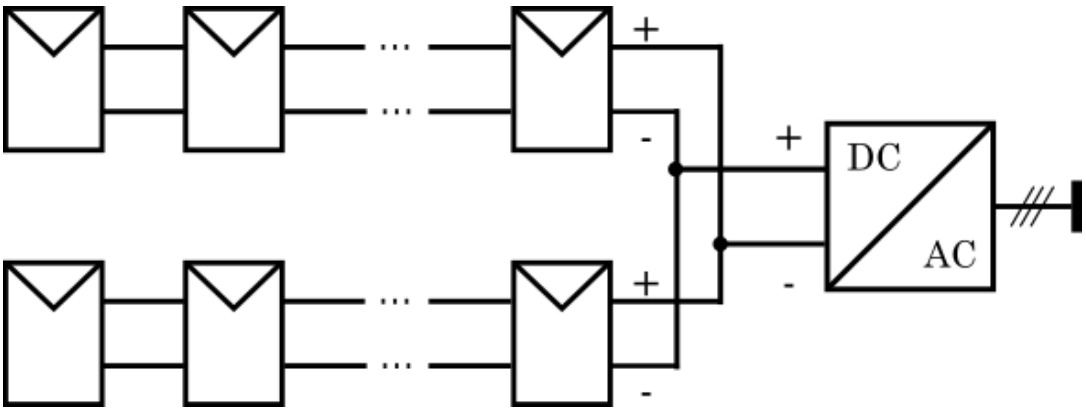

Figure 1.2 Central inverter topology

- String topology (Figure 1.3): In this topology each PV string is connected to an inverter, greatly reducing the power that flows through each of the inverters. This solution implies higher modularity, reducing the losses associated to one of the inverters breaking down, to the detriment of the power it is capable of outputting, which is considerably lower for each of the strings.

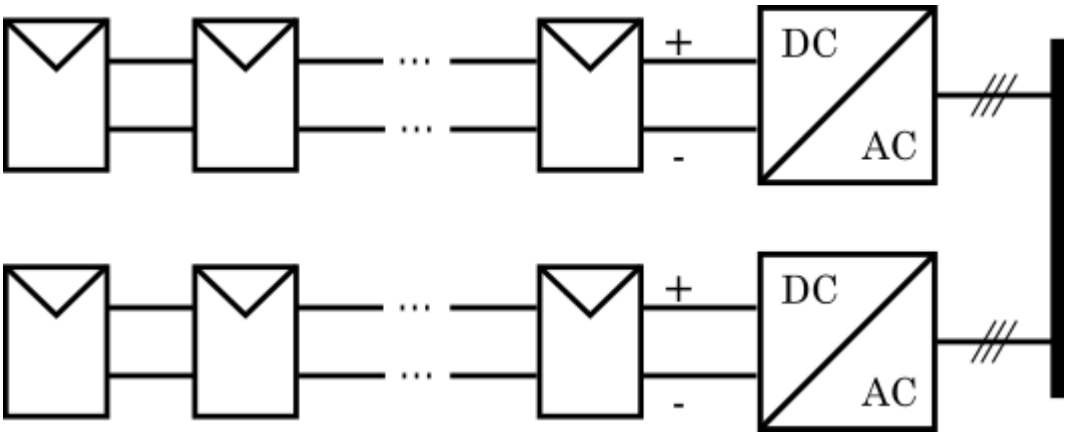

Figure 1.3 String inverter topology

- String topology (Figure 1.4): In this topology each PV string is connected to an inverter, greatly reducing the power that flows through each of the inverters. This solution implies higher modularity, reducing the losses associated to one of the inverters breaking down, to the detriment of the power it is capable of outputting, which is considerably lower for each of the strings.

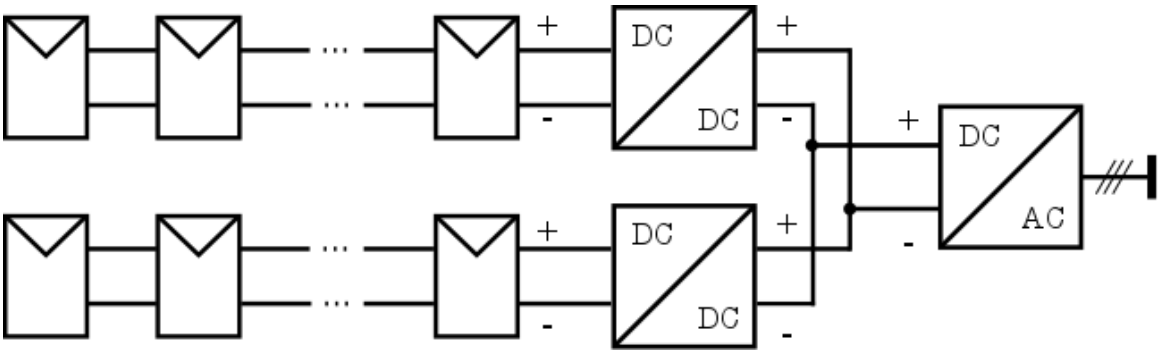

Figure 1.4 Multi-String Inverter topology

The inverter topology choice in every PV generation system design is always based on the system's rated power output and the installation restrictions of the plant's allocation. In any case, a grand majority of the high-power PVPP facilities around the world are based around the central inverter due to its power output capacity and its cost-effectiveness. The main issue with the central inverter topology is in the effect a PV panel failure can have on the DC side of the inverter and its operation. The power losses associated to failing PV panels in a PV array has previously been studied in the literature [15] and although it does have an effect on the central inverter's output power, it has not been assessed as a critical vulnerability.

1.5 Internal AC grid

In order to achieve high power PVPP plants like examples presented in the introduction to this chapter, many inverters must be used. The interconnection of the inverters and the evacuation line into the grid can be done following several layout designs.

The internal AC grid topologies can be summarized into 3 categories:

- Radial inverter connection (Figure 1.5): The output voltage of each inverter is elevated to medium voltage by means of a step-up transformer. The high voltage side of the transformers are connected forming inverter strings. The inverter strings are connected to a point of common coupling from which the power is injected into the utility grid. The main issue with this internal AC grid is that if one of the inverters fails, the inverters further down the string are basically disconnected from the PCC and the power is lost. Thus, its reliability can sometimes be compromised.

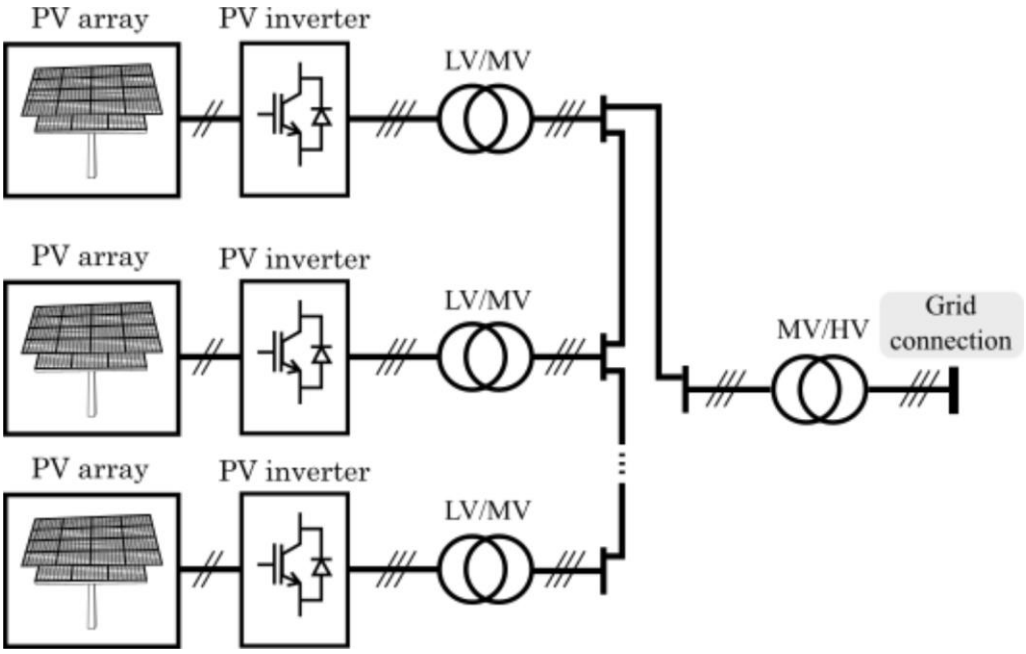

Figure 1.5 Radial internal AC PVPP grid

- Ring inverter connection (Figure 1.6): In this topology, only one inverter is connected to the grid via a power evacuation line. The rest of the converters are connected to the grid connected inverter forming a ring. The usual design of this topology attempts to minimise cable distances and looks for symmetry in order to balance the power losses of each of the system's medium voltage lines. The general operation of a system with this topology is more complex than the other two designs because maintaining power balance can be challenging. As an interesting fact, the 10 MW PV power plant in Vanju Mare Romania uses this layout.

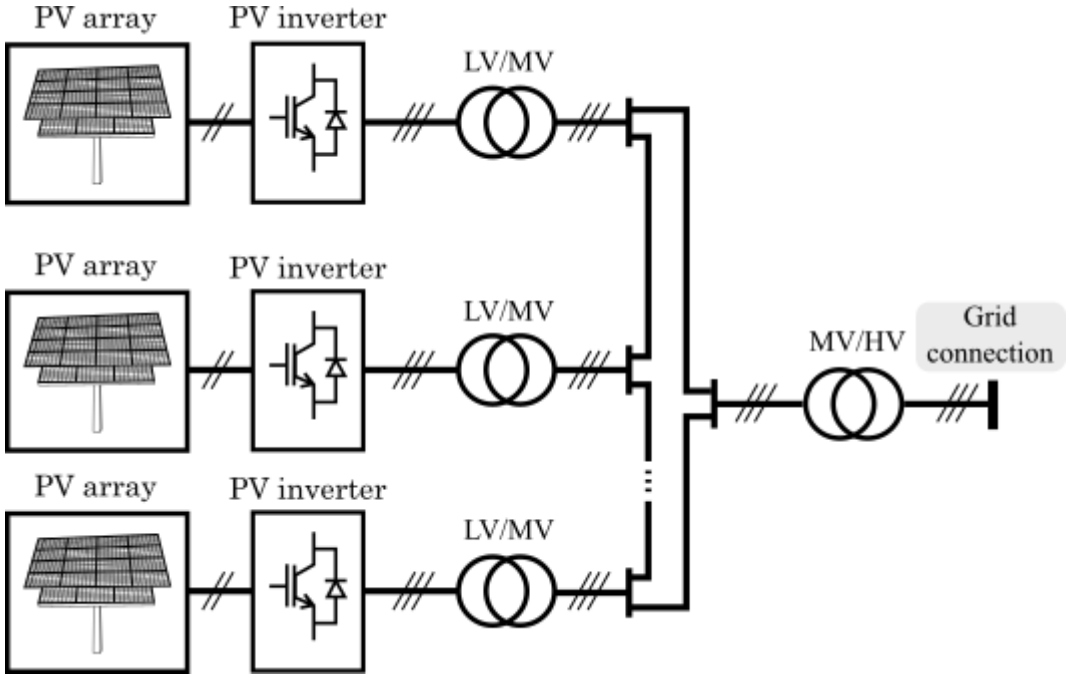

Figure 1.6 Ring internal AC PVPP grid

- Star inverter Connection (Figure 1.7): In this topology, each of the inverters are connected directly to the grid. This solution is the most reliable as a problem in one of the inverters does not imply the disconnection of any of the others. However, the increased reliability comes at a cost, the average distances in this topology are longer requiring more expensive cables.

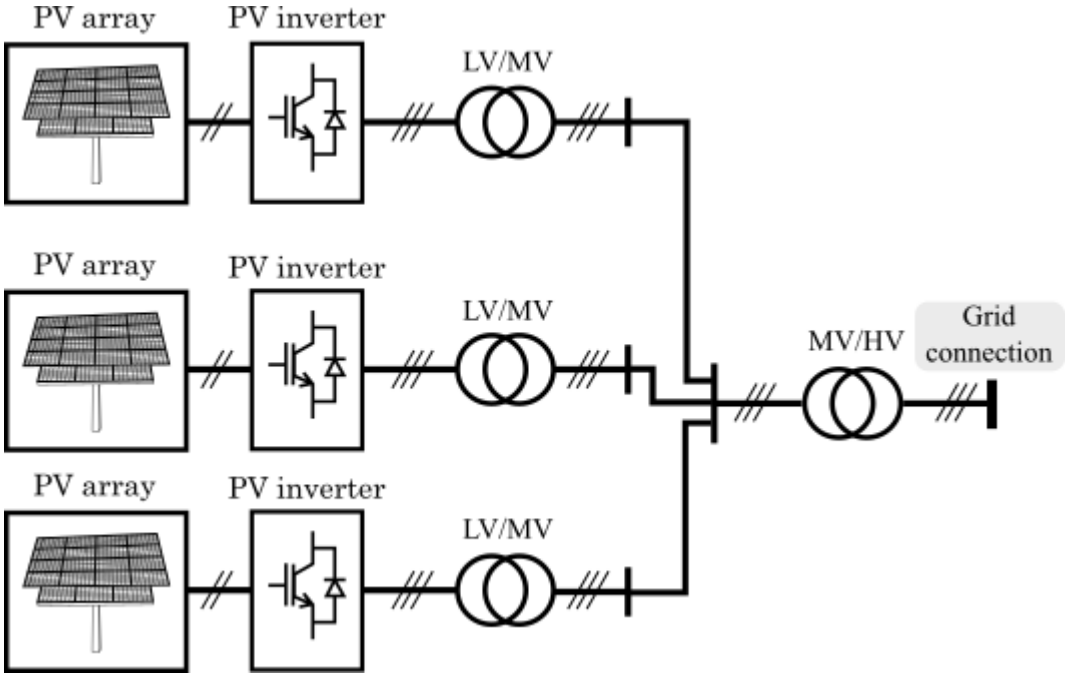

Figure 1.7 Star Inverter AC PVPP grid

2 The Voltage Source Converter

2.1 Introduction

As detailed in the previous chapter, a photovoltaic power plant requires the use of an inverter in order to convert the DC power generated by the PV panels into a grid-suitable, code-compliant AC form. In this chapter, the basic functioning principles and the control of the voltage source converter are detailed. This chapter is profoundly relevant to the project, since the interaction study has been conducted on a system including the VSC as the PV inverter.

2.2 The VSC topology

Essentially, the converter consists on a DC bus which is connected to the three branches that constitute the three phase AC side. Two IGBTs (Insulated Gate Bipolar Transistors) are used to connect the branches to the DC bus. An impedance is connected between the IGBTs and the grid in order to filter some of the harmonics introduced by the commutation.

Regarding the DC side, it is usually connected to a storage system or a DC voltage source, depending on the application for which the converter is intended. In a PV system like the one studied in this project, the DC side will be connected to the PV panel strings. The latter implies that in this project, the DC side will be treated as a voltage source and the power flow of the system will be unidirectional and into the AC grid.

Figure 2.1 shows the layout of the two-level voltage source converter topology:

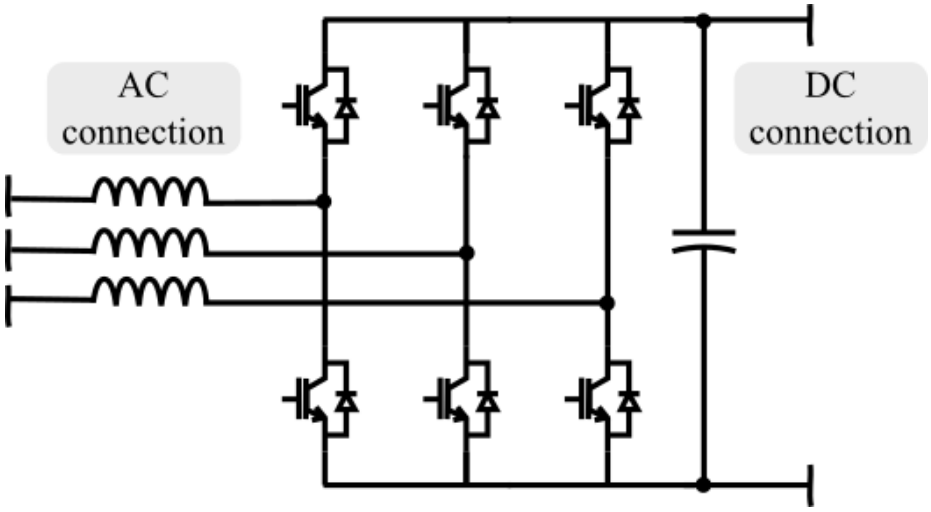

Figure 2.1 Overview of the two-level VSC topology

Having seen what, the VSC converter topology looks like, one can comprehend that the DC to AC voltage conversion essentially consists on opening and closing the IGBT switches at a given rate in order to generate the appropriate sinusoidal voltage wave on the AC side.

For its correct operation, the IGBT switches that are connected to the same phase of the AC side must never be in the same state. The commutation is operated by means of six logic signals that are calculated within the control system.

Naturally, there are many variations of the converter topology shown in this section. Multi-level converters offer a higher quality three-phase AC voltage output at the cost of complicating the control system [16]. However, in this project, the study will be carried out using the two-level voltage source converter.

Taking into consideration both computation time and that the main focus of this thesis is not entirely on the converter itself but on its interactions with other elements of the PV power plant connection to the grid, a simplification of the previously shown VSC topology will be used.

The averaged model that will be used substitutes the IGBT modules for AC voltage sources [17], greatly reducing simulation times. This is a very simplified version of the VSC since the DC side of the converter will not be modelled. This implies that the dynamics of the capacitor that is allocated in the DC bus will not be included in the study. This decision has been taken in order to represent a controlled generation scenario where the control system demands a certain amount of the available power from the PV generation system. Had the DC bus been included, in order to control the active power injected into the grid, the current generated by the PV panels would have had to be controlled. A more realistic approach would have included the DC side with storage batteries and an energy management system in which the excess power generated by the PV panels would have been stored.

Figure 2.2 depicts the VSC modelled as a three-phase controllable voltage source:

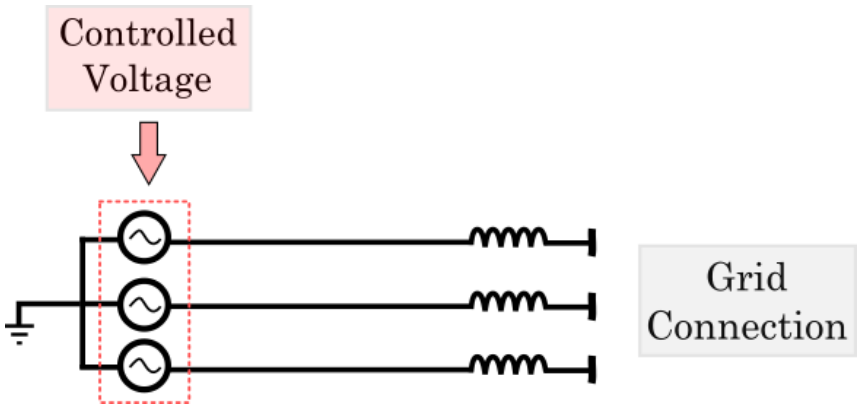

Figure 2.2 Voltage source converter modelled as a three-phase controllable voltage source

2.3 General overview of the VSC control scheme

The control scheme of a Voltage Source converter is based on a series of cascaded control loops containing proportional-integral controllers which generate the AC signal which is injected into the grid.

The signal flow of the control scheme is fairly simple. Firstly, the input signals for the VSC control loop are active and reactive power reference values. These references are compared to the actual active and reactive powers injected to the grid and controlled by the local active and reactive power loops. The output of said loops are the reference currents that should circulate through the impedances in the connection between the converter and the grid. These current references are compared to the actual currents that circulate through the impedances by means of another PI-based control loop known as the current loop. The current loop generates the voltage references for the AC side of the converter, closing the full control loop and ensuring that the referenced active and reactive power requirements have been satisfied.

Figure 2.3 shows the signal flow of the cascaded control loop of the voltage source converter:

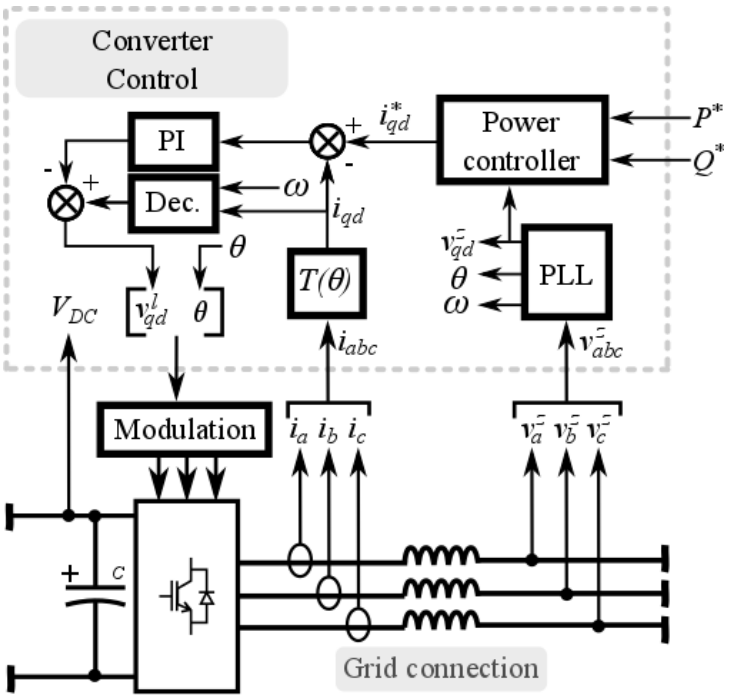

Figure 2.3 Overview of the VSC control loop

The control system of a voltage source converter may vary depending on the depth at which it is being modelled, and its application. In this case, since the modelling of the converter is reduced to an AC voltage source, no more loops are needed. However, when the DC side of the converter is modelled as a current source, a voltage loop is used to control the voltage of the capacitor of the DC bus, preventing DC voltage surges that could damage the capacitor or destabilise the system's power balance. Additionally, the modulation used to apply the voltages calculated by the current loop is not necessary either.

The VSC control system heavily relies on the Park transform, greatly simplifying its structure. The Park transform enables the mathematical conversion of three-phase voltage and current sinusoidal waves into constant values. Naturally, the complexity of mathematical operations is greatly reduced in the new reference, which is commonly referred to as $qd0$.

Given the importance of said transformation, an appendix of this thesis is dedicated to explaining the synchronous reference frame and the transformation from abc reference to $qd0$.

2.4 Instantaneous power equations in $qd0$ reference

Considering that the power injected into the grid by the converter is highly relevant to this study, the usual three-phase AC power equations must be converted into a form in which the $qd0$ values are used [18], [19].

The following expression is used to calculate the instantaneous power of a balanced three-phase AC system. Where $\underline{V}$ is the phase to neutral voltage and $\underline{I}$ is the current.

$$\underline{S} = P + jQ = 3 \cdot \underline{V} \cdot \underline{I}^{*} \tag{2.1}$$

Applying the Park transform to the both voltage and current phasors in abc reference will yield voltage and current phasors in the $qd0$ reference as shown in equations (2.2) and (2.3):

$$v_{qd} = \frac{v_q - jv_d}{\sqrt{2}} \tag{2.2}$$

$$i_{qd} = \frac{i_q - ji_d}{\sqrt{2}} \tag{2.3}$$

Substituting (2) and (3) into (1) the expression for the instantaneous power is obtained in $qd0$ reference:

$$\underline{S} = P + jQ = 3 \cdot \left(\frac{v_q - jv_d}{\sqrt{2}}\right) \cdot \left(\frac{i_q + ji_d}{\sqrt{2}}\right) \tag{2.4}$$

Upon expanding and reorganising terms within (4), expressions for active and reactive power in $qd0$ reference can be obtained:

$$P = \frac{3}{2} \cdot (v_q i_q + v_d i_d) \tag{2.5}$$

$$Q = \frac{3}{2} \cdot (v_q i_d - v_d i_q) \tag{2.6}$$

The obtained active and reactive power equations using the voltage and current magnitudes in $qd0$ reference will be pivotal to the control of the PV plant.

2.5 Circuit resolution in $qd0$ reference

Taking into account that the convert control works in the $qd0$ reference, the definition of the voltage equations of the circuit in said reference is an important tool to be considered.

The instantaneous voltage equations of a three-phase balanced circuit like the one shown in Figure 2.4 are:

$$\begin{bmatrix} v_a^2 \\ v_b^2 \\ v_c^2 \end{bmatrix} - \begin{bmatrix} v_a^1 \\ v_b^1 \\ v_c^1 \end{bmatrix} = \begin{bmatrix} r_l & 0 & 0 \\ 0 & r_l & 0 \\ 0 & 0 & r_l \end{bmatrix} \cdot \begin{bmatrix} i_a \\ i_b \\ i_c \end{bmatrix} + \begin{bmatrix} l_l & 0 & 0 \\ 0 & l_l & 0 \\ 0 & 0 & l_l \end{bmatrix} \frac{d}{dt} \begin{bmatrix} i_a \\ i_b \\ i_c \end{bmatrix} \tag{2.7}$$

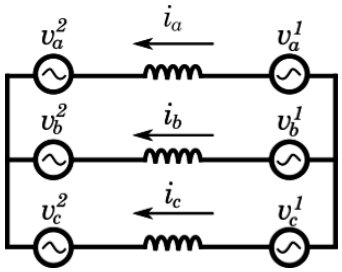

Figure 2.4 Three-phase balanced circuit

Applying the Park transformation to the previous equation, the result yields the relationship between v_{qd0} and i_{dq0}:

$$\begin{bmatrix} v_q^2 \\ v_d^2 \end{bmatrix} - \begin{bmatrix} v_q^1 \\ v_d^1 \end{bmatrix} = \begin{bmatrix} r_l & l_l \cdot \omega \\ -l_l \cdot \omega & r_l \end{bmatrix} \begin{bmatrix} i_q \\ i_d \end{bmatrix} + \begin{bmatrix} l_l & 0 \\ 0 & l_l \end{bmatrix} \frac{d}{dt} \begin{bmatrix} i_q \\ i_d \end{bmatrix} \tag{2.8}$$

2.6 Converter power control loops

As previously introduced in the overview of the converter's control signal flow, the first step in the general control system is the local power control. The power control loop is required to control the power the converter injects into the grid. For this purpose, the active and reactive power measured at the point of connection between the grid and the converter is compared and corrected by two negative feedback PI loop. The output of the converter's power control is a vector formed by the reference $i_q{}^*$ and $i_d{}^*$ which is used later within the control chain.

This is done by means of the power equations that were introduced earlier on:

$$P = \frac{3}{2} \cdot (v_q i_q + v_d i_d) \tag{2.9}$$

$$Q = \frac{3}{2} \cdot (v_q i_d - v_d i_q) \tag{2.10}$$

The phase locked loop imposes that $v_d = 0$, therefore the expressions can be simplified to:

$$P = \frac{3}{2} \cdot (v_q i_q) \tag{2.11}$$

$$Q = \frac{3}{2} \cdot (v_q i_d) \tag{2.12}$$

Finally, one can obtain the current needed to satisfy the power references using:

$$i_q = \frac{2 \cdot P}{3 \cdot v_q} \tag{2.13}$$

$$i_d = \frac{2 \cdot Q}{3 \cdot v_q} \tag{2.14}$$

Where v_q is the constant peak phase voltage at the point of measurement. The general overview of the converter power loop is depicted in Figure 2.5:

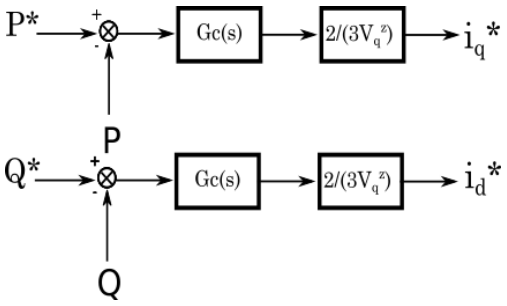

Figure 2.5 Diagram of the VSC power loop control

Regarding the controller design, there are many possible techniques that can be used to approach this matter. The main idea behind the design of this PI controller is that it must be approximately 10 times slower than the current loop. The exact parameters can be found using internal model control theory, and can be tuned by iterating the participation factor analysis detailed later in this project in order to optimise the dynamic response of the system. In this thesis, the power loop time constant was of 0.1 seconds.

2.7 Current loop

The current loop is in charge of imposing the reference $qd0$ current calculated by the active and reactive power loops. This control loop is based on the current-voltage equation in $qd0$ reference and outputs the necessary voltage in order to satisfy said current reference. Essentially, the voltage equation is applied to the converter filter impedance as is shown in the following expression:

$$\begin{bmatrix} v_q^z \\ v_d^z \end{bmatrix} - \begin{bmatrix} v_q^l \\ v_d^l \end{bmatrix} = \begin{bmatrix} r_l & l_l \cdot \omega \\ -l_l \cdot \omega & r_l \end{bmatrix} \begin{bmatrix} i_q^l \\ i_d^l \end{bmatrix} + \begin{bmatrix} l_l & 0 \\ 0 & l_l \end{bmatrix} \frac{d}{dt} \begin{bmatrix} i_q^l \\ i_d^l \end{bmatrix} \tag{2.15}$$

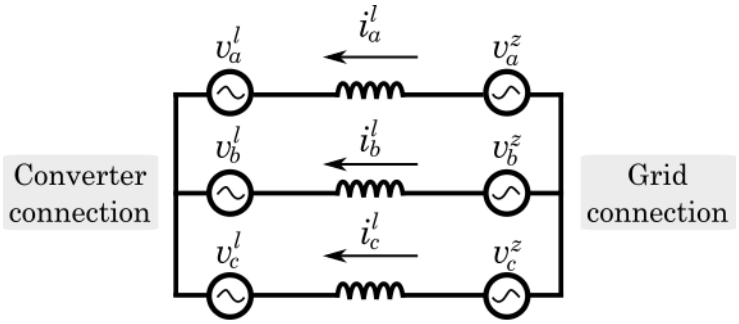

Figure 2.6 Averaged model of the AC side of a voltage source converter

Where v_q^z and v_d^z correspond to the grid side of the impedance and v_q^l and v_d^l correspond to the converter side of the impedance. The converter side voltages will essentially be the output of the current loop. On the other hand, the d component of the grid side voltage will be fixed at 0 by the phase locked loop which will be detailed later in the chapter. Therefore, the equation will look like so:

$$\begin{bmatrix} v_q^z \\ 0 \end{bmatrix} - \begin{bmatrix} v_q^l \\ v_d^l \end{bmatrix} = \begin{bmatrix} r_l & l_l \cdot \omega \\ -l_l \cdot \omega & r_l \end{bmatrix} \begin{bmatrix} i_q^l \\ i_d^l \end{bmatrix} + \begin{bmatrix} l_l & 0 \\ 0 & l_l \end{bmatrix} \frac{d}{dt} \begin{bmatrix} i_q^l \\ i_d^l \end{bmatrix} \tag{2.16}$$

In order to control both q and d current components without using a more complicated multiple input/output controller, both components must be decoupled enabling individual control of each one of them. The decoupled expressions of I_q and I_d are the following:

$$\begin{bmatrix} v_q^l \\ v_d^l \end{bmatrix} = \begin{bmatrix} -v_q^{l*} + v_q^z - l_l \cdot \omega \cdot i_d^l \\ -v_d^{l*} + l_l \cdot \omega \cdot i_q^l \end{bmatrix} \tag{2.17}$$

The v_q^{l*} and v_d^{l*} parameters are the outputs of the current controller, whereas v_q^l and v_d^l are the actual voltages the converter must apply in order to satisfy the current reference.

Substituting the decoupled voltage expressions into the impedance voltage equation:

$$\begin{bmatrix} v_q^{l*} \\ v_d^{l*} \end{bmatrix} = \begin{bmatrix} r_l & 0 \\ 0 & r_l \end{bmatrix} \begin{bmatrix} i_q^l \\ i_d^l \end{bmatrix} + \begin{bmatrix} l_l & 0 \\ 0 & l_l \end{bmatrix} \frac{d}{dt} \begin{bmatrix} i_q^l \\ i_d^l \end{bmatrix} \tag{2.18}$$

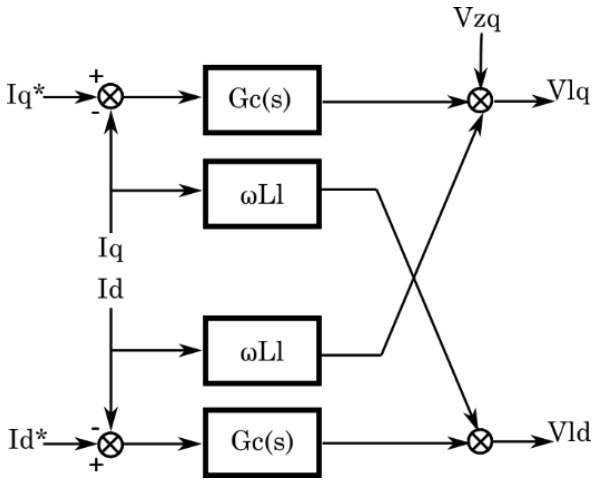

Figure 2.7 Block diagram of the current loop

Upon application of the Laplace transform:

$$\frac{v_q^{l*}(s)}{i_q^l(s)} = \frac{1}{l_l \cdot s + r_l} \tag{2.19}$$

$$\frac{v_d^{l*}(s)}{i_d^l(s)} = \frac{1}{l_l \cdot s + r_l} \tag{2.20}$$

A PI controller will be used to control the dynamic response of the afore exposed transfer functions. The design of said PI controller has been conducted by means of the internal model control technique. Its parameters are calculated with the following expressions:

$$Gc(s) = \frac{K_p \cdot s + K_i}{s} \tag{2.21}$$

$$K_p = \frac{l_l}{\tau} \tag{2.22}$$

$$K_i = \frac{r_l}{\tau} \tag{2.23}$$

Where τ is the time constant associated to the control loop of the electrical system.

2.8 The Phase-Locked Loop

The Phase Locked Loop (PLL) is a control system that tracks and outputs the phase of a given input signal. Its role within the control of a VSC is pivotal as it enables the conversion of voltage and current signals from abc to $qd0$ reference and vice-versa.

The three-phase voltage signal is transformed from abc to $qd0$ reference by means of the Clarke and Park matrices. The angular position of the reference frame is controlled by a feedback loop that fixes the value of v_d^z at 0. The difference between v_d^z and 0 is filtered by a PI controller. Integration of the output of the filter produces the voltage wave's phase [20].

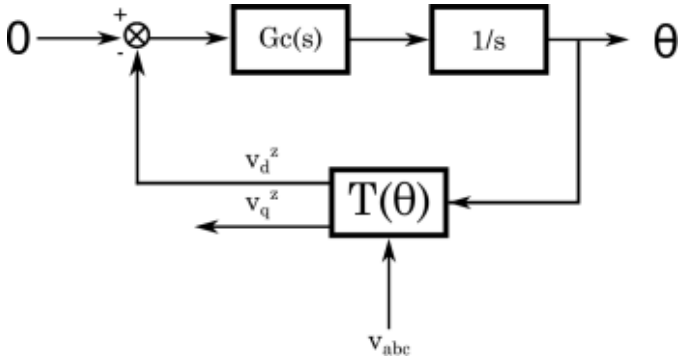

Figure 2.8 Block diagram of the synchronous reference frame phase-locked loop

The controller is in charge of adjusting ω^* to a value close enough to that of the frequency of the voltage input in order to minimise the difference between the real phase and the estimated phase. Upon reaching a small enough phase difference, v_d^z will be 0 and therefore the angular frequency will stabilise.

The design of the PI controller upon which the PLL is based can be approached by linearizing the system and assuming that the angle error is negligible. The result is a second order transfer function of the sort:

$$\frac{\theta'(s)}{\theta(s)} = \frac{2\xi\omega_n s + {\omega_n}^2}{s^2 + 2\xi\omega_n + {\omega_n}^2} \tag{2.24}$$

The PI controller can be defined as:

$$Gc(s) = K_p\left(\frac{\frac{1}{\tau} + s}{s}\right) \tag{2.25}$$

The following expressions provide computation of the controller parameters:

$$K_p = \frac{2\xi\omega_n}{Em} \tag{2.26}$$

$$\tau = \frac{2\xi}{\omega_n} \tag{2.27}$$

Where ξ is the dampening ratio (usually $\frac{1}{\sqrt{2}}$), Em is the peak phase voltage and ω_n is the electrical grid angular velocity.

3 Case study and initial model

3.1 Introduction

The study proposed in this project relies on a series of simulation techniques that must be properly explained in this thesis. The objective of this section is to explain the methodology used in the study and to provide a detailed explanation of the initial non-linear model.

3.2 Experimental procedure

The study conducted upon the electrical system in question is commonly referred to as a modal analysis. This technique provides numerical results that enable quantification of the internal oscillations of a mathematical model. In this case, the mathematical model describes the behaviour of three VSC which are connected in parallel to the AC-grid. Taking into account that one of the drawbacks of the static converter technology resides in the harmonic injection associated to its working principles, comprehending the frequencies of the harmonics introduced into the grid can be of great value. In other words, this type of study is commonly used in this particular area of electrical engineering in a satisfactory way.

The equations of the converters have been detailed in earlier sections of this thesis and show that some of them are non-linear. Non-linearity greatly complicates the interaction study and therefore a linearized model must be used. For this reason, the first step in this project consists on producing a linearized state-space equivalent model of the converters and their interconnection. Said linearization is carried out by using the first term of the Taylor series derived from each of the non-linear equations around a certain initial set point of the system. The linearization values are obtained by recording the steady state values of all the relevant parameters of the non-linear simulation model. The values are then substituted in the linearized expressions producing the linear model.

The precision of the linearized model must be validated in order to draw correct conclusions and therefore the following step of the study consists on graphically comparing the response of all the interesting variables in the linear and non-linear simulations.

Then, upon validation of the linearized model, a participation factor study of the model produces the oscillation frequencies of the system's transient behaviour, the dampening ratio of said frequencies and their contributing factors.

Finally, a graphical inspection of the non-linear simulation results is carried out in order to validate the internal oscillation frequency variations of the different simulation tests.

The MATLAB® software has been used to conduct all the different steps of the study.

3.3 Linearization

The linearization used in this project is very simple. It essentially consists on using first order Taylor series of the non-linear components as can be seen in the following expression:

$$f(x) \approx f(a) + f'(a) \cdot (x - a) + Rn \tag{3.1}$$

Where $f(x)$ is the approximated function, a is the linearization point and Rn is the residue of the operation. Since the linearization of the different modules is a mere approximation, certain error will always be part of the linear model. Therefore, the degree of precision of the linear model must be validated.

On the other hand, as can be seen in the first order Taylor expression, linearization requires certain linearization points. For this reason, the Non-linear model is always run before computing the linear model in order to save the correct steady-state operation points of the necessary variables for the linearization.

3.4 Participation Factor

In order to quantify the different oscillation modes of a power system and their contributing parameters, a participation factor study can be applied. This technique has widely been applied in the many different power systems and defined in detail in the literature [21].

In order to carry out said participation factor study, the study case must be modelled as a linear state-space system. The A matrix of the state-space system must then be diagonalised, obtaining the system's Eigen Values.

Regarding the system's Eigen values, two important considerations must be taken into account. On one hand, the real components of all of the system's Eigen values must be lower than or equal to zero for stable operation of the system. On the other hand, the imaginary component of each of the Eigen values provides information about the frequency of the oscillation mode associated to each value.

The next step to be taken in the participation factor study is to calculate the left and right Eigen vectors of the system defined by the following properties:

$$[A] \cdot r_i = \lambda_i \cdot r_i \tag{3.2}$$

$$l_i \cdot [A] = l_i \cdot \lambda_i \tag{3.3}$$

Where r_i is the right Eigen vector, l_i is the left Eigen vector and λ_i is the Eigen value to which they are associated.

The participation factors are computed using (3.4):

$$p_i^k = \left| r_i^k \cdot l_i^k \right| \tag{3.4}$$

Where k represents each state and i each oscillation mode.

The frequency of each oscillation mode is computed with (3.5):

$$f = |Im\{\lambda_i\}| \tag{3.5}$$

Finally, the dampening ratio of each of the oscillation modes is computed using (3.6):

$$\xi = \frac{Re\{\lambda_i\}}{|\lambda_i|} \tag{3.6}$$

Where ξ is the dampening ratio associated to each oscillation mode.

3.5 Study Case

The electrical system studied in this project is a simplified model of the power injection of three 1 MW voltage source converters like the ones commonly used in the PV generation application. The general PV power plant layout was derived from a project developed in Romania, the Vanju Mare PV plant (10 MW). Said PVPP uses a ring internal AC grid layout. However, in this project the studied internal AC grid is of the star type in.

The converters output a 400 V voltage and are connected to a step-up transformer which elevates the voltage to 20 kV. Each of the branches are then connected to a point of common coupling by means of cables. Finally, the PCC is connected to the grid. Figure 3.1 shows the studied system:

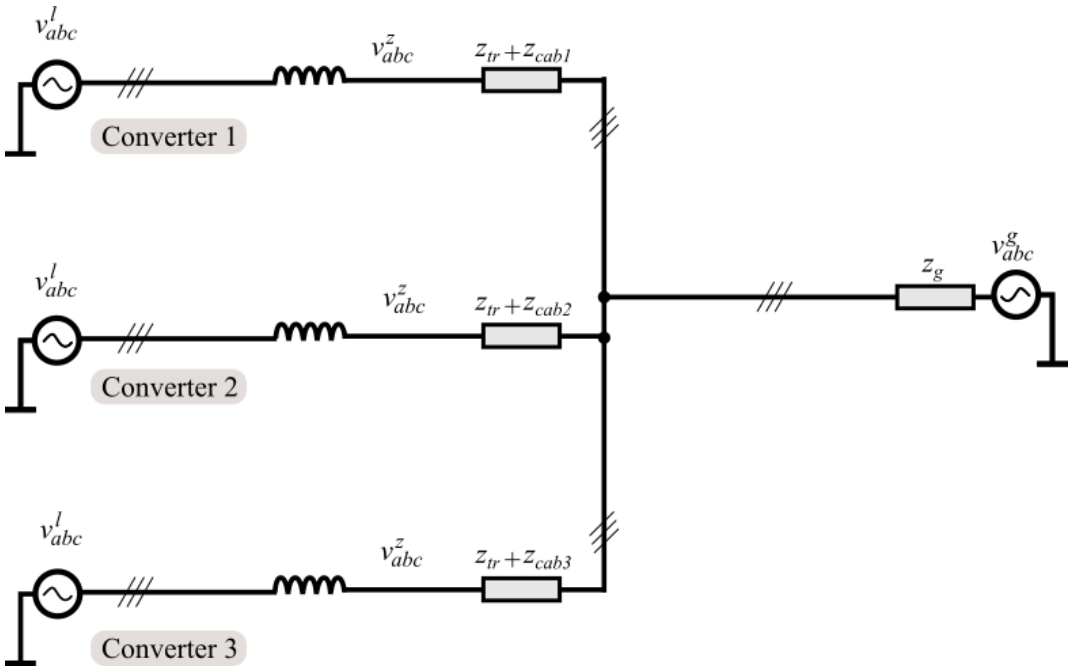

Figure 3.1 Diagram of the studied system

The grid-injected power measurement is usually taken at high voltage right after an elevator transformer. However, in this project the effect the elevating transformer has on the power transmission has been ignored in order to simplify the posterior mathematical model of the internal grid.

3.6 The non-linear model

As previously detailed in this chapter, generating a non-linear model of the system to be studied is a requirement for this study. The non-linear model can be separated into 4 main parts; the voltage source converter, the internal grid, the AC grid and the Photovoltaic power controller (PPC).

3.6.1 Converter parameters

The VSC is modelled as has been detailed in previous sections. The most relevant parameters of the VSC modelling are included in Table 1.

Table 1 Voltage source converter model parameters

NAME	VALUE
$\boldsymbol{Z_l}$	0.01 +j0.2 *p.u.*
$\boldsymbol{K_{p_{pll}}}$	0.4899
$\boldsymbol{K_{i_{pll}}}$	39.2
$\boldsymbol{K_{p_{cl}}}$	0.034
$\boldsymbol{K_{i_{cl}}}$	0.533
$\boldsymbol{K_{p_{Pc}}}$	0.75
$\boldsymbol{K_{i_{Pc}}}$	100

The control parameters used for the converter control system have been derived from other existing VSC models used in similar studies at CITCEA-UPC.

3.6.2 Internal Grid Model

Regarding the internal grid, considering it includes a step-up transformer, the electrical components of the system will be reduced to per-unit values. An important consideration to be taken into account is the fact that even though the converter impedance will be introduced into the model in pu, both the converter control system and the PPC will work invert the per-unit conversion and work with ISU variables.

Following Table 2 provides insight as to how the per unit conversion of the model has been carried out. The converter variables have been switched to per-unit using the table defined in [22]:

Table 2 Base voltage parameters for per unit conversion

Base Variable	Expression	Low Voltage Value	Medium Voltage Value
Rated base power	S_b	3 MVA	3 MVA
Base Voltage	V_b	0.4 kV	20 kV
Base current	$I_b = \frac{2}{3} \cdot \frac{S_b}{V_b}$	6123.7 A	122.47 A
Base impedance	$Z_b = \frac{V_b}{I_b}$	0.0533 Ω	133.33 Ω
Base inductance	$L_b = \frac{Z_b}{\omega}$	1.6977e-04 H	0.4244 H

In per-unit, the converter equations include a series of small differences. The following expressions show the new converter equations in pu.

$$\frac{1}{\omega_b} \cdot \frac{\delta i_d}{\delta t} = -R \cdot i_d + L \cdot \omega \cdot i_q - v_d^z + v_d^l \tag{3.7}$$

$$\frac{1}{\omega_b} \cdot \frac{\delta i_q}{\delta t} = -R \cdot i_q - L \cdot \omega \cdot i_d - v_q^z + v_q^l \tag{3.8}$$

The elements included in the internal grid include the step-up transformer and the medium voltage cables. For the sake of simplicity, the transformer has been modelled as a single impedance in order to simplify the modelling of the internal grid. The cable impedance and transformer impedance parameters were extracted from the mentioned PVPP project in the introduction.

3.6.3 AC grid model

The AC grid has been modelled using a Thévenin equivalent defined by the following expressions using an SCR value:

$$S_{CC} = S_N \cdot SCR \tag{3.9}$$

$$L_g = \frac{{V_N}^2}{S_{CC} \cdot 2 \cdot \pi \cdot f} \tag{3.10}$$

$$\frac{X_g}{R_g} = 10 \tag{3.11}$$

Where in this case $S_N = 3\ \text{MVA}$ and $V_N = 20\ \text{kV}$. The assigned value of the SCR parameter will vary throughout the interaction study.

3.6.4 Photovoltaic Power Converter

The Photovoltaic Power Converter or PPC is the power loop that controls active and reactive power injection from the converters into the AC grid. It does so by reading the angle, the current and the voltage at the point of common coupling and calculating the power flowing through the node. The calculated power is then compared to the active and reactive power references introduced into the system. The active and reactive power error is then filtered through negative feedback PI control loops and the PPC outputs the active and reactive power references for each of the converters. The PPC structure can be seen in Figure 3.2

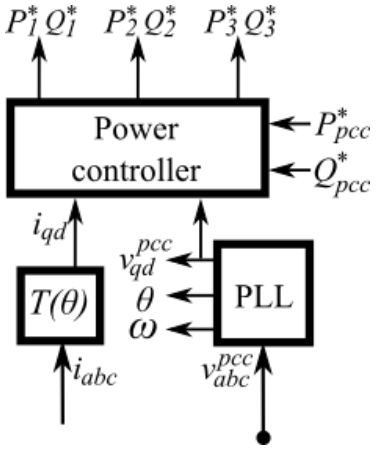

Figure 3.2 Block diagram of the photovoltaic power controller

Generally, a PV generation system outputs a set DC current depending on a series of boundary conditions that vary throughout the day consequently varying the available PV generated power. In this project, the PPC will only request a portion of the available power, assuming that the rest is dealt with in the DC side of the system.

In order to achieve stable operation of the system, the PPC's control loop must be slower than the rest of the control loops that follow it in the general control chain. For this reason, the parameters for the PPC used in this project have been determined using the internal model control theory, with an internal loop time constant of one second.

Expanding on the subject of the PPC, the one used in this project is a fairly simple design. Other PV projects include PPC designs which enable the TSO to input the power references in different forms and to control other variables [23]. Following Figure 3.3 shows the general scheme of a PPC which is capable of controlling output voltage and frequency as well as applying droop and ramp controls:

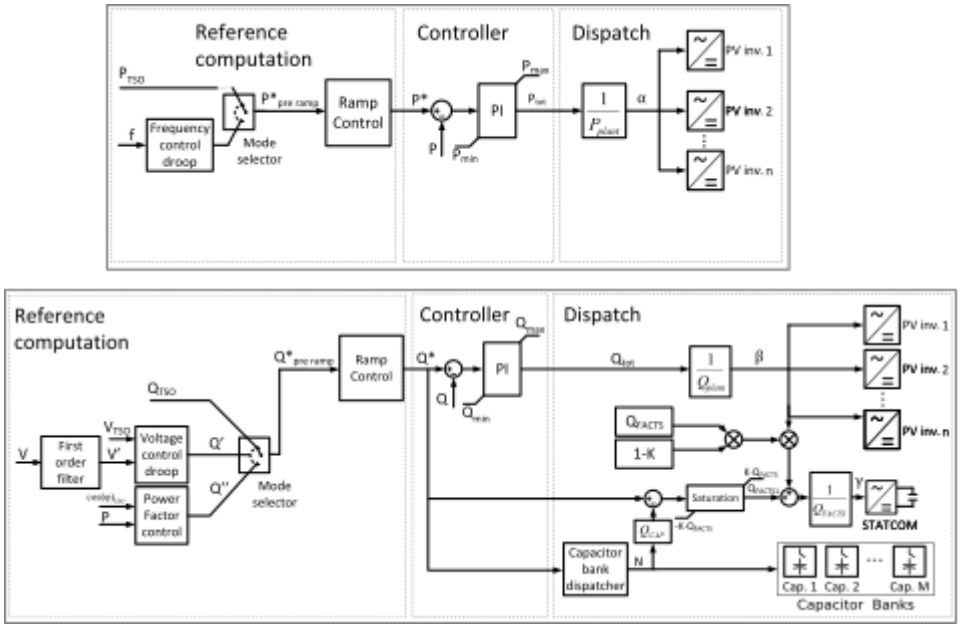

Figure 3.3 PPC complete general control scheme

The way this PPC translates the control's orders to the inverters is in form of the α and β variables. These variables translate to a certain ratio of the available power in form of i_q or i_d current at the output of the inverter, thus enabling the control of the P and Q injected by each converter without exceeding the available power at any given time.

3.6.5 Complete Model

Finally, upon integrating all the defined subparts of the model, the full Non-linear model is obtained Figure 3.4:

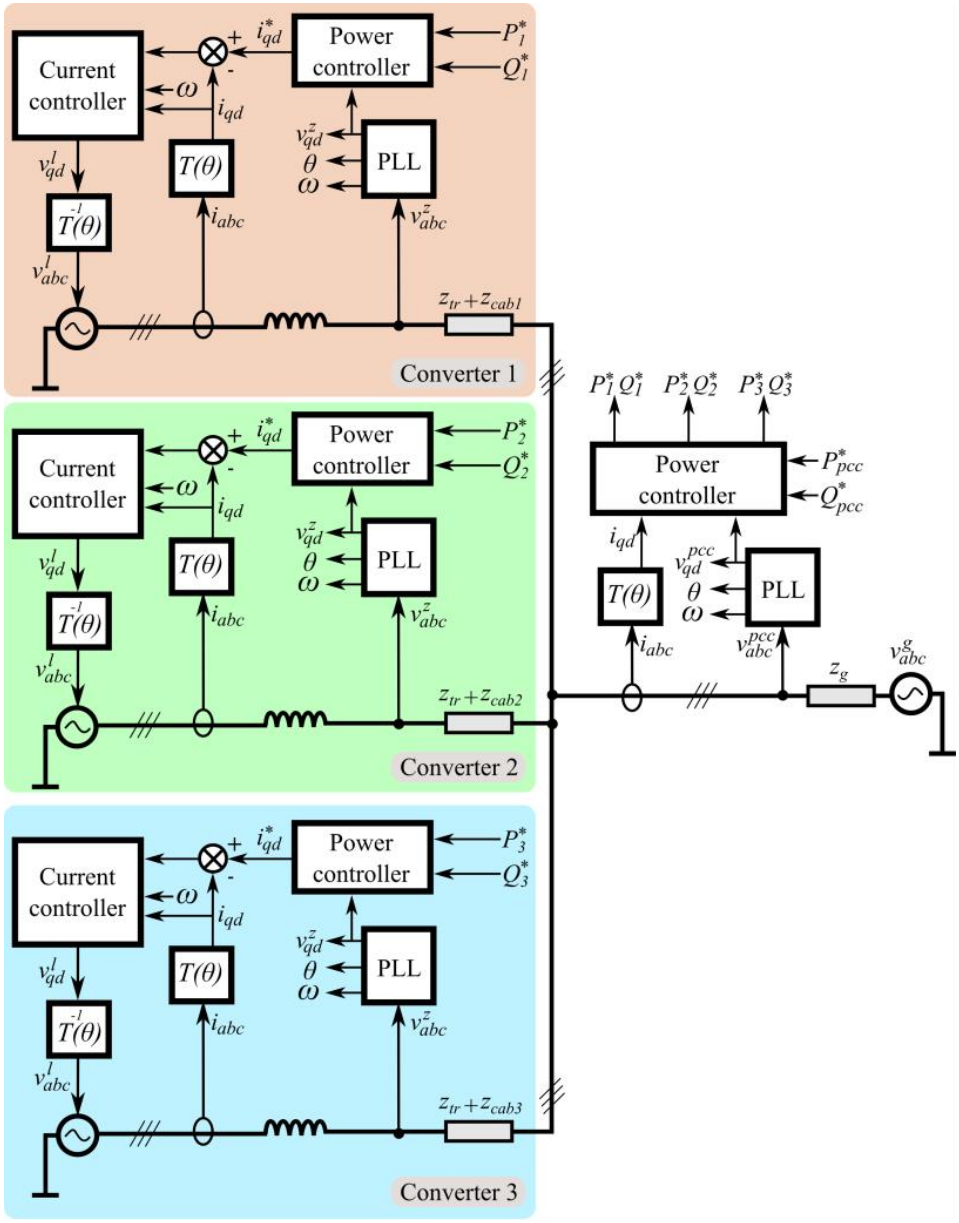

Figure 3.4 Complete Non-linear mode electric and control diagram.

4 The small signal-model

4.1 Introduction

Having obtained the complete non-linear model, the next step in the interaction study consists on formulating a linear mathematical model in state-space form capable of reproducing the transient behaviour of the non-linear system with a high degree of precision. In this section, the linearization process and the small-signal model are presented.

4.2 Internal Grid State Space Model

Within the linear model, most of the control blocks require the input of different variables such as the voltage or current of different points of the circuit. For this reason, taking advantage of the continuity of the electric circuit, all of the electrical equations have been combined in a single state space representation from which all of the remaining control blocks can acquire the information.

In this subsection the electrical equations used in this process and the final state space representation is shown. The following Figure 4.1 depicts the electrical model of the system:

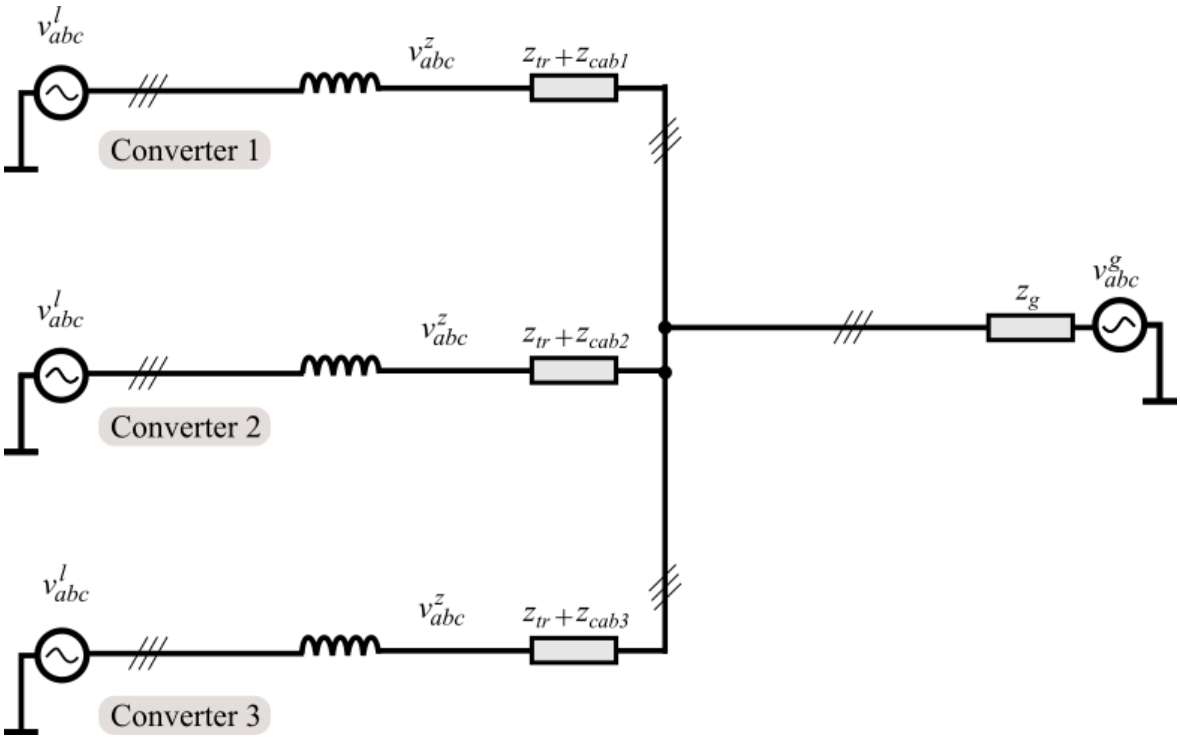

Figure 4.1 Internal PVPP AC grid connection to the grid

The electrical equations of the circuit in $qd0$ reference are shown:

Converter impedance balance:

$$\begin{aligned}
v_{q1}^{l} - v_{q1}^{z} &= R_{lpu} \cdot i_{q1} + L_{lpu} \cdot \left(\frac{di_{q1}}{dt}\right) + L_{lpu} \cdot \omega \cdot i_{d1} \\
v_{d1}^{l} - v_{d1}^{z} &= R_{lpu} \cdot i_{d1} + L_{lpu} \cdot \left(\frac{di_{d1}}{dt}\right) - L_{lpu} \cdot \omega \cdot i_{q1} \\
v_{q2}^{l} - v_{q2}^{z} &= R_{lpu} \cdot i_{q2} + L_{lpu} \cdot \left(\frac{di_{q2}}{dt}\right) + L_{lpu} \cdot \omega \cdot i_{d2} \\
v_{d2}^{l} - v_{d2}^{z} &= R_{lpu} \cdot i_{d2} + L_{lpu} \cdot \left(\frac{di_{d2}}{dt}\right) - L_{lpu} \cdot \omega \cdot i_{q2} \\
v_{q3}^{l} - v_{q3}^{z} &= R_{lpu} \cdot i_{q3} + L_{lpu} \cdot \left(\frac{di_{q3}}{dt}\right) + L_{lpu} \cdot \omega \cdot i_{d3} \\
v_{d3}^{l} - v_{d3}^{z} &= R_{lpu} \cdot i_{d3} + L_{lpu} \cdot \left(\frac{di_{d3}}{dt}\right) - L_{lpu} \cdot \omega \cdot i_{q3}
\end{aligned} \tag{4.1}$$

Cable and transformer impedance balance:

$$\begin{aligned}
v_{q}^{pcc} - v_{q1}^{z} &= R_{cabpu} \cdot i_{q1} + L_{cabpu} \cdot \left(\frac{di_{q1}}{dt}\right) + L_{cabpu} \cdot \omega \cdot i_{d1} \\
v_{d}^{pcc} - v_{d1}^{z} &= R_{cabpu} \cdot i_{d1} + L_{cabpu} \cdot \left(\frac{di_{d1}}{dt}\right) - L_{cabpu} \cdot \omega \cdot i_{q1} \\
v_{q}^{pcc} - v_{q2}^{z} &= R_{cabpu} \cdot i_{q2} + L_{cabpu} \cdot \left(\frac{di_{q2}}{dt}\right) + L_{cabpu} \cdot \omega \cdot i_{d2} \\
v_{d}^{pcc} - v_{d2}^{z} &= R_{cabpu} \cdot i_{d2} + L_{cabpu} \cdot \left(\frac{di_{d2}}{dt}\right) - L_{cabpu} \cdot \omega \cdot i_{q2} \\
v_{q}^{pcc} - v_{q3}^{z} &= R_{cabpu} \cdot i_{q3} + L_{cabpu} \cdot \left(\frac{di_{q3}}{dt}\right) + L_{cabpu} \cdot \omega \cdot i_{d3} \\
v_{d}^{pcc} - v_{d3}^{z} &= R_{cabpu} \cdot i_{d1} + L_{cabpu} \cdot \left(\frac{di_{d3}}{dt}\right) - L_{cabpu} \cdot \omega \cdot i_{q3}
\end{aligned} \tag{4.2}$$

Grid impedance balance:

$$\begin{aligned}
v_{q}^{g} - v_{q}^{pcc} &= R_{gpu} \cdot i_{gq} + L_{gpu} \cdot \left(\frac{di_{gq}}{dt}\right) + L_{gpu} \cdot \omega \cdot i_{gd} \\
v_{d}^{g} - v_{d}^{pcc} &= R_{gpu} \cdot i_{gd} + L_{gpu} \cdot \left(\frac{di_{gd}}{dt}\right) - L_{gpu} \cdot \omega \cdot i_{gq}
\end{aligned} \tag{4.3}$$

Finally, the current balance equations:

$$\begin{aligned}
v_{q}^{g} - v_{q}^{pcc} &= R_{gpu} \cdot i_{gq} + L_{gpu} \cdot \left(\frac{di_{gq}}{dt}\right) + L_{gpu} \cdot \omega \cdot i_{gd} \\
v_{d}^{g} - v_{d}^{pcc} &= R_{gpu} \cdot i_{gd} + L_{gpu} \cdot \left(\frac{di_{gd}}{dt}\right) - L_{gpu} \cdot \omega \cdot i_{gq}
\end{aligned} \tag{4.4}$$

Using the maple software, the equations are rearranged and converted into a state space representation in which the different current values for each of the converter branches are states. The inputs and outputs of the state-space are shown in Figure 4.2:

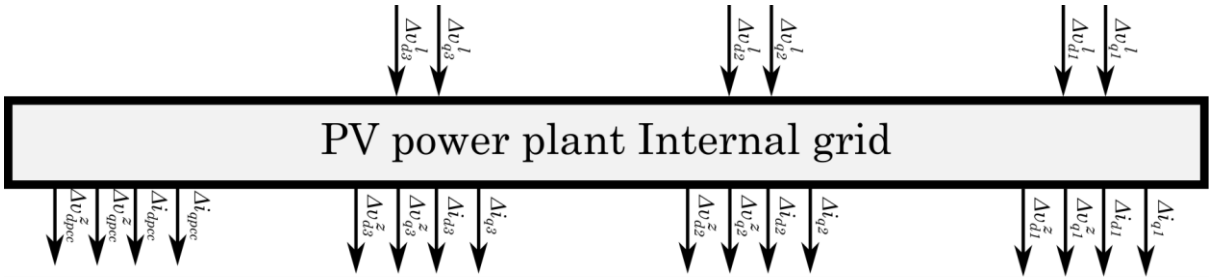

Figure 4.2 Block diagram of the state-space representation of the AC PVPP Internal grid

$$u = \{\Delta v_{q1}^{l}, \Delta v_{d1}^{l}, \Delta v_{q2}^{l}, \Delta v_{d2}^{l}, \Delta v_{q3}^{l}, \Delta v_{d3}^{l}\}$$

$$x = \{\Delta i_{q1}, \Delta i_{d1}, \Delta i_{q2}, \Delta i_{d2}, \Delta i_{q3}, \Delta i_{d3}\}$$

$$y = \{\Delta i_{q1}, \Delta i_{d1}, \Delta i_{q2}, \Delta i_{d2}, i\Delta_{q3}, \Delta i_{d3}, \Delta v_{q1}^{z}, \Delta v_{d1}^{z}, \Delta v_{q2}^{z}, \Delta v_{d2}^{z}, \Delta v_{q3}^{z}, v_{d3}^{z}, \Delta v_{q}^{pcc}, \Delta v_{d}^{pcc}, \Delta i_{gq}, \Delta i_{gd}\}$$

4.3 The Current Loop

The current loop state-space representation is presented in the following expressions:

$$A = \begin{bmatrix} 0 & 0 & 0 & 0 \\ 0 & 0 & 0 & 0 \\ 0 & 0 & 0 & 0 \\ 0 & 0 & 0 & 0 \end{bmatrix} \tag{4.5}$$

$$B = \begin{bmatrix} 1 & 0 & 0 & 0 & 0 & 0 \\ 0 & 1 & 0 & 0 & 0 & 0 \\ 0 & 0 & 1 & 0 & 0 & 0 \\ 0 & 0 & 0 & 1 & 0 & 0 \end{bmatrix}$$

$$C = \begin{bmatrix} -k_{i_{cl}} & 0 & k_{i_{cl}} & 0 \\ 0 & -k_{i_{cl}} & 0 & k_{i_{cl}} \end{bmatrix}$$

$$D = \begin{bmatrix} -k_{p_{cl}} & 0 & k_{p_{cl}} & \omega_n \cdot L_L & 1 & 0 \\ 0 & -k_{p_{cl}} & \omega_n \cdot L_L & k_{p_{cl}} & 0 & 1 \end{bmatrix}$$

$$u = \{\Delta i_{q1-c1}^{*}, \Delta i_{d1-c1}^{*}, \Delta i_{q1-c1}, \Delta i_{d1-c1}, \Delta v_{q1-c1}^{z}, \Delta v_{d1-c1}^{z}\}$$
$$x = \{Si_{q1}^{*}, Si_{d1}^{*}, Si_{q1-c1}, Si_{d1-c1}\}$$
$$y = \{\Delta v_{q1-c1}^{l}, \Delta v_{d1-c1}^{l}\}$$

The following Figure 4.3 depicts the inputs and outputs of the current loop controller:

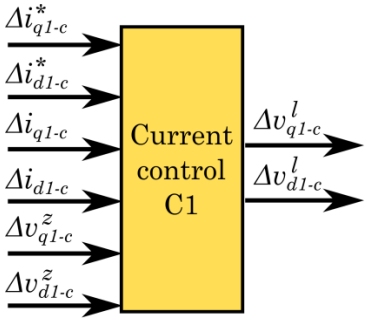

Figure 4.3 Block diagram for the state-space representation of the current loop

As can be deduced from the current loop equations presented in Chapter 2, the current loop is already linear and therefore does not require any form of linearization.

4.4 Phase Locked Loop

The phase locked loop state-space representation has been separated into two submodels which have been concatenated. The first block corresponds to the PI control used to minimise the error of the V^c_{dz} variable which should always be 0 under correct operation of the system. The following expressions represent the PI control component of the PLL:

$$A_1 = \begin{bmatrix} 0 & 0 \\ 0 & 0 \end{bmatrix} \tag{4.6}$$

$$B_1 = \begin{bmatrix} 1 & 0 \\ 0 & 1 \end{bmatrix}$$

$$C_1 = \begin{bmatrix} k_{i_{pll}} & -k_{i_{pll}} \end{bmatrix}$$

$$D_1 = \begin{bmatrix} k_{p_{pll}} & -k_{p_{pll}} \end{bmatrix}$$

$$u_1 = \{\Delta v^{z*}_{d1-c1} *, \Delta v^z_{d1-c1}\}$$

$$x_1 = \{Sv^{z*}_{d1-c1} *, Sv^z_{d1-c1}\}$$

$$y_1 = \{\Delta\omega_1\}$$

The output of the first block is the frequency of the sine wave corresponding to the measured voltage. The frequency must be fed through an integrator in order to obtain the phase estimation in coherence with the synchronous reference frame control topology presented in a previous chapter.

The following expressions represent the integrator state-space model used in the study:

$$A_2 = [0] \tag{4.7}$$

$$B_2 = [1]$$

$$C_2 = [1]$$

$$D_2 = [0]$$

$$u_2 = \{\Delta\omega_1\}$$

$$x_2 = \{\theta_1\}$$

$$y_2 = \{\Delta\theta_1\}$$

Concatenation of both subsystems constitutes the PLL state space model that generates the phase variable used in the reference conversion of other variables. The following Figure 4.4 depicts the inputs and outputs of the phase-locked loop in the linear model:

Figure 4.4 Block diagram of the state-space representation of the Phase-locked loop

4.5 Variable reference

In this study, the different control systems work in different synchronous reference frames that are related to the angle difference associated to each of the points of the circuit to which they are connected. In order to correctly control each of the converters and the PPC, a PLL is used in order to generate the phase estimation for each part of the control. Since the Park rotation is a non-linear application, it must be linearized. For this purpose, the rotation equations have been introduced into the maple software and a linearization of the matrix has been produced. The following expression is the non-linear rotation matrix that converts 2 variables in one reference to another depending on the angle difference between them:

$$\begin{bmatrix} v_q^{ref1} \\ v_d^{ref1} \end{bmatrix} = \begin{bmatrix} \cos(\theta_1 - \theta_2) & -\sin(\theta_1 - \theta_2) \\ \sin(\theta_1 - \theta_2) & \cos(\theta_1 - \theta_2) \end{bmatrix} \begin{bmatrix} v_q^{ref2} \\ v_d^{ref2} \end{bmatrix} \tag{4.8}$$

In this case, the Park and inverse Park rotations are used to change from each of the PLL references to the grid reference. The grid reference is considered $\theta_g = 0$. Therefore, rotation can be simplified to the following expression:

$$\begin{bmatrix} v_q^{c1} \\ v_d^{c1} \end{bmatrix} = \begin{bmatrix} \cos(\theta_1) & -\sin(\theta_1) \\ \sin(\theta_1) & \cos(\theta_1) \end{bmatrix} \begin{bmatrix} v_q^{g} \\ v_d^{g} \end{bmatrix} \tag{4.9}$$

The following state space model represents the voltage Park transformation from grid reference to converter 1 reference:

$$A = [0] \tag{4.10}$$

$$B = [0 \quad 0 \quad 0]$$

$$C = \begin{bmatrix} 0 \\ 0 \end{bmatrix}$$

$$D = \begin{bmatrix} \cos(\theta_{10}) \cdot V_b & -\sin(\theta_{10}) \cdot V_b & -\sin(\theta_{10}) \cdot v_{q10}^z - \cos(\theta_{10}) \cdot v_{d10}^z \\ \sin(\theta_{10}) \cdot V_b & \cos(\theta_{10}) \cdot V_b & \cos(\theta_{10}) \cdot v_{q10}^z - \sin(\theta_{10}) \cdot v_{d10}^z \end{bmatrix}$$

$$u = \{\Delta v_{q1}^z, \Delta v_{d1}^z, \Delta\theta_1\}$$

$$x = \{''\}$$

$$y = \{\Delta v_{q1-c}^z, \Delta v_{d1-c}^z\}$$

Where v_{zq10}^g and v_{zd10}^g are the linearization points corresponding to the steady state values of v_{zqd}^g in grid reference and θ_{10} corresponds to the initial phase difference of the converter.

The following Figure 4.5 depicts the inputs and outputs of the grid-to-converter transformation in the linear model:

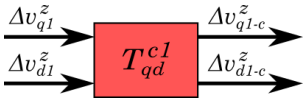

Figure 4.5 Block diagram of the Grid-to-converter reference transformation model

Similarly to the voltage transformation, the same has to be done for the current flowing through each of the branches into the PCC. The current reference transformation is shown in the following expressions:

$$A = [0] \tag{4.11}$$

$$B = [0 \quad 0 \quad 0]$$

$$C = \begin{bmatrix} 0 \\ 0 \end{bmatrix}$$

$$D = \begin{bmatrix} \cos(\theta_{10}) \cdot I_b & -\sin(\theta_{10}) \cdot I_b & -\sin(\theta_{10}) \cdot i_{q10} - \cos(\theta_{10}) \cdot i_{d10} \\ \sin(\theta_{10}) \cdot I_b & \cos(\theta_{10}) \cdot I_b & \cos(\theta_{10}) \cdot i_{q10} - \sin(\theta_{10}) \cdot i_{d10} \end{bmatrix}$$

$$u = \{\Delta i_{q1}, \Delta i_{d1}, \Delta\theta_1\}$$

$$x = \{''\}$$

$$y = \{\Delta i_{q1-c}, \Delta i_{d1-c}\}$$

Finally, the converter control's output value must be converted from converter reference to grid reference. This is done by inverting the rotation matrix:

$$\begin{bmatrix} v_q^g \\ v_d^g \end{bmatrix} = \begin{bmatrix} \cos(\theta_1) & \sin(\theta_1) \\ -\sin(\theta_1) & \cos(\theta_1) \end{bmatrix} \begin{bmatrix} v_q^{c1} \\ v_d^{c1} \end{bmatrix} \tag{4.12}$$

Upon repeating the linearization procedure, the resulting linearized state-space model is obtained:

$$A = [0] \tag{4.13}$$

$$B = [0 \quad 0 \quad 0]$$

$$C = \begin{bmatrix} 0 \\ 0 \end{bmatrix}$$

$$D = \begin{bmatrix} \cos(\theta_{10})/V_b & \sin(\theta_{10})/V_b & -\sin(\theta_{10}) \cdot v_{q10}^l/V_b - \cos(\theta_{10}) \cdot v_{d10}^l/V_b \\ -\sin(\theta_{10}) \cdot V_b & \cos(\theta_{10}) \cdot V_b & \cos(\theta_{10}) \cdot v_{q10}^l/V_b - \sin(\theta_{10}) \cdot v_{d10}^l/V_b \end{bmatrix}$$

$$u = \{\Delta v_{q1-c}^l, \Delta v_{d1-c}^l, \Delta\theta_1\}$$

$$x = \{''\}$$

$$y = \{\Delta v_{q1}^l, \Delta v_{d1}^l\}$$

The base values seen throughout the state-space matrices of the transforms are included only to convert from international system units to per unit and vice-versa.

Figure 4.6 shows the inverse rotation block:

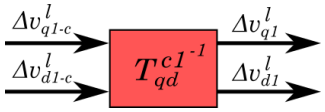

Figure 4.6 Block diagram of the Converter-to-Grid reference transformation model

4.6 Converter Power Control

The converter power control loop controls the power the converter injects to the grid and translates the output error into a current reference. For this purpose, two state-space models have been implemented. They correspond to the converter power loops detailed in the previous chapter. Their state-space equations are shown in the following expressions:

$$A_{Pc1} = \begin{bmatrix} 0 & 0 \\ 0 & 0 \end{bmatrix} \tag{4.14}$$

$$B_{Pc1} = \begin{bmatrix} 1 & 0 \\ 0 & 1 \end{bmatrix}$$

$$C_{Pc1} = [ki_{Pc} \quad -ki_{Pc}]$$

$$D_{Pc1} = [kp_{Pc} \quad -kp_{Pc}]$$

$$u_{Pc1} = \{\Delta P^*_{c1}, \Delta P_{m1}\}$$

$$x_{Pc1} = \{SP^*_{c1}, SP_{c1}\}$$

$$y_{Pc1} = \{\Delta P_{c1}\}$$

And:

$$A_{Qc1} = \begin{bmatrix} 0 & 0 \\ 0 & 0 \end{bmatrix} \tag{4.15}$$

$$B_{Qc1} = \begin{bmatrix} 1 & 0 \\ 0 & 1 \end{bmatrix}$$

$$C_{Qc1} = [ki_{Qc} \quad -ki_{Qc}]$$

$$D_{Qc1} = [kp_{Qc} \quad -kp_{Qc}]$$

$$u_{Qc1} = \{\Delta Q^*_{c1} \Delta Q_{m1}\}$$

$$x_{Qc1} = \{SQ^*_{c1}, SQ_{c1}\}$$

$$y_{Qc1} = \{\Delta Q_{c1}\}$$

Where the gain parameters of both controllers are identical.

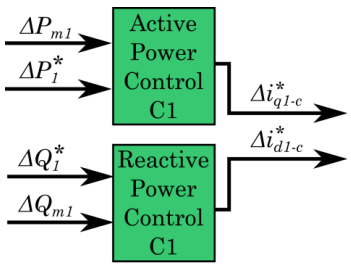

Figure 4.7 Block diagram of the state-space form of the Converter power control

4.7 Power Computation

Throughout the model, the power must be measured at the PCC and at the connection point of each of the converters. As previously explained in the introductory chapters, the power equations in $qd0$ reference are as follows:

$$P = \frac{3}{2} \cdot (v_q i_q + v_d i_d) \tag{4.16}$$

$$Q = \frac{3}{2} \cdot (v_q i_d - v_d i_q) \tag{4.17}$$

As can be seen, the equations must be linearized. Upon application of the linearization procedure, the linearized expressions are obtained:

$$P = \frac{3}{2} \cdot (v_q i_{q0} + v_{q0} i_q + v_{d0} i_d + v_d i_{d0})$$

$$Q = \frac{3}{2} \cdot (v_q i_{d0} + v_q i_{d0} - v_{d0} i_q - v_d i_{q0})$$

The following state-space model describes the power measurement for converter 1:

$$A = [0] \tag{4.18}$$

$$B = [0 \quad 0 \quad 0 \quad 0]$$

$$C = \begin{bmatrix} 0 \\ 0 \end{bmatrix}$$

$$D = \begin{bmatrix} \frac{3}{2} \cdot i_{q10-c} & \frac{3}{2} \cdot i_{d10-c} & \frac{3}{2} \cdot v^z_{q10-c} & \frac{3}{2} \cdot v^z_{d10-c} \\ \frac{3}{2} \cdot i_{d10-c} & -\frac{3}{2} \cdot i_{q10-c} & -\frac{3}{2} \cdot v^z_{d10-c} & \frac{3}{2} \cdot v^z_{q10-c} \end{bmatrix}$$

$$u = \{\Delta v^z_{q1-c}, \Delta v^z_{d1-c}, \Delta i_{q1-c}, \Delta i_{d1-c}\}$$

$$x = \{''\}$$

$$y = \{\Delta P_{m1}, \Delta Q_{m1}\}$$

The power computation state space block for converter 1 is depicted in the following Figure 4.8:

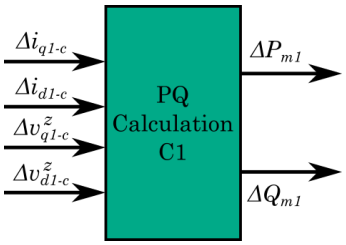

Figure 4.8 Block diagram of the state-space form of the Active and reactive power measurement model

4.8 Total power controller

The PPC's control loop is in charge of regulating the power flowing into the AC grid. It receives the calculated power at the point of common coupling and compares it with the total P and Q references which are the main inputs to the whole system.

The PV Park power control loop has been defined in two state-space models as follows:

$$A_{Ppcc} = \begin{bmatrix} 0 & 0 \\ 0 & 0 \end{bmatrix} \tag{4.19}$$

$$B_{Ppcc} = \begin{bmatrix} 1 & 0 \\ 0 & 1 \end{bmatrix}$$

$$C_{Ppcc} = \begin{bmatrix} K_{i_P}/3 & -K_{i_P}/3 \\ K_{i_P}/3 & -K_{i_P}/3 \\ K_{i_P}/3 & -K_{i_P}/3 \end{bmatrix}$$

$$D_{Ppcc} = \begin{bmatrix} K_{p_P}/3 & -K_{p_P}/3 \\ K_{p_P}/3 & -K_{p_P}/3 \\ K_{p_P}/3 & -K_{p_P}/3 \end{bmatrix}$$

$$u_{Ppcc} = \{\Delta P^*_{pcc}, \Delta P_{mpcc}\}$$

$$x_{Ppcc} = \{SP^*_{pcc}, SP_{mpcc}\}$$

$$y_{Ppcc} = \{\Delta P^*_{c1}, \Delta P^*_{c2}, \Delta P^*_{c3}\}$$

And:

$$A_{Qpcc} = \begin{bmatrix} 0 & 0 \\ 0 & 0 \end{bmatrix} \tag{4.20}$$

$$B_{Qpcc} = \begin{bmatrix} 1 & 0 \\ 0 & 1 \end{bmatrix}$$

$$C_{Qpcc} = \begin{bmatrix} K_{i_Q}/3 & -K_{i_Q}/3 \\ K_{i_Q}/3 & -K_{i_Q}/3 \\ K_{i_Q}/3 & -K_{i_Q}/3 \end{bmatrix}$$

$$D_{Qpcc} = \begin{bmatrix} K_{p_Q}/3 & -K_{p_Q}/3 \\ K_{p_Q}/3 & -K_{p_Q}/3 \\ K_{p_Q}/3 & -K_{p_Q}/3 \end{bmatrix}$$

$$u_{Qpcc} = \{\Delta Q^*_{pcc}, \Delta Q_{mpcc}\}$$

$$x_{Qpcc} = \{SQ^*_{pcc}, SQ_{mpcc}\}$$

$$y_{Qpcc} = \{\Delta Q^*_{c1}, \Delta Q^*_{c2}, \Delta Q^*_{c3}\}$$

Where the gain parameters for the P and Q control are identical.

As can be seen, this control loop calculates how much power must be injected and divides it equally between the converters. The PPC state space block is depicted in the following Figure 4.9:

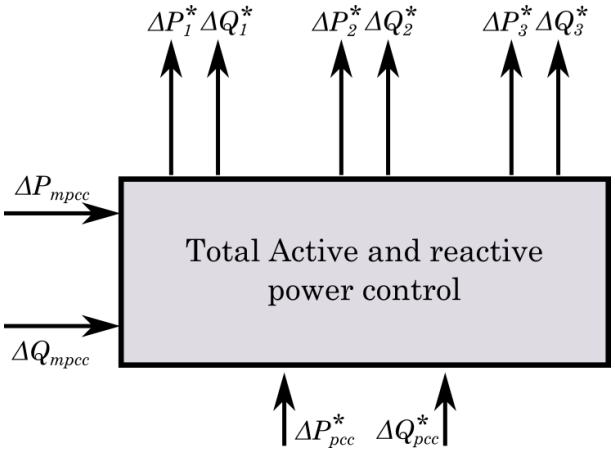

Figure 4.9 Block Diagram of the PPC state-space model

4.9 Model initialisation

A fairly common problem in the simulation of a model like the one described in this chapter is associated to its initialisation. The MATLAB® simulation software has problems starting the simulation because the programme attempts to compute all the calculations starting at 0 value. The consequences of said computation are usually very slow simulation times or unstable simulation.

The most common solutions used to address this issue consist on specialised MATLAB® Simulink blocks that initialise certain variables (memory block), or the use of logical signals that disable certain control loops for the first few microseconds. Naturally, producing an exact mathematical model of a memory block is not trivial. Therefore, the solution implemented in this project consists on introducing a small delay into the control signal sent to the controllable AC voltage sources.

This solution has been implemented by using a first order transfer function with a very small time delay value which can be seen in the following expression:

$$\frac{v_{qd}{}'(s)}{v_{qd}(s)} = \frac{1}{\tau_{delay} \cdot s + 1} \tag{4.21}$$

Where $v_{qd}^{l}(s)$ is the output of the current control of each converter and $v_{qd}{}'(s)$ is the delayed signal. The value for τ_{delay} can have a great impact on the dynamic response of the system. For this reason, the delay constant has to be small enough in order to prevent the filtering of the system oscillations that are studied in this project.

The impact of the delay transfer function can be seen in the following bode plots for different τ_{delay} values:

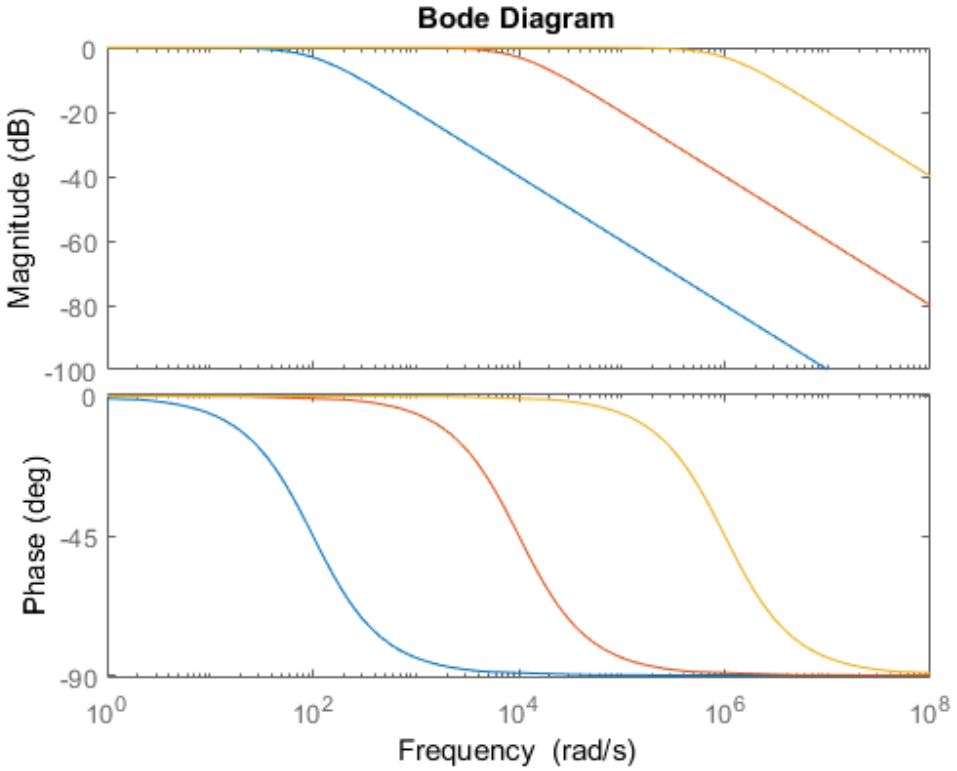

Figure 4.10 Bode Plot for the delay block transfer function for different delay values

Where the blue line $\tau_{delay} = 1 \cdot 10^{-2}$ red line $\tau_{delay} = 1 \cdot 10^{-4}$ and the yellow line corresponds to $\tau_{delay} = 1 \cdot 10^{-6}$ .As can be seen in both graphs, the lower the τ_{delay} parameter is, the smaller the dynamic filtering produced. However, using a very small delay time greatly increases the computation time of the simulation. For that reason, the chosen delay time for the model initialisation has been $\tau_{delay} = 1 \cdot 10^{-4}$.

Thus, the delay transfer function used in the model is obtained:

$$\frac{v_{qd}{}'(s)}{v_{qd}(s)} = \frac{1}{(1 \cdot 10^{-4} \cdot s + 1)} \tag{4.22}$$

The delay has been converted to state-space and included in the linear mathematical model.

4.10 Full small-signal model

The complete small signal model is obtained by interconnecting all of the previously detailed state-space models. This task has been carried out by using the connect command of the MATLAB® software. Figure 4.11 shows the complete signal flow of the complete small-signal model:

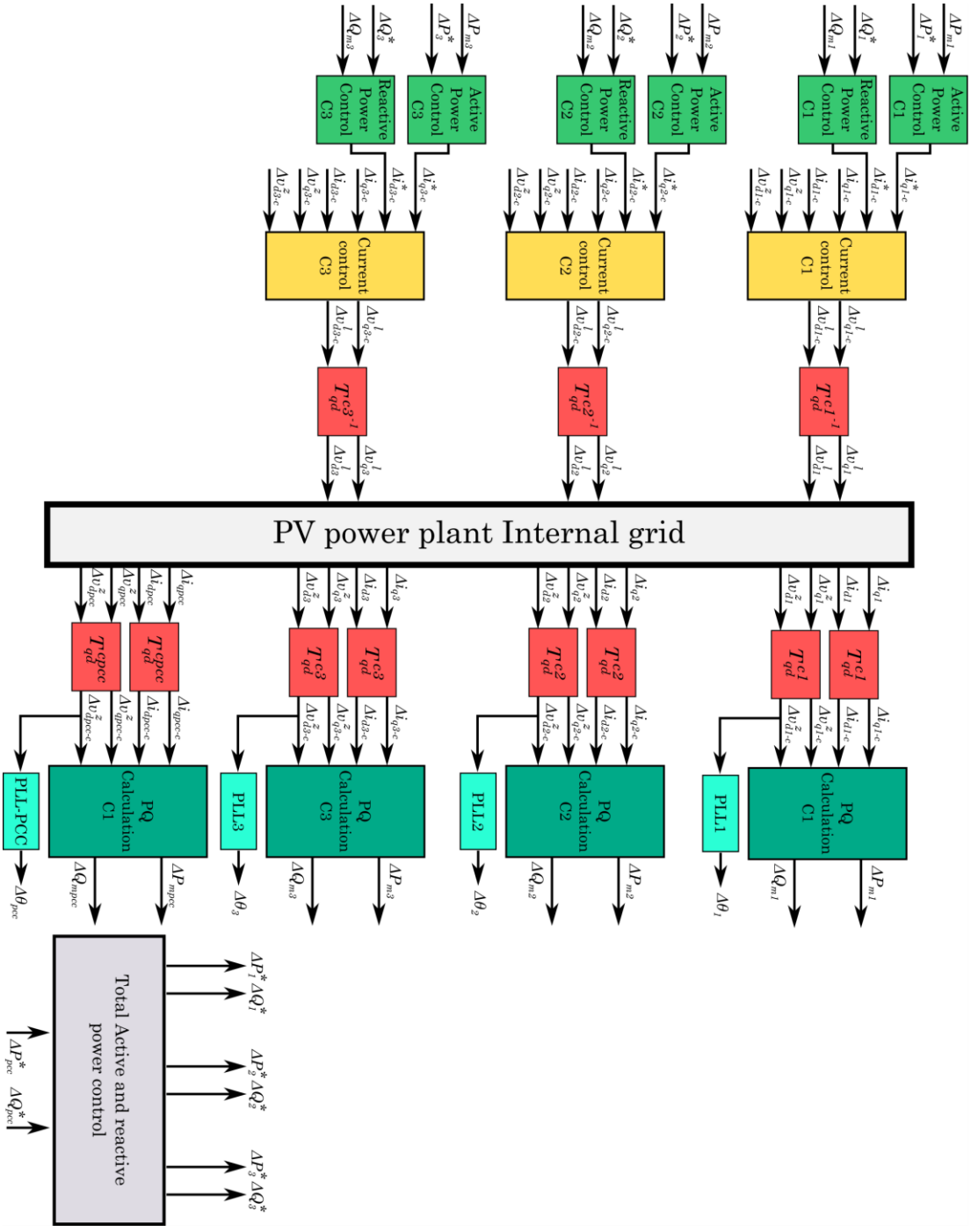

Figure 4.11 Diagram of the complete linear model

5 Results and Findings

5.1 Introduction

This section presents the results obtained from the different simulations and other mathematical operations. These include the linear model validation, the participation factor computations for the different SCR values and the time domain simulations of the non-linear model showing the oscillations for each SCR.

5.2 Model Validation

In order to ensure satisfactory results from the small signal study, the linearized mathematical model must be validated. The validation process is simple, both the linear and non-linear models must be simulated in the same boundary conditions. The electrical signals of both models are compared in order to confirm that the linear mathematical model is precise enough. Since the linear model is an approximation of the non-linear model at a certain operation point, a certain amount of error is unavoidable. Therefore, the further the simulation goes from the linearized operation point, the bigger the error. This effect can be seen in the following Figure 5.1 and Figure 5.2 where different power increases over the operation point are performed and the v_q^{pcc} values are compared:

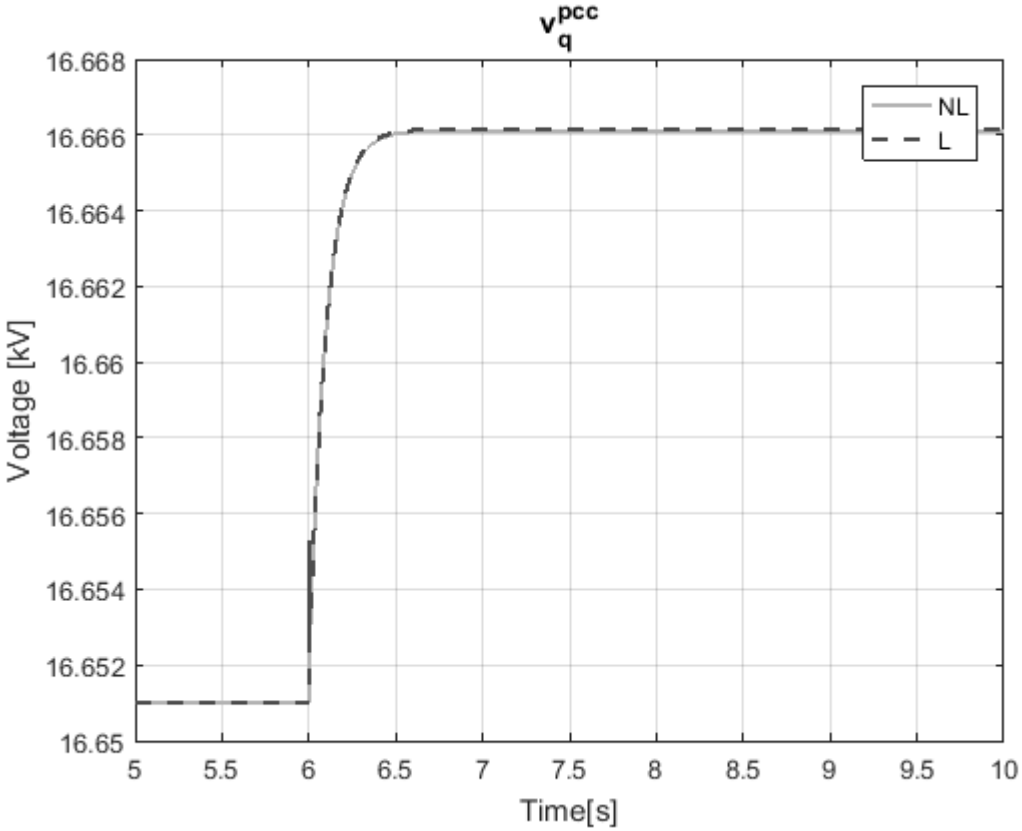

Figure 5.1 v_q comparison at the PCC between the Linear and Non-linear models for a 5% Power Reference increase

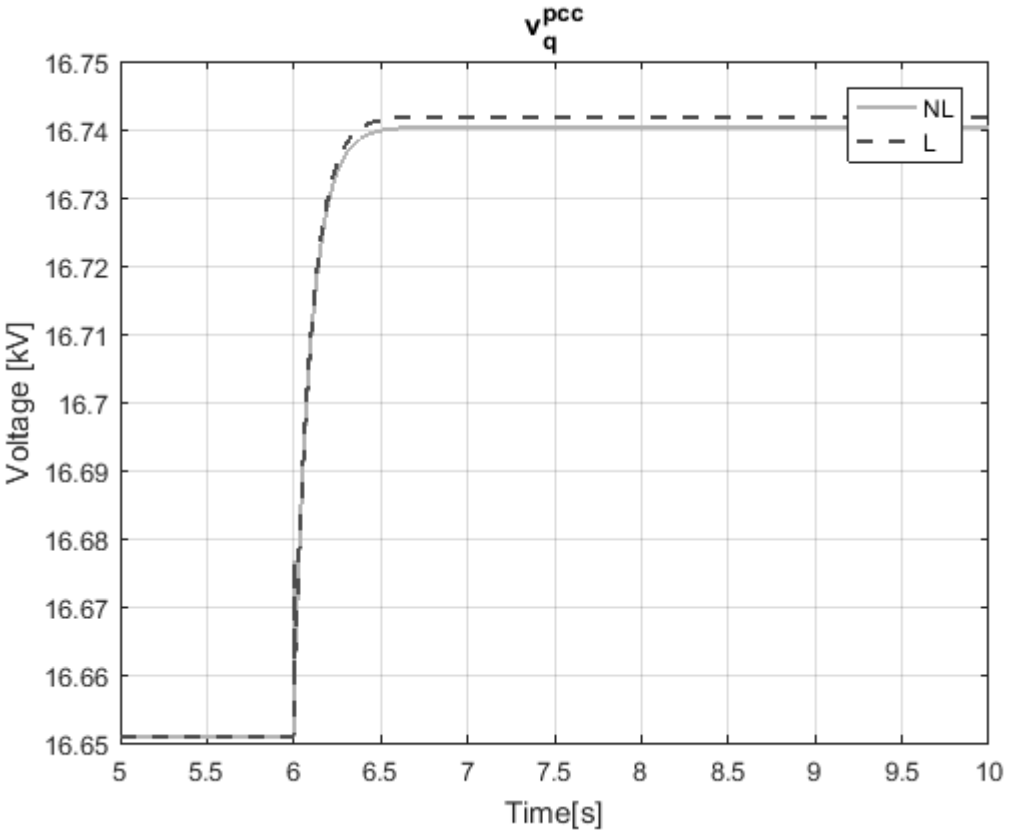

Figure 5.2 v_d comparison at the PCC between the Linear and Non-linear models for a 30% Power Reference increase

The first simulation has been carried out applying a 5% power reference increase at the 6 second time mark. Similarly, in the second simulation a 30% power reference increase has been applied. As can be seen, the linear model is much more precise when the power references are closer to the linearization point.

The model validation has been conducted comparing the time domain simulation of both the linear and non-linear models, applying a 5 % active and reactive power increase at t=6s and linearizing at an initial power output of 2.5 MW and 1 Mvar.

The following Figure 5.3 to Figure 5.14 depict the signal comparison from both models for several relevant parameters:

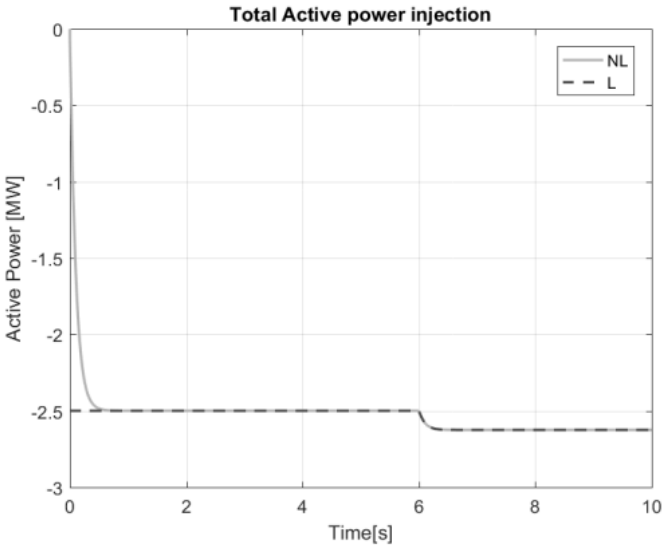

Figure 5.3 Total Active power comparison flowing through the PCC between the Linear and Non-linear models

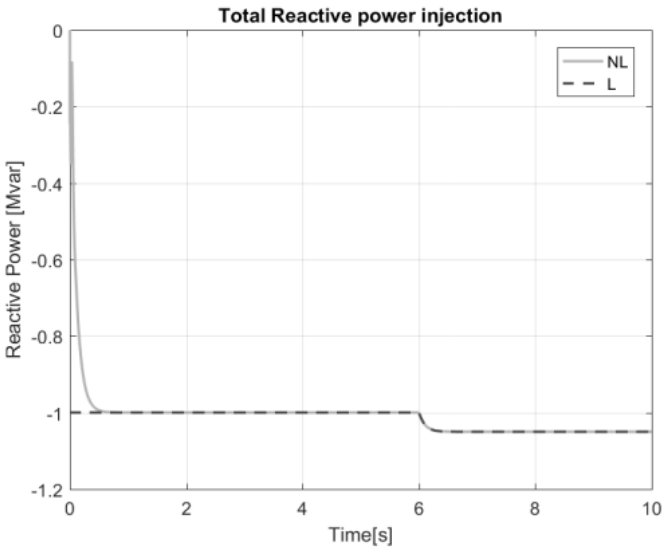

Figure 5.4 Total Reactive power comparison flowing through the PCC between the Linear and Non-linear models

The linear and non-linear power measurements at the PCC can be seen. Both signals show practically no error for the 5% power reference increase.

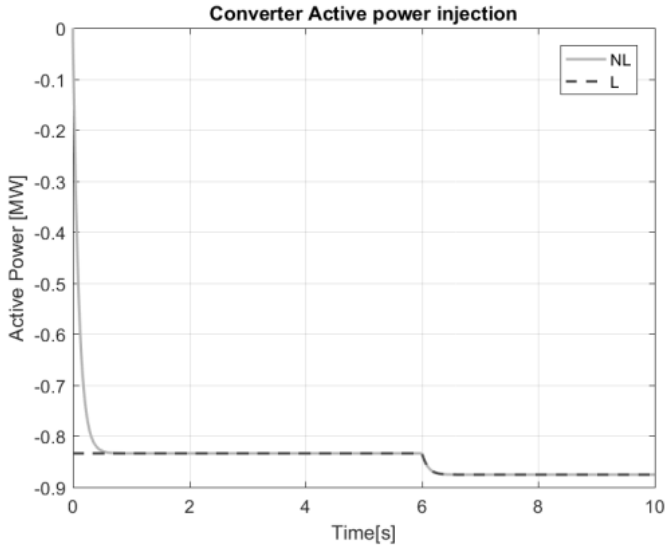

Figure 5.5 Total Active power comparison flowing through Converter 1 between the Linear and Non-linear models

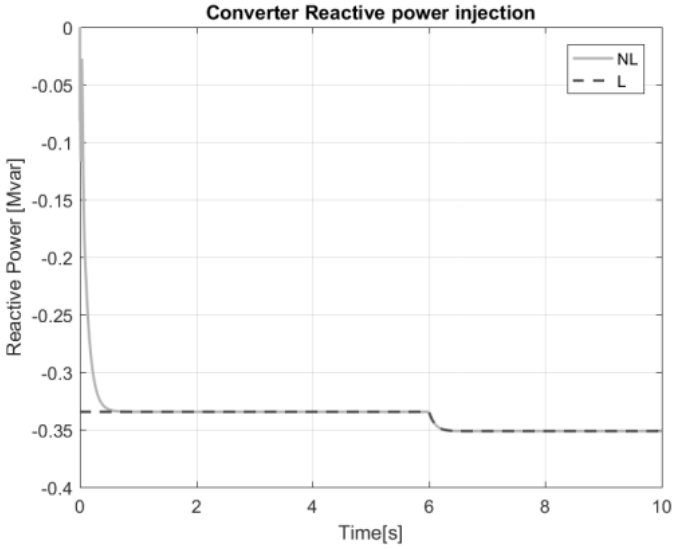

Figure 5.6 Total Reactive power comparison flowing through Converter 1 between the Linear and Non-linear models

The linear and non-linear power measurements at the connection point of converter 1 can be seen. Both signals show practically no error for the 5% power reference increase.

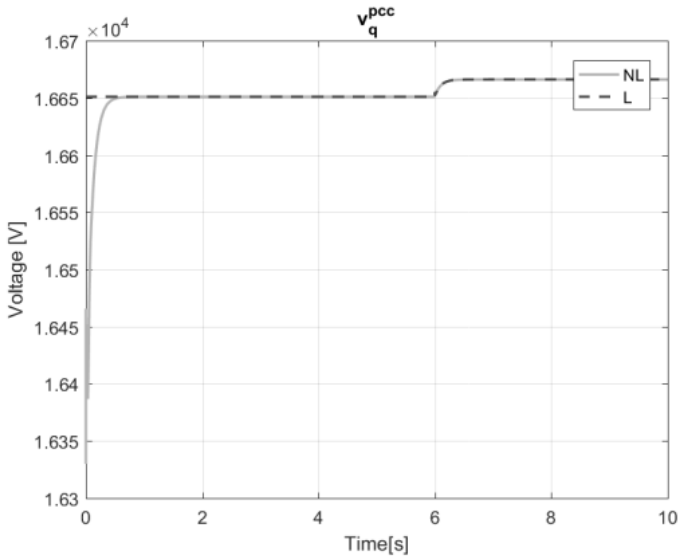

Figure 5.7 v_q comparison at the PCC between the Linear and Non-linear models

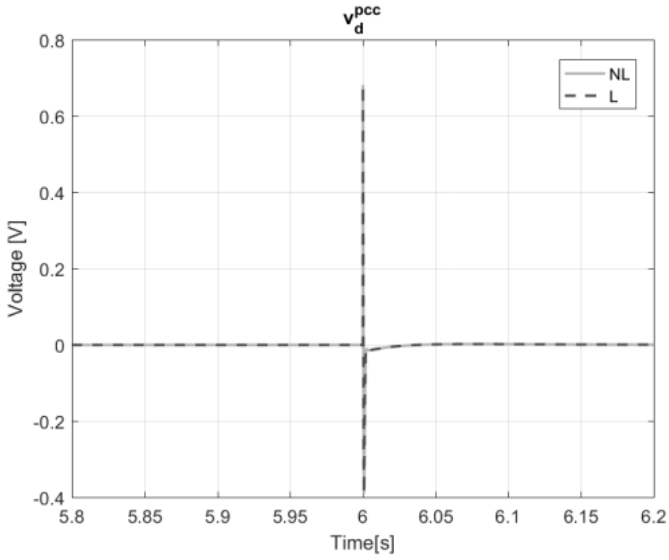

Figure 5.8 v_d comparison at the PCC between the Linear and Non-linear models

The linear and non-linear power $qd0$ voltage measured at the PCC can be seen. Both signals show practically no error for the 5% power reference increase.

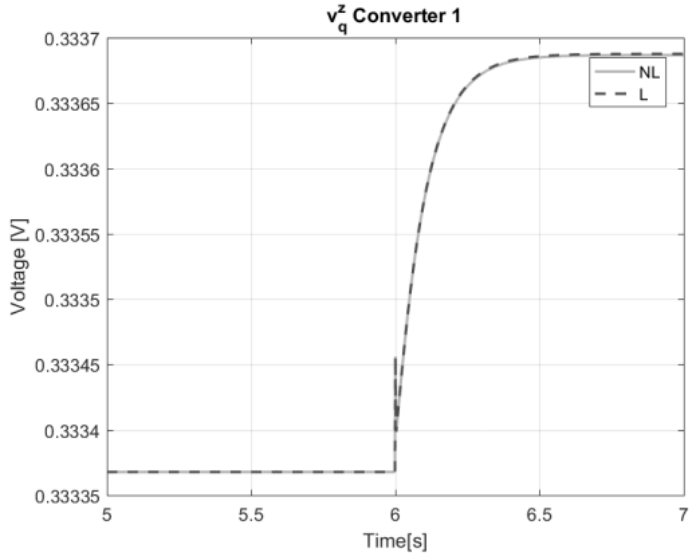

Figure 5.9 v_q comparison at the converter 1 at the impedance grid-side between the Linear and Non-linear models

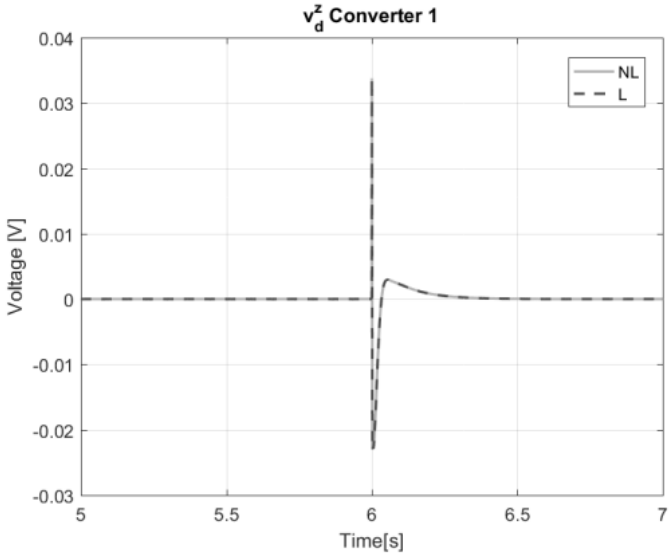

Figure 5.10 v_d comparison at the converter 1 at the impedance grid-side between the Linear and Non-linear models

The linear and non-linear power $qd0$ voltage measured at the converter 1 connection point can be seen. Both signals show practically no error for the 5% power reference increase.

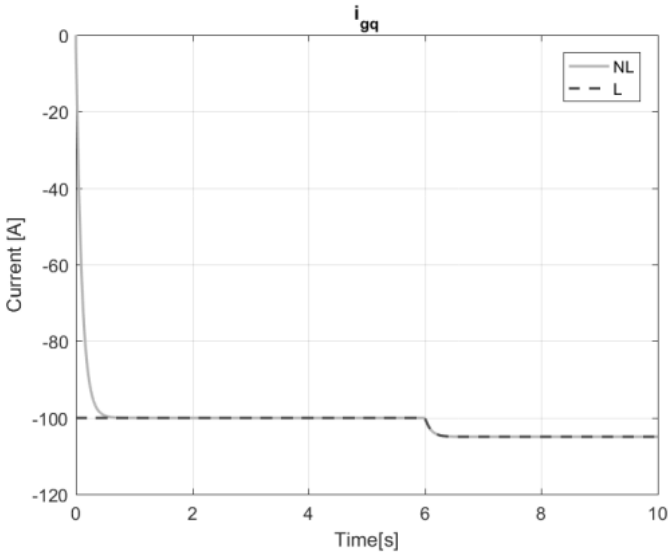

Figure 5.11 Current q component comparison flowing through the PCC between the Linear and Non-linear model

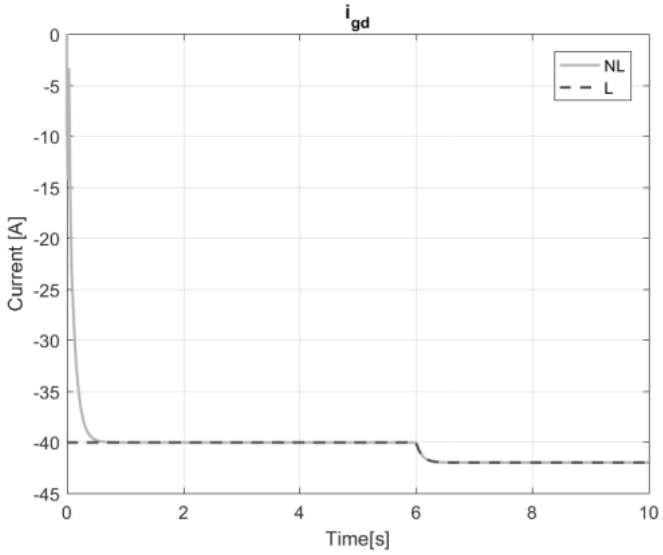

Figure 5.12 Current d component comparison flowing through the PCC between the Linear and Non-linear model

The linear and non-linear power $qd0$ current measured at the PCC can be seen. Both signals show practically no error for the 5% power reference increase.

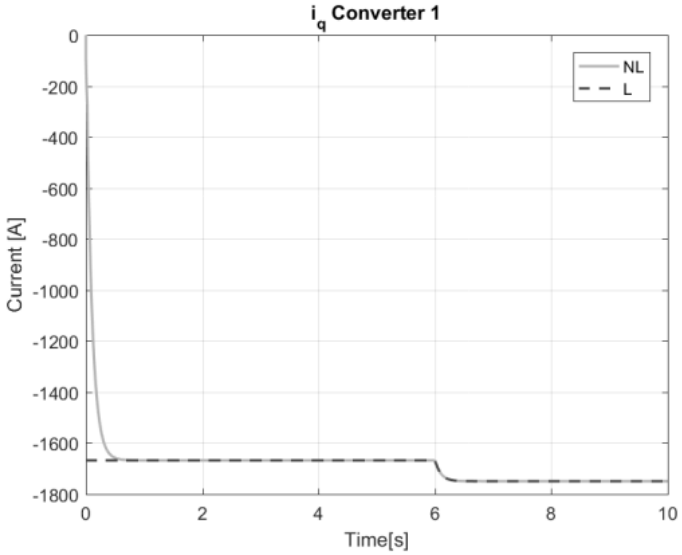

Figure 5.13 Current q component comparison flowing through the converter 1 impedance between the Linear and Non-linear model

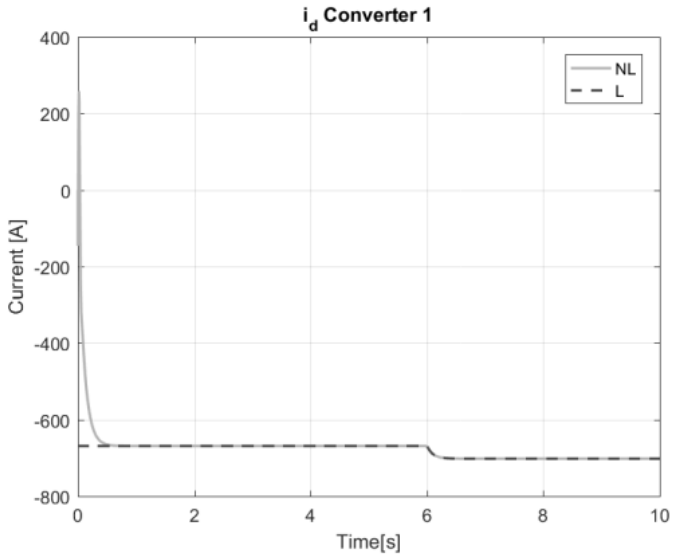

Figure 5.14 Current d component comparison flowing through the converter 1 impedance between the Linear and Non-linear model

The linear and non-linear power $qd0$ current measured flowing through the converter 1 branch can be seen. Both signals show practically no error for the 5% power reference increase.

The linear model has proved to behave like the non-linear model for the specific operation point without excessive error. Therefore, the model validation has been successful.

5.4 Different SCR values

The effect that grid strength can have on the dynamic behaviour of the system has been studied in this system. In this section the critical Eigen values of the system are plotted. Additionally, the results of the participation factor study are included showing the predominant oscillatory behaviour of the system as well as the internal states which participate in said oscillations. Finally, time domain simulations are used to compare the dynamic behaviour for different SCR values for the most relevant variables.

5.4.1 Eigen Values

A decrease the SCR of the AC grid pushes the system into unstable operation as can be seen by plotting the linear model's Eigen values. The real zero value is the stability threshold as is known from general continuous control theory. The evolution of the systems poles for SCR values lower than three can be seen in Figure 5.15:

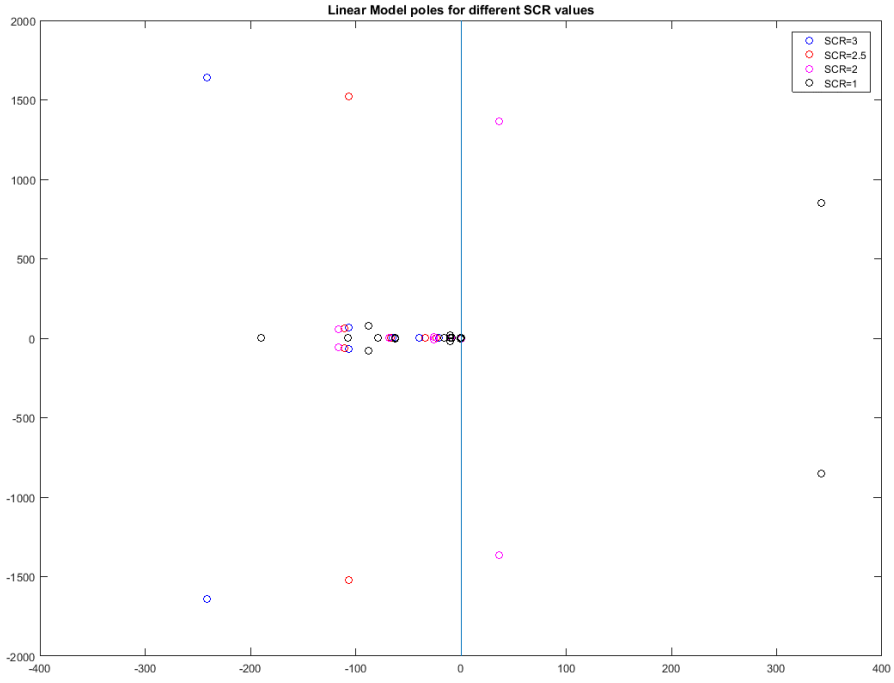

Figure 5.15 Eigenvalue plot for SCR values under three.

As can be gathered from the pole map, an SCR lower or equal than two proves to destabilize the system since there are positive real components of the system's poles. Simulations on the non-linear model for SCR values lower than three were unstable and therefore could not yield results.

5.4.2 Participation factory analysis

Upon validating the linear model, a modal analysis is performed on the state matrix of the linear model. The participation factor computation has been carried out for different SCR values. The results are presented in the present section.

Figure 5.16 shows the internal oscillations and participation factor computation results for an SCR of 20:

SCR=20	M1	M2	M3	M4	M5	M6	M7	M8	M9	M10	M11	M12	M13	M14	M15	M16	M17	M18
'f (Hz)'	71,229	71,229	71,386	71,386	295,928	295,928	115,330	115,330	21,454	21,454	21,773	21,773	12,906	12,906	12,740	12,740	12,742	12,742
'damp'	0,998	0,998	0,998	0,998	0,803	0,803	0,973	0,973	0,998	0,998	0,998	0,998	0,707	0,707	0,714	0,714	0,714	0,714
'Suc1_d '	0,00	0,00	0,00	0,00	0,00	0,00	0,00	0,00	0,00	0,00	0,00	0,00	0,98	0,98	1,00	1,00	0,25	0,25
'e_theta'	0,00	0,00	0,00	0,00	0,01	0,01	0,00	0,00	0,00	0,00	0,00	0,00	1,00	1,00	1,00	1,00	0,25	0,25
'SPinv1'	0,00	0,00	0,00	0,00	0,00	0,00	0,00	0,00	0,00	0,00	0,00	0,00	0,00	0,00	0,00	0,00	0,00	0,00
'SPc1 '	0,00	0,00	0,00	0,00	0,00	0,00	0,01	0,01	0,03	0,03	0,01	0,01	0,01	0,01	0,00	0,00	0,00	0,00
'SQinv1'	0,00	0,00	0,00	0,00	0,00	0,00	0,00	0,00	0,00	0,00	0,00	0,00	0,00	0,00	0,00	0,00	0,00	0,00
'SQc1 '	0,00	0,00	0,00	0,00	0,02	0,02	0,00	0,00	0,03	0,03	0,01	0,01	0,01	0,01	0,00	0,00	0,00	0,00
'Sic1_q_ref'	0,00	0,00	0,00	0,00	0,00	0,00	0,00	0,00	0,00	0,00	0,00	0,00	0,00	0,00	0,00	0,00	0,00	0,00
'Sic1_d_ref'	0,00	0,00	0,00	0,00	0,00	0,00	0,00	0,00	0,00	0,00	0,00	0,00	0,00	0,00	0,00	0,00	0,00	0,00
'Sic1_q'	0,00	0,00	0,00	0,00	0,00	0,00	0,00	0,00	0,00	0,00	0,00	0,00	0,00	0,00	0,00	0,00	0,00	0,00
'Sic1_d'	0,00	0,00	0,00	0,00	0,00	0,00	0,00	0,00	0,00	0,00	0,00	0,00	0,00	0,00	0,00	0,00	0,00	0,00
'Rmem1q'	1,00	1,00	0,26	0,26	0,07	0,07	0,94	0,94	0,30	0,30	0,08	0,08	0,00	0,00	0,00	0,00	0,00	0,00
'Rmem1d'	0,99	0,99	0,25	0,25	0,91	0,91	0,02	0,02	0,29	0,29	0,08	0,08	0,00	0,00	0,00	0,00	0,00	0,00
'Suc2_d '	0,00	0,00	0,00	0,00	0,00	0,00	0,00	0,00	0,00	0,00	0,00	0,00	0,99	0,99	0,00	0,00	1,00	1,00
'e_theta2'	0,00	0,00	0,00	0,00	0,01	0,01	0,00	0,00	0,00	0,00	0,00	0,00	1,00	1,00	0,00	0,00	1,00	1,00
'SPinv2'	0,00	0,00	0,00	0,00	0,00	0,00	0,00	0,00	0,00	0,00	0,00	0,00	0,00	0,00	0,00	0,00	0,00	0,00
'SPc2 '	0,00	0,00	0,00	0,00	0,00	0,00	0,01	0,01	0,00	0,00	0,03	0,03	0,01	0,01	0,00	0,00	0,00	0,00
'SQinv2'	0,00	0,00	0,00	0,00	0,00	0,00	0,00	0,00	0,00	0,00	0,00	0,00	0,00	0,00	0,00	0,00	0,00	0,00
'SQc2 '	0,00	0,00	0,00	0,00	0,03	0,03	0,00	0,00	0,00	0,00	0,03	0,03	0,01	0,01	0,00	0,00	0,00	0,00
'Sic2_q_ref'	0,00	0,00	0,00	0,00	0,00	0,00	0,00	0,00	0,00	0,00	0,00	0,00	0,00	0,00	0,00	0,00	0,00	0,00
'Sic2_d_ref'	0,00	0,00	0,00	0,00	0,00	0,00	0,00	0,00	0,00	0,00	0,00	0,00	0,00	0,00	0,00	0,00	0,00	0,00
'Sic2_q'	0,00	0,00	0,00	0,00	0,00	0,00	0,00	0,00	0,00	0,00	0,00	0,00	0,00	0,00	0,00	0,00	0,00	0,00
'Sic2_d'	0,00	0,00	0,00	0,00	0,00	0,00	0,00	0,00	0,00	0,00	0,00	0,00	0,00	0,00	0,00	0,00	0,00	0,00
'Rmem2q'	0,00	0,00	1,00	1,00	0,07	0,07	0,96	0,96	0,00	0,00	0,30	0,30	0,00	0,00	0,00	0,00	0,00	0,00
'Rmem2d'	0,00	0,00	0,99	0,99	0,93	0,93	0,02	0,02	0,00	0,00	0,29	0,29	0,00	0,00	0,00	0,00	0,00	0,00
'Suc3_d '	0,00	0,00	0,00	0,00	0,00	0,00	0,00	0,00	0,00	0,00	0,00	0,00	0,98	0,98	1,00	1,00	0,25	0,25
'e_theta3'	0,00	0,00	0,00	0,00	0,01	0,01	0,00	0,00	0,00	0,00	0,00	0,00	1,00	1,00	1,00	1,00	0,25	0,25
'SPinv3'	0,00	0,00	0,00	0,00	0,00	0,00	0,00	0,00	0,00	0,00	0,00	0,00	0,00	0,00	0,00	0,00	0,00	0,00
'SPc3 '	0,00	0,00	0,00	0,00	0,00	0,00	0,01	0,01	0,03	0,03	0,01	0,01	0,01	0,01	0,00	0,00	0,00	0,00
'SQinv3'	0,00	0,00	0,00	0,00	0,00	0,00	0,00	0,00	0,00	0,00	0,00	0,00	0,00	0,00	0,00	0,00	0,00	0,00
'SQc3 '	0,00	0,00	0,00	0,00	0,02	0,02	0,00	0,00	0,03	0,03	0,01	0,01	0,01	0,01	0,00	0,00	0,00	0,00
'Sic3_q_ref'	0,00	0,00	0,00	0,00	0,00	0,00	0,00	0,00	0,00	0,00	0,00	0,00	0,00	0,00	0,00	0,00	0,00	0,00
'Sic3_d_ref'	0,00	0,00	0,00	0,00	0,00	0,00	0,00	0,00	0,00	0,00	0,00	0,00	0,00	0,00	0,00	0,00	0,00	0,00
'Sic3_q'	0,00	0,00	0,00	0,00	0,00	0,00	0,00	0,00	0,00	0,00	0,00	0,00	0,00	0,00	0,00	0,00	0,00	0,00
'Sic3_d'	0,00	0,00	0,00	0,00	0,00	0,00	0,00	0,00	0,00	0,00	0,00	0,00	0,00	0,00	0,00	0,00	0,00	0,00
'Rmem3q'	1,00	1,00	0,26	0,26	0,07	0,07	0,94	0,94	0,30	0,30	0,08	0,08	0,00	0,00	0,00	0,00	0,00	0,00
'Rmem3d'	0,99	0,99	0,25	0,25	0,91	0,91	0,02	0,02	0,29	0,29	0,08	0,08	0,00	0,00	0,00	0,00	0,00	0,00
'SP '	0,00	0,00	0,00	0,00	0,00	0,00	0,00	0,00	0,00	0,00	0,00	0,00	0,00	0,00	0,00	0,00	0,00	0,00
'SQ '	0,00	0,00	0,00	0,00	0,01	0,01	0,00	0,00	0,00	0,00	0,00	0,00	0,00	0,00	0,00	0,00	0,00	0,00
'ic1_q'	0,31	0,31	0,08	0,08	0,10	0,10	0,97	0,97	1,00	1,00	0,26	0,26	0,00	0,00	0,00	0,00	0,00	0,00
'ic1_d'	0,30	0,30	0,08	0,08	0,97	0,97	0,05	0,05	0,99	0,99	0,25	0,25	0,01	0,01	0,00	0,00	0,00	0,00
'ic2_q'	0,00	0,00	0,32	0,32	0,10	0,10	1,00	1,00	0,00	0,00	1,00	1,00	0,00	0,00	0,00	0,00	0,00	0,00
'ic2_d'	0,00	0,00	0,31	0,31	1,00	1,00	0,05	0,05	0,00	0,00	0,99	0,99	0,01	0,01	0,00	0,00	0,00	0,00
'ic3_q'	0,31	0,31	0,08	0,08	0,10	0,10	0,97	0,97	1,00	1,00	0,26	0,26	0,00	0,00	0,00	0,00	0,00	0,00
'ic3_d'	0,30	0,30	0,08	0,08	0,97	0,97	0,05	0,05	0,99	0,99	0,25	0,25	0,01	0,01	0,00	0,00	0,00	0,00

Figure 5.16 Participation factor study results for SCR=20.

Figure 5.17 shows the internal oscillations and participation factor computation results for an SCR of 10:

SCR=10	M1	M2	M3	M4	M5	M6	M7	M8	M9	M10	M11	M12	M13	M14	M15	M16	M17	M18
'f (Hz)'	72,465	72,465	72,695	72,695	305,864	305,864	198,636	198,636	22,673	22,673	23,052	23,052	12,399	12,399	12,708	12,708	12,707	12,707
'damp'	0,998	0,998	0,998	0,998	0,342	0,342	0,810	0,810	0,998	0,998	0,998	0,998	0,756	0,756	0,731	0,731	0,731	0,731
'Suc1_d '	0,00	0,00	0,00	0,00	0,00	0,00	0,00	0,00	0,00	0,00	0,00	0,00	0,97	0,97	1,00	1,00	0,26	0,26
'e_theta'	0,00	0,00	0,00	0,00	0,03	0,03	0,00	0,00	0,00	0,00	0,00	0,00	0,96	0,96	1,00	1,00	0,26	0,26
'SPinv1'	0,00	0,00	0,00	0,00	0,00	0,00	0,00	0,00	0,00	0,00	0,00	0,00	0,00	0,00	0,00	0,00	0,00	0,00
'SPc1 '	0,00	0,00	0,00	0,00	0,00	0,00	0,02	0,02	0,03	0,03	0,01	0,01	0,04	0,04	0,00	0,00	0,00	0,00
'SQinv1'	0,00	0,00	0,00	0,00	0,00	0,00	0,00	0,00	0,00	0,00	0,00	0,00	0,00	0,00	0,00	0,00	0,00	0,00
'SQc1 '	0,00	0,00	0,00	0,00	0,05	0,05	0,00	0,00	0,03	0,03	0,01	0,01	0,02	0,02	0,00	0,00	0,00	0,00
'Sic1_q_ref'	0,00	0,00	0,00	0,00	0,00	0,00	0,00	0,00	0,00	0,00	0,00	0,00	0,00	0,00	0,00	0,00	0,00	0,00
'Sic1_d_ref'	0,00	0,00	0,00	0,00	0,01	0,01	0,00	0,00	0,00	0,00	0,00	0,00	0,00	0,00	0,00	0,00	0,00	0,00
'Sic1_q'	0,00	0,00	0,00	0,00	0,00	0,00	0,00	0,00	0,00	0,00	0,00	0,00	0,01	0,01	0,00	0,00	0,00	0,00
'Sic1_d'	0,00	0,00	0,00	0,00	0,00	0,00	0,00	0,00	0,00	0,00	0,00	0,00	0,00	0,00	0,00	0,00	0,00	0,00
'Rmem1q'	1,00	1,00	0,25	0,25	0,04	0,04	0,99	0,99	0,31	0,31	0,08	0,08	0,00	0,00	0,00	0,00	0,00	0,00
'Rmem1d'	0,99	0,99	0,25	0,25	0,90	0,90	0,01	0,01	0,30	0,30	0,08	0,08	0,00	0,00	0,00	0,00	0,00	0,00
'Suc2_d '	0,00	0,00	0,00	0,00	0,00	0,00	0,00	0,00	0,00	0,00	0,00	0,00	1,00	1,00	0,00	0,00	1,00	1,00
'e_theta2'	0,00	0,00	0,00	0,00	0,03	0,03	0,00	0,00	0,00	0,00	0,00	0,00	0,98	0,98	0,00	0,00	1,00	1,00
'SPinv2'	0,00	0,00	0,00	0,00	0,00	0,00	0,00	0,00	0,00	0,00	0,00	0,00	0,00	0,00	0,00	0,00	0,00	0,00
'SPc2 '	0,00	0,00	0,00	0,00	0,00	0,00	0,02	0,02	0,00	0,00	0,03	0,03	0,04	0,04	0,00	0,00	0,00	0,00
'SQinv2'	0,00	0,00	0,00	0,00	0,00	0,00	0,00	0,00	0,00	0,00	0,00	0,00	0,00	0,00	0,00	0,00	0,00	0,00
'SQc2 '	0,00	0,00	0,00	0,00	0,05	0,05	0,00	0,00	0,00	0,00	0,03	0,03	0,02	0,02	0,00	0,00	0,00	0,00
'Sic2_q_ref'	0,00	0,00	0,00	0,00	0,00	0,00	0,00	0,00	0,00	0,00	0,00	0,00	0,00	0,00	0,00	0,00	0,00	0,00
'Sic2_d_ref'	0,00	0,00	0,00	0,00	0,01	0,01	0,00	0,00	0,00	0,00	0,00	0,00	0,00	0,00	0,00	0,00	0,00	0,00
'Sic2_q'	0,00	0,00	0,00	0,00	0,00	0,00	0,00	0,00	0,00	0,00	0,00	0,00	0,01	0,01	0,00	0,00	0,00	0,00
'Sic2_d'	0,00	0,00	0,00	0,00	0,00	0,00	0,00	0,00	0,00	0,00	0,00	0,00	0,00	0,00	0,00	0,00	0,00	0,00
'Rmem2q'	0,00	0,00	1,00	1,00	0,04	0,04	0,99	0,99	0,00	0,00	0,31	0,31	0,00	0,00	0,00	0,00	0,00	0,00
'Rmem2d'	0,00	0,00	0,99	0,99	0,90	0,90	0,01	0,01	0,00	0,00	0,31	0,31	0,00	0,00	0,00	0,00	0,00	0,00
'Suc3_d '	0,00	0,00	0,00	0,00	0,00	0,00	0,00	0,00	0,00	0,00	0,00	0,00	0,97	0,97	1,00	1,00	0,26	0,26
'e_theta3'	0,00	0,00	0,00	0,00	0,03	0,03	0,00	0,00	0,00	0,00	0,00	0,00	0,96	0,96	1,00	1,00	0,26	0,26
'SPinv3'	0,00	0,00	0,00	0,00	0,00	0,00	0,00	0,00	0,00	0,00	0,00	0,00	0,00	0,00	0,00	0,00	0,00	0,00
'SPc3 '	0,00	0,00	0,00	0,00	0,00	0,00	0,02	0,02	0,03	0,03	0,01	0,01	0,04	0,04	0,00	0,00	0,00	0,00
'SQinv3'	0,00	0,00	0,00	0,00	0,00	0,00	0,00	0,00	0,00	0,00	0,00	0,00	0,00	0,00	0,00	0,00	0,00	0,00
'SQc3 '	0,00	0,00	0,00	0,00	0,05	0,05	0,00	0,00	0,03	0,03	0,01	0,01	0,02	0,02	0,00	0,00	0,00	0,00
'Sic3_q_ref'	0,00	0,00	0,00	0,00	0,00	0,00	0,00	0,00	0,00	0,00	0,00	0,00	0,00	0,00	0,00	0,00	0,00	0,00
'Sic3_d_ref'	0,00	0,00	0,00	0,00	0,01	0,01	0,00	0,00	0,00	0,00	0,00	0,00	0,00	0,00	0,00	0,00	0,00	0,00
'Sic3_q'	0,00	0,00	0,00	0,00	0,00	0,00	0,00	0,00	0,00	0,00	0,00	0,00	0,01	0,01	0,00	0,00	0,00	0,00
'Sic3_d'	0,00	0,00	0,00	0,00	0,00	0,00	0,00	0,00	0,00	0,00	0,00	0,00	0,00	0,00	0,00	0,00	0,00	0,00
'Rmem3q'	1,00	1,00	0,25	0,25	0,04	0,04	0,99	0,99	0,31	0,31	0,08	0,08	0,00	0,00	0,00	0,00	0,00	0,00
'Rmem3d'	0,99	0,99	0,25	0,25	0,90	0,90	0,01	0,01	0,30	0,30	0,08	0,08	0,00	0,00	0,00	0,00	0,00	0,00
'SP '	0,00	0,00	0,00	0,00	0,00	0,00	0,00	0,00	0,00	0,00	0,00	0,00	0,01	0,01	0,00	0,00	0,00	0,00
'SQ '	0,00	0,00	0,00	0,00	0,01	0,01	0,00	0,00	0,00	0,00	0,00	0,00	0,00	0,00	0,00	0,00	0,00	0,00
'ic1_q'	0,32	0,32	0,08	0,08	0,05	0,05	0,99	0,99	1,00	1,00	0,25	0,25	0,01	0,01	0,00	0,00	0,00	0,00
'ic1_d'	0,31	0,31	0,08	0,08	0,99	0,99	0,02	0,02	0,99	0,99	0,25	0,25	0,03	0,03	0,00	0,00	0,00	0,00
'ic2_q'	0,00	0,00	0,33	0,33	0,05	0,05	1,00	1,00	0,00	0,00	1,00	1,00	0,01	0,01	0,00	0,00	0,00	0,00
'ic2_d'	0,00	0,00	0,32	0,32	1,00	1,00	0,02	0,02	0,00	0,00	0,99	0,99	0,03	0,03	0,00	0,00	0,00	0,00
'ic3_q'	0,32	0,32	0,08	0,08	0,05	0,05	0,99	0,99	1,00	1,00	0,25	0,25	0,01	0,01	0,00	0,00	0,00	0,00
'ic3_d'	0,31	0,31	0,08	0,08	0,99	0,99	0,02	0,02	0,99	0,99	0,25	0,25	0,03	0,03	0,00	0,00	0,00	0,00

Figure 5.17 Participation factor study results for SCR=10.

Figure 5.18 shows the internal oscillations and participation factor computation results for an SCR of 5:

SCR=5	M1	M2	M3	M4	M5	M6	M7	M8	M9	M10	M11	M12	M13	M14	M15	M16	M17	M18
'f (Hz)'	72,465	72,465	72,695	72,695	305,864	305,864	198,636	198,636	22,673	22,673	23,052	23,052	12,399	12,399	12,708	12,708	12,707	12,707
'damp'	0,998	0,998	0,998	0,998	0,342	0,342	0,810	0,810	0,998	0,998	0,998	0,998	0,756	0,756	0,731	0,731	0,731	0,731
'Suc1_d '	0,00	0,00	0,00	0,00	0,00	0,00	0,00	0,00	0,00	0,00	0,00	0,00	0,97	0,97	1,00	1,00	0,26	0,26
'e_theta'	0,00	0,00	0,00	0,00	0,03	0,03	0,00	0,00	0,00	0,00	0,00	0,00	0,96	0,96	1,00	1,00	0,26	0,26
'SPinv1'	0,00	0,00	0,00	0,00	0,00	0,00	0,00	0,00	0,00	0,00	0,00	0,00	0,00	0,00	0,00	0,00	0,00	0,00
'SPc1 '	0,00	0,00	0,00	0,00	0,00	0,00	0,02	0,02	0,03	0,03	0,01	0,01	0,04	0,04	0,00	0,00	0,00	0,00
'SQinv1'	0,00	0,00	0,00	0,00	0,00	0,00	0,00	0,00	0,00	0,00	0,00	0,00	0,00	0,00	0,00	0,00	0,00	0,00
'SQc1 '	0,00	0,00	0,00	0,00	0,05	0,05	0,00	0,00	0,03	0,03	0,01	0,01	0,02	0,02	0,00	0,00	0,00	0,00
'Sic1_q_ref'	0,00	0,00	0,00	0,00	0,00	0,00	0,00	0,00	0,00	0,00	0,00	0,00	0,00	0,00	0,00	0,00	0,00	0,00
'Sic1_d_ref'	0,00	0,00	0,00	0,00	0,01	0,01	0,00	0,00	0,00	0,00	0,00	0,00	0,00	0,00	0,00	0,00	0,00	0,00
'Sic1_q'	0,00	0,00	0,00	0,00	0,00	0,00	0,00	0,00	0,00	0,00	0,00	0,00	0,01	0,01	0,00	0,00	0,00	0,00
'Sic1_d'	0,00	0,00	0,00	0,00	0,00	0,00	0,00	0,00	0,00	0,00	0,00	0,00	0,00	0,00	0,00	0,00	0,00	0,00
'Rmem1q'	1,00	1,00	0,25	0,25	0,04	0,04	0,99	0,99	0,31	0,31	0,08	0,08	0,00	0,00	0,00	0,00	0,00	0,00
'Rmem1d'	0,99	0,99	0,25	0,25	0,90	0,90	0,01	0,01	0,30	0,30	0,08	0,08	0,00	0,00	0,00	0,00	0,00	0,00
'Suc2_d '	0,00	0,00	0,00	0,00	0,00	0,00	0,00	0,00	0,00	0,00	0,00	0,00	1,00	1,00	0,00	0,00	1,00	1,00
'e_theta2'	0,00	0,00	0,00	0,00	0,03	0,03	0,00	0,00	0,00	0,00	0,00	0,00	0,98	0,98	0,00	0,00	1,00	1,00
'SPinv2'	0,00	0,00	0,00	0,00	0,00	0,00	0,00	0,00	0,00	0,00	0,00	0,00	0,00	0,00	0,00	0,00	0,00	0,00
'SPc2 '	0,00	0,00	0,00	0,00	0,00	0,00	0,02	0,02	0,00	0,00	0,03	0,03	0,04	0,04	0,00	0,00	0,00	0,00
'SQinv2'	0,00	0,00	0,00	0,00	0,00	0,00	0,00	0,00	0,00	0,00	0,00	0,00	0,00	0,00	0,00	0,00	0,00	0,00
'SQc2 '	0,00	0,00	0,00	0,00	0,05	0,05	0,00	0,00	0,00	0,00	0,03	0,03	0,02	0,02	0,00	0,00	0,00	0,00
'Sic2_q_ref'	0,00	0,00	0,00	0,00	0,00	0,00	0,00	0,00	0,00	0,00	0,00	0,00	0,00	0,00	0,00	0,00	0,00	0,00
'Sic2_d_ref'	0,00	0,00	0,00	0,00	0,01	0,01	0,00	0,00	0,00	0,00	0,00	0,00	0,00	0,00	0,00	0,00	0,00	0,00
'Sic2_q'	0,00	0,00	0,00	0,00	0,00	0,00	0,00	0,00	0,00	0,00	0,00	0,00	0,01	0,01	0,00	0,00	0,00	0,00
'Sic2_d'	0,00	0,00	0,00	0,00	0,00	0,00	0,00	0,00	0,00	0,00	0,00	0,00	0,00	0,00	0,00	0,00	0,00	0,00
'Rmem2q'	0,00	0,00	1,00	1,00	0,04	0,04	0,99	0,99	0,00	0,00	0,31	0,31	0,00	0,00	0,00	0,00	0,00	0,00
'Rmem2d'	0,00	0,00	0,99	0,99	0,90	0,90	0,01	0,01	0,00	0,00	0,31	0,31	0,00	0,00	0,00	0,00	0,00	0,00
'Suc3_d '	0,00	0,00	0,00	0,00	0,00	0,00	0,00	0,00	0,00	0,00	0,00	0,00	0,97	0,97	1,00	1,00	0,26	0,26
'e_theta3'	0,00	0,00	0,00	0,00	0,03	0,03	0,00	0,00	0,00	0,00	0,00	0,00	0,96	0,96	1,00	1,00	0,26	0,26
'SPinv3'	0,00	0,00	0,00	0,00	0,00	0,00	0,00	0,00	0,00	0,00	0,00	0,00	0,00	0,00	0,00	0,00	0,00	0,00
'SPc3 '	0,00	0,00	0,00	0,00	0,00	0,00	0,02	0,02	0,03	0,03	0,01	0,01	0,04	0,04	0,00	0,00	0,00	0,00
'SQinv3'	0,00	0,00	0,00	0,00	0,00	0,00	0,00	0,00	0,00	0,00	0,00	0,00	0,00	0,00	0,00	0,00	0,00	0,00
'SQc3 '	0,00	0,00	0,00	0,00	0,05	0,05	0,00	0,00	0,03	0,03	0,01	0,01	0,02	0,02	0,00	0,00	0,00	0,00
'Sic3_q_ref'	0,00	0,00	0,00	0,00	0,00	0,00	0,00	0,00	0,00	0,00	0,00	0,00	0,00	0,00	0,00	0,00	0,00	0,00
'Sic3_d_ref'	0,00	0,00	0,00	0,00	0,01	0,01	0,00	0,00	0,00	0,00	0,00	0,00	0,00	0,00	0,00	0,00	0,00	0,00
'Sic3_q'	0,00	0,00	0,00	0,00	0,00	0,00	0,00	0,00	0,00	0,00	0,00	0,00	0,01	0,01	0,00	0,00	0,00	0,00
'Sic3_d'	0,00	0,00	0,00	0,00	0,00	0,00	0,00	0,00	0,00	0,00	0,00	0,00	0,00	0,00	0,00	0,00	0,00	0,00
'Rmem3q'	1,00	1,00	0,25	0,25	0,04	0,04	0,99	0,99	0,31	0,31	0,08	0,08	0,00	0,00	0,00	0,00	0,00	0,00
'Rmem3d'	0,99	0,99	0,25	0,25	0,90	0,90	0,01	0,01	0,30	0,30	0,08	0,08	0,00	0,00	0,00	0,00	0,00	0,00
'SP '	0,00	0,00	0,00	0,00	0,00	0,00	0,00	0,00	0,00	0,00	0,00	0,00	0,01	0,01	0,00	0,00	0,00	0,00
'SQ '	0,00	0,00	0,00	0,00	0,01	0,01	0,00	0,00	0,00	0,00	0,00	0,00	0,00	0,00	0,00	0,00	0,00	0,00
'ic1_q'	0,32	0,32	0,08	0,08	0,05	0,05	0,99	0,99	1,00	1,00	0,25	0,25	0,01	0,01	0,00	0,00	0,00	0,00
'ic1_d'	0,31	0,31	0,08	0,08	0,99	0,99	0,02	0,02	0,99	0,99	0,25	0,25	0,03	0,03	0,00	0,00	0,00	0,00
'ic2_q'	0,00	0,00	0,33	0,33	0,05	0,05	1,00	1,00	0,00	0,00	1,00	1,00	0,01	0,01	0,00	0,00	0,00	0,00
'ic2_d'	0,00	0,00	0,32	0,32	1,00	1,00	0,02	0,02	0,00	0,00	0,99	0,99	0,03	0,03	0,00	0,00	0,00	0,00
'ic3_q'	0,32	0,32	0,08	0,08	0,05	0,05	0,99	0,99	1,00	1,00	0,25	0,25	0,01	0,01	0,00	0,00	0,00	0,00
'ic3_d'	0,31	0,31	0,08	0,08	0,99	0,99	0,02	0,02	0,99	0,99	0,25	0,25	0,03	0,03	0,00	0,00	0,00	0,00

Figure 5.18 Participation factor study results for SCR=5.

Figure 5.19 shows the internal oscillations and participation factor computation results for an SCR of 4:

SCR=4	M1	M2	M3	M4	M5	M6	M7	M8	M9	M10	M11	M12	M13	M14	M15	M16	M17	M18
'f (Hz)'	72,808	72,808	73,060	73,060	287,820	287,820	191,031	191,031	23,012	23,012	23,410	23,410	11,854	11,854	12,694	12,694	12,693	12,693
'damp'	0,998	0,998	0,998	0,998	0,258	0,258	0,791	0,791	0,998	0,998	0,998	0,998	0,788	0,788	0,735	0,735	0,735	0,735
'Suc1_d '	0,00	0,00	0,00	0,00	0,00	0,00	0,00	0,00	0,00	0,00	0,00	0,00	0,98	0,98	1,00	1,00	0,25	0,25
'e_theta'	0,00	0,00	0,00	0,00	0,04	0,04	0,00	0,00	0,00	0,00	0,00	0,00	0,94	0,94	1,00	1,00	0,25	0,25
'SPinv1'	0,00	0,00	0,00	0,00	0,00	0,00	0,00	0,00	0,00	0,00	0,00	0,00	0,00	0,00	0,00	0,00	0,00	0,00
'SPc1 '	0,00	0,00	0,00	0,00	0,00	0,00	0,02	0,02	0,03	0,03	0,01	0,01	0,07	0,07	0,00	0,00	0,00	0,00
'SQinv1'	0,00	0,00	0,00	0,00	0,00	0,00	0,00	0,00	0,00	0,00	0,00	0,00	0,00	0,00	0,00	0,00	0,00	0,00
'SQc1 '	0,00	0,00	0,00	0,00	0,05	0,05	0,00	0,00	0,03	0,03	0,01	0,01	0,02	0,02	0,00	0,00	0,00	0,00
'Sic1_q_ref'	0,00	0,00	0,00	0,00	0,00	0,00	0,00	0,00	0,00	0,00	0,00	0,00	0,01	0,01	0,00	0,00	0,00	0,00
'Sic1_d_ref'	0,00	0,00	0,00	0,00	0,01	0,01	0,00	0,00	0,00	0,00	0,00	0,00	0,00	0,00	0,00	0,00	0,00	0,00
'Sic1_q'	0,00	0,00	0,00	0,00	0,00	0,00	0,00	0,00	0,00	0,00	0,00	0,00	0,02	0,02	0,00	0,00	0,00	0,00
'Sic1_d'	0,00	0,00	0,00	0,00	0,00	0,00	0,00	0,00	0,00	0,00	0,00	0,00	0,00	0,00	0,00	0,00	0,00	0,00
'Rmem1q'	1,00	1,00	0,25	0,25	0,04	0,04	0,99	0,99	0,31	0,31	0,08	0,08	0,00	0,00	0,00	0,00	0,00	0,00
'Rmem1d'	0,99	0,99	0,25	0,25	0,89	0,89	0,01	0,01	0,31	0,31	0,08	0,08	0,00	0,00	0,00	0,00	0,00	0,00
'Suc2_d '	0,00	0,00	0,00	0,00	0,00	0,00	0,00	0,00	0,00	0,00	0,00	0,00	1,00	1,00	0,00	0,00	1,00	1,00
'e_theta2'	0,00	0,00	0,00	0,00	0,04	0,04	0,00	0,00	0,00	0,00	0,00	0,00	0,95	0,95	0,00	0,00	1,00	1,00
'SPinv2'	0,00	0,00	0,00	0,00	0,00	0,00	0,00	0,00	0,00	0,00	0,00	0,00	0,00	0,00	0,00	0,00	0,00	0,00
'SPc2 '	0,00	0,00	0,00	0,00	0,00	0,00	0,02	0,02	0,00	0,00	0,03	0,03	0,07	0,07	0,00	0,00	0,00	0,00
'SQinv2'	0,00	0,00	0,00	0,00	0,00	0,00	0,00	0,00	0,00	0,00	0,00	0,00	0,00	0,00	0,00	0,00	0,00	0,00
'SQc2 '	0,00	0,00	0,00	0,00	0,05	0,05	0,00	0,00	0,00	0,00	0,03	0,03	0,02	0,02	0,00	0,00	0,00	0,00
'Sic2_q_ref'	0,00	0,00	0,00	0,00	0,00	0,00	0,00	0,00	0,00	0,00	0,00	0,00	0,01	0,01	0,00	0,00	0,00	0,00
'Sic2_d_ref'	0,00	0,00	0,00	0,00	0,01	0,01	0,00	0,00	0,00	0,00	0,00	0,00	0,00	0,00	0,00	0,00	0,00	0,00
'Sic2_q'	0,00	0,00	0,00	0,00	0,00	0,00	0,00	0,00	0,00	0,00	0,00	0,00	0,02	0,02	0,00	0,00	0,00	0,00
'Sic2_d'	0,00	0,00	0,00	0,00	0,00	0,00	0,00	0,00	0,00	0,00	0,00	0,00	0,00	0,00	0,00	0,00	0,00	0,00
'Rmem2q'	0,00	0,00	1,00	1,00	0,04	0,04	1,00	1,00	0,00	0,00	0,32	0,32	0,00	0,00	0,00	0,00	0,00	0,00
'Rmem2d'	0,00	0,00	0,99	0,99	0,90	0,90	0,01	0,01	0,00	0,00	0,31	0,31	0,00	0,00	0,00	0,00	0,00	0,00
'Suc3_d '	0,00	0,00	0,00	0,00	0,00	0,00	0,00	0,00	0,00	0,00	0,00	0,00	0,98	0,98	1,00	1,00	0,25	0,25
'e_theta3'	0,00	0,00	0,00	0,00	0,04	0,04	0,00	0,00	0,00	0,00	0,00	0,00	0,94	0,94	1,00	1,00	0,25	0,25
'SPinv3'	0,00	0,00	0,00	0,00	0,00	0,00	0,00	0,00	0,00	0,00	0,00	0,00	0,00	0,00	0,00	0,00	0,00	0,00
'SPc3 '	0,00	0,00	0,00	0,00	0,00	0,00	0,02	0,02	0,03	0,03	0,01	0,01	0,07	0,07	0,00	0,00	0,00	0,00
'SQinv3'	0,00	0,00	0,00	0,00	0,00	0,00	0,00	0,00	0,00	0,00	0,00	0,00	0,00	0,00	0,00	0,00	0,00	0,00
'SQc3 '	0,00	0,00	0,00	0,00	0,05	0,05	0,00	0,00	0,03	0,03	0,01	0,01	0,02	0,02	0,00	0,00	0,00	0,00
'Sic3_q_ref'	0,00	0,00	0,00	0,00	0,00	0,00	0,00	0,00	0,00	0,00	0,00	0,00	0,01	0,01	0,00	0,00	0,00	0,00
'Sic3_d_ref'	0,00	0,00	0,00	0,00	0,01	0,01	0,00	0,00	0,00	0,00	0,00	0,00	0,00	0,00	0,00	0,00	0,00	0,00
'Sic3_q'	0,00	0,00	0,00	0,00	0,00	0,00	0,00	0,00	0,00	0,00	0,00	0,00	0,02	0,02	0,00	0,00	0,00	0,00
'Sic3_d'	0,00	0,00	0,00	0,00	0,00	0,00	0,00	0,00	0,00	0,00	0,00	0,00	0,00	0,00	0,00	0,00	0,00	0,00
'Rmem3q'	1,00	1,00	0,25	0,25	0,04	0,04	0,99	0,99	0,31	0,31	0,08	0,08	0,00	0,00	0,00	0,00	0,00	0,00
'Rmem3d'	0,99	0,99	0,25	0,25	0,89	0,89	0,01	0,01	0,31	0,31	0,08	0,08	0,00	0,00	0,00	0,00	0,00	0,00
'SP '	0,00	0,00	0,00	0,00	0,00	0,00	0,00	0,00	0,00	0,00	0,00	0,00	0,01	0,01	0,00	0,00	0,00	0,00
'SQ '	0,00	0,00	0,00	0,00	0,01	0,01	0,00	0,00	0,00	0,00	0,00	0,00	0,00	0,00	0,00	0,00	0,00	0,00
'ic1_q'	0,33	0,33	0,08	0,08	0,04	0,04	0,99	0,99	1,00	1,00	0,25	0,25	0,02	0,02	0,00	0,00	0,00	0,00
'ic1_d'	0,32	0,32	0,08	0,08	0,99	0,99	0,02	0,02	0,99	0,99	0,25	0,25	0,03	0,03	0,00	0,00	0,00	0,00
'ic2_q'	0,00	0,00	0,33	0,33	0,04	0,04	1,00	1,00	0,00	0,00	1,00	1,00	0,02	0,02	0,00	0,00	0,00	0,00
'ic2_d'	0,00	0,00	0,32	0,32	1,00	1,00	0,02	0,02	0,00	0,00	0,99	0,99	0,03	0,03	0,00	0,00	0,00	0,00
'ic3_q'	0,33	0,33	0,08	0,08	0,04	0,04	0,99	0,99	1,00	1,00	0,25	0,25	0,02	0,02	0,00	0,00	0,00	0,00
'ic3_d'	0,32	0,32	0,08	0,08	0,99	0,99	0,02	0,02	0,99	0,99	0,25	0,25	0,03	0,03	0,00	0,00	0,00	0,00

Figure 5.19 Participation factor study results for SCR=4.

Figure 5.20 shows the internal oscillations and participation factor computation results for an SCR of 3:

SCR=3	M1	M2	M3	M4	M5	M6	M7	M8	M9	M10	M11	M12	M13	M14	M15	M16	M17	M18
'f (Hz)'	73,308	73,308	73,592	73,592	261,359	261,359	177,048	177,048	23,507	23,507	23,932	23,932	10,410	10,410	12,667	12,667	12,670	12,670
'damp'	0,998	0,998	0,998	0,998	0,145	0,145	0,771	0,771	0,998	0,998	0,998	0,998	0,852	0,852	0,741	0,741	0,741	0,741
'Suc1_d '	0,00	0,00	0,00	0,00	0,00	0,00	0,00	0,00	0,00	0,00	0,00	0,00	0,99	0,99	0,25	0,25	1,00	1,00
'e_theta'	0,00	0,00	0,00	0,00	0,04	0,04	0,01	0,01	0,00	0,00	0,00	0,00	0,87	0,87	0,25	0,25	1,00	1,00
'SPinv1'	0,00	0,00	0,00	0,00	0,00	0,00	0,00	0,00	0,00	0,00	0,00	0,00	0,01	0,01	0,00	0,00	0,00	0,00
'SPc1 '	0,00	0,00	0,00	0,00	0,00	0,00	0,03	0,03	0,03	0,03	0,01	0,01	0,14	0,14	0,00	0,00	0,00	0,00
'SQinv1'	0,00	0,00	0,00	0,00	0,00	0,00	0,00	0,00	0,00	0,00	0,00	0,00	0,00	0,00	0,00	0,00	0,00	0,00
'SQc1 '	0,00	0,00	0,00	0,00	0,06	0,06	0,00	0,00	0,03	0,03	0,01	0,01	0,03	0,03	0,00	0,00	0,00	0,00
'Sic1_q_ref'	0,00	0,00	0,00	0,00	0,00	0,00	0,00	0,00	0,00	0,00	0,00	0,00	0,01	0,01	0,00	0,00	0,00	0,00
'Sic1_d_ref'	0,00	0,00	0,00	0,00	0,01	0,01	0,00	0,00	0,00	0,00	0,00	0,00	0,00	0,00	0,00	0,00	0,00	0,00
'Sic1_q'	0,00	0,00	0,00	0,00	0,00	0,00	0,00	0,00	0,00	0,00	0,00	0,00	0,03	0,03	0,00	0,00	0,00	0,00
'Sic1_d'	0,00	0,00	0,00	0,00	0,00	0,00	0,00	0,00	0,00	0,00	0,00	0,00	0,00	0,00	0,00	0,00	0,00	0,00
'Rmem1q'	1,00	1,00	0,25	0,25	0,04	0,04	1,00	1,00	0,32	0,32	0,08	0,08	0,00	0,00	0,00	0,00	0,00	0,00
'Rmem1d'	0,99	0,99	0,25	0,25	0,89	0,89	0,01	0,01	0,31	0,31	0,08	0,08	0,00	0,00	0,00	0,00	0,00	0,00
'Suc2_d '	0,00	0,00	0,00	0,00	0,00	0,00	0,00	0,00	0,00	0,00	0,00	0,00	1,00	1,00	1,00	1,00	0,00	0,00
'e_theta2'	0,00	0,00	0,00	0,00	0,04	0,04	0,01	0,01	0,00	0,00	0,00	0,00	0,88	0,88	1,00	1,00	0,00	0,00
'SPinv2'	0,00	0,00	0,00	0,00	0,00	0,00	0,00	0,00	0,00	0,00	0,00	0,00	0,01	0,01	0,00	0,00	0,00	0,00
'SPc2 '	0,00	0,00	0,00	0,00	0,00	0,00	0,03	0,03	0,00	0,00	0,03	0,03	0,14	0,14	0,00	0,00	0,00	0,00
'SQinv2'	0,00	0,00	0,00	0,00	0,00	0,00	0,00	0,00	0,00	0,00	0,00	0,00	0,00	0,00	0,00	0,00	0,00	0,00
'SQc2 '	0,00	0,00	0,00	0,00	0,06	0,06	0,00	0,00	0,00	0,00	0,03	0,03	0,03	0,03	0,00	0,00	0,00	0,00
'Sic2_q_ref'	0,00	0,00	0,00	0,00	0,00	0,00	0,00	0,00	0,00	0,00	0,00	0,00	0,01	0,01	0,00	0,00	0,00	0,00
'Sic2_d_ref'	0,00	0,00	0,00	0,00	0,01	0,01	0,00	0,00	0,00	0,00	0,00	0,00	0,00	0,00	0,00	0,00	0,00	0,00
'Sic2_q'	0,00	0,00	0,00	0,00	0,00	0,00	0,00	0,00	0,00	0,00	0,00	0,00	0,03	0,03	0,00	0,00	0,00	0,00
'Sic2_d'	0,00	0,00	0,00	0,00	0,00	0,00	0,00	0,00	0,00	0,00	0,00	0,00	0,00	0,00	0,00	0,00	0,00	0,00
'Rmem2q'	0,00	0,00	1,00	1,00	0,04	0,04	1,00	1,00	0,00	0,00	0,32	0,32	0,00	0,00	0,00	0,00	0,00	0,00
'Rmem2d'	0,00	0,00	0,99	0,99	0,90	0,90	0,01	0,01	0,00	0,00	0,31	0,31	0,00	0,00	0,00	0,00	0,00	0,00
'Suc3_d '	0,00	0,00	0,00	0,00	0,00	0,00	0,00	0,00	0,00	0,00	0,00	0,00	0,99	0,99	0,25	0,25	1,00	1,00
'e_theta3'	0,00	0,00	0,00	0,00	0,04	0,04	0,01	0,01	0,00	0,00	0,00	0,00	0,87	0,87	0,25	0,25	1,00	1,00
'SPinv3'	0,00	0,00	0,00	0,00	0,00	0,00	0,00	0,00	0,00	0,00	0,00	0,00	0,01	0,01	0,00	0,00	0,00	0,00
'SPc3 '	0,00	0,00	0,00	0,00	0,00	0,00	0,03	0,03	0,03	0,03	0,01	0,01	0,14	0,14	0,00	0,00	0,00	0,00
'SQinv3'	0,00	0,00	0,00	0,00	0,00	0,00	0,00	0,00	0,00	0,00	0,00	0,00	0,00	0,00	0,00	0,00	0,00	0,00
'SQc3 '	0,00	0,00	0,00	0,00	0,06	0,06	0,00	0,00	0,03	0,03	0,01	0,01	0,03	0,03	0,00	0,00	0,00	0,00
'Sic3_q_ref'	0,00	0,00	0,00	0,00	0,00	0,00	0,00	0,00	0,00	0,00	0,00	0,00	0,01	0,01	0,00	0,00	0,00	0,00
'Sic3_d_ref'	0,00	0,00	0,00	0,00	0,01	0,01	0,00	0,00	0,00	0,00	0,00	0,00	0,00	0,00	0,00	0,00	0,00	0,00
'Sic3_q'	0,00	0,00	0,00	0,00	0,00	0,00	0,00	0,00	0,00	0,00	0,00	0,00	0,03	0,03	0,00	0,00	0,00	0,00
'Sic3_d'	0,00	0,00	0,00	0,00	0,00	0,00	0,00	0,00	0,00	0,00	0,00	0,00	0,00	0,00	0,00	0,00	0,00	0,00
'Rmem3q'	1,00	1,00	0,25	0,25	0,04	0,04	1,00	1,00	0,32	0,32	0,08	0,08	0,00	0,00	0,00	0,00	0,00	0,00
'Rmem3d'	0,99	0,99	0,25	0,25	0,89	0,89	0,01	0,01	0,31	0,31	0,08	0,08	0,00	0,00	0,00	0,00	0,00	0,00
'SP '	0,00	0,00	0,00	0,00	0,00	0,00	0,01	0,01	0,00	0,00	0,00	0,00	0,02	0,02	0,00	0,00	0,00	0,00
'SQ '	0,00	0,00	0,00	0,00	0,01	0,01	0,00	0,00	0,00	0,00	0,00	0,00	0,00	0,00	0,00	0,00	0,00	0,00
'ic1_q'	0,33	0,33	0,08	0,08	0,03	0,03	0,99	0,99	1,00	1,00	0,25	0,25	0,04	0,04	0,00	0,00	0,00	0,00
'ic1_d'	0,32	0,32	0,08	0,08	1,00	1,00	0,03	0,03	0,99	0,99	0,25	0,25	0,02	0,02	0,00	0,00	0,00	0,00
'ic2_q'	0,00	0,00	0,33	0,33	0,03	0,03	0,99	0,99	0,00	0,00	1,00	1,00	0,04	0,04	0,00	0,00	0,00	0,00
'ic2_d'	0,00	0,00	0,32	0,32	1,00	1,00	0,03	0,03	0,00	0,00	0,99	0,99	0,01	0,01	0,00	0,00	0,00	0,00
'ic3_q'	0,33	0,33	0,08	0,08	0,03	0,03	0,99	0,99	1,00	1,00	0,25	0,25	0,04	0,04	0,00	0,00	0,00	0,00
'ic3_d'	0,32	0,32	0,08	0,08	1,00	1,00	0,03	0,03	0,99	0,99	0,25	0,25	0,02	0,02	0,00	0,00	0,00	0,00

Figure 5.20 Participation factor study results for SCR=3.

The most relevant participation factors have been highlighted in two different shades of red, where the darker red is used for those parameters which exceed the 0,85 participation threshold.

Regarding the internal oscillation modes obtained from the modal analysis, there are 5 main types of oscillations depending on the participating factors:

- Modes (M1-M4): The first four modes that can be seen in the participation factor computation are related to the delay that was introduced to the system enabling a correct initialisation of the model. The oscillation modes do not change significantly with the changes in the short circuit ratio of the AC grid. As a matter of fact, the dampening ratio of this oscillation is so high it barely compromises the operation of the system.

- Modes (M5-M8): These oscillation modes are associated to the interactions between the initialisation delay and the current loop variables (Modes 5 and 6 correspond to the q component and 7 and 8 to the d components). The dampening ratio of this modes greatly decreases with the grid's strength. Regarding the frequency of these oscillations, the frequency of the modes associated to the q component of the current loop variables decreases with the SCR (from 300 Hz to 260 Hz) while the d components remain more or less the same (195 Hz).

- Modes (M9-M12): These mode oscillations are essentially produced by the current loop control of the converters. The dampening ratio is higher than 0,95 for all the studied SCR values and the frequency remains around the 23 Hz mark.

- Modes (M13-M18): There are six modes that oscillate at an approximately 12 Hz frequency mainly caused by the interactions between the Phase-Locked Loops. In the first two, all 3 PLLs are involved with practically the same participation level. The dampening ratio of this oscillation increases slightly while the frequency decreases when the AC grid is weaker. Frequency modes 14 and 15 are mainly produced by the second converter's PLL and the last two are produced by the first and third PLLs. This is due to the fact that the length of the cable used to connect the second converter to the PCC is longer than the cables that connect the first and third converter. The last 4 oscillation modes do not vary greatly with the changes in the grid strength.

As can be deducted from the obtained results, variations in the SCR reduces the dampening ratio of the previously mentioned oscillation modes. The system becomes more oscillatory and less stable when the SCR decreases.

5.4.3 Time domain simulation comparing different SCR values

The effect that a weaker grid has on the internal oscillations of the model has been presented in the participation factor study in the previous section.

In this section, time domain simulations will be carried out on the non-linear model comparing different SCR value, validating the conclusions from the small signal analysis.

In Figure 5.21 and Figure 5.22 the simulation results for the active and reactive power measured at the PCC are shown:

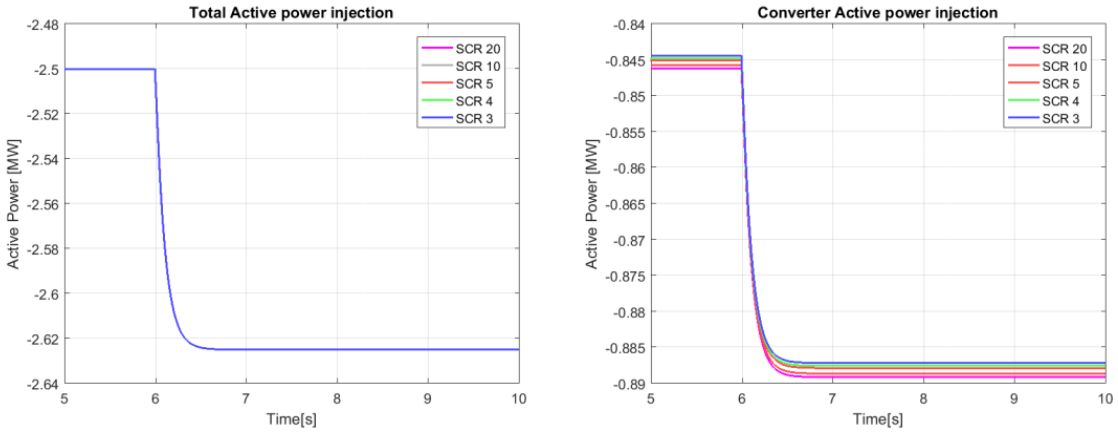

Figure 5.21 Time-domain results comparison for the PCC Active power for different SCRs.

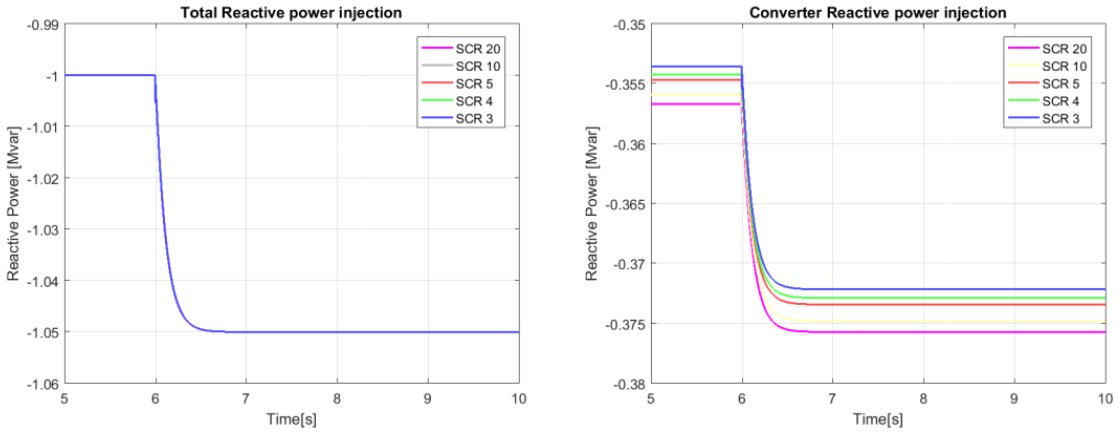

Figure 5.22 Time-domain results comparison for the PCC Reactive power for different SCRs.

As can be seen, the active and reactive power values measured at the PCC show that there are more oscillations for SCR=3 than for higher values. As can be seen, the Q measurement at the PCC shows more oscillations mainly due to the fact that the d component is much more relevant in the reactive power equation, and said voltage value is greatly affected by the PLL dynamics.

The following Figure 5.23 and Figure 5.24 compare the d and q voltage components of the voltage values at the PCC and at converter 1 for different SCR values.

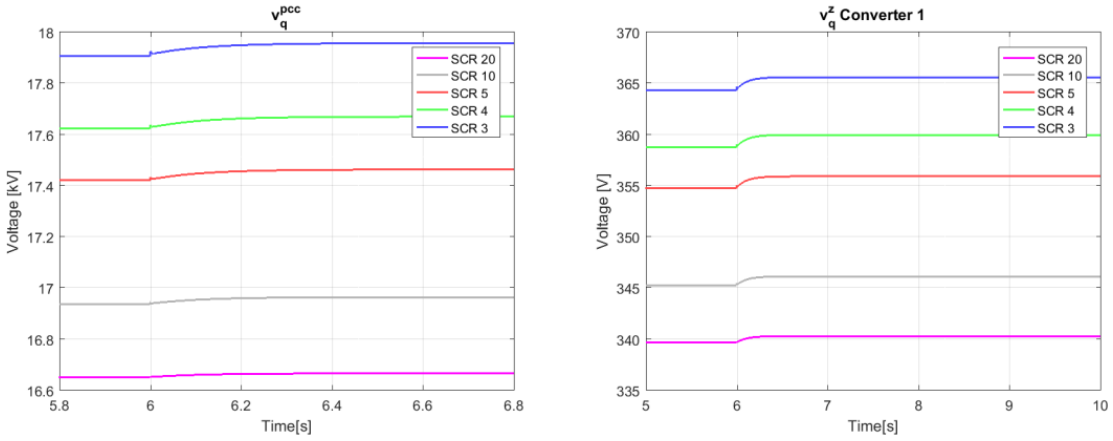

Figure 5.23 Time-domain results comparison for the q voltage components (PCC and grid-side impedance voltage) for different SCRs.

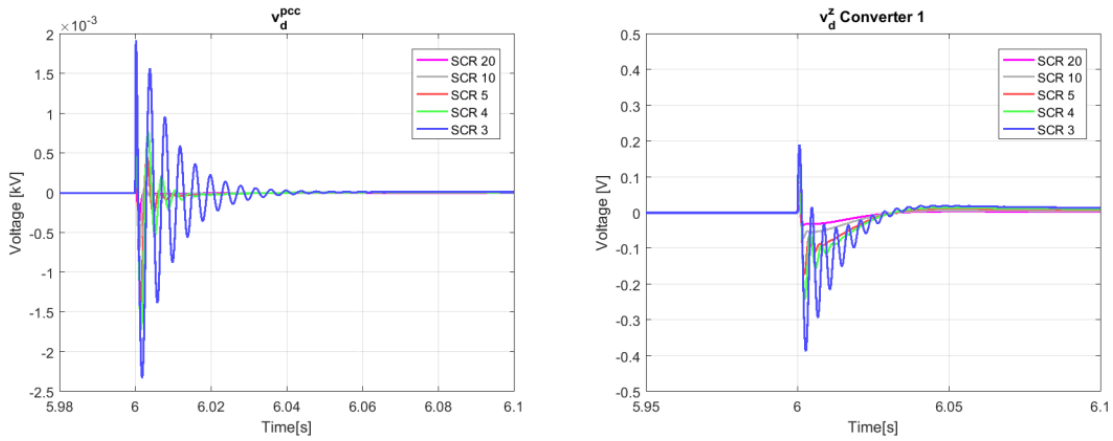

Figure 5.24 Time-domain results comparison for the d voltage components (PCC and grid-side impedance voltage) for different SCRs.

Regarding the q components, considering that changing the SCR value modifies the grid equivalent impedance, the voltage needed at the different points of the circuit must also change in proportion to enable correct power reference satisfaction. As can be seen, a lower SCR implies a higher grid impedance.

Regarding the d components of the voltage, considering that the four phase-locked loops (PLL) connected at different points of the circuit impose that the d component of the voltage must stay at the 0 value, all the PLL dynamics can be seen in the transient behaviour of this variable. Considering that the modal analysis showed that the interactions between the current loop and the initialisation block were more unstable when the SCR was lower, and the fact that the PLL angle estimation is used to transform the signal outputted by the delay block from converter reference to grid reference, the oscillations seen at the d component of the circuit are coherent with the obtained results from the small signal analysis.

The delay block oscillations seen in modes 5-8 of the participation factor study can be seen in the controllable AC voltage source input signals shown in the following Figure 5.25:

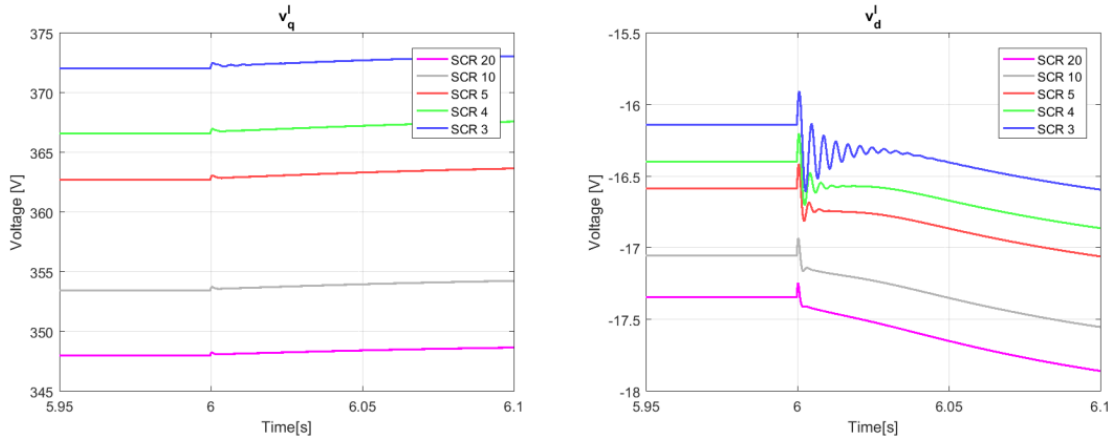

Figure 5.25 Time-domain results comparison for the d and q voltage components at converter 1 converter side for different SCRs.

As can be seen for the SCR=3 simulation, a high frequency oscillation occurs in the transient behaviour. In comparison to the other SCR simulations, the oscillation frequency is of a similar order of magnitude, but the stabilisation time is much higher due to the worse dampening ratio.

Finally, regarding the current flowing through the PCC and the converter branches, they can be seen in Figure 5.26 and Figure 5.27:

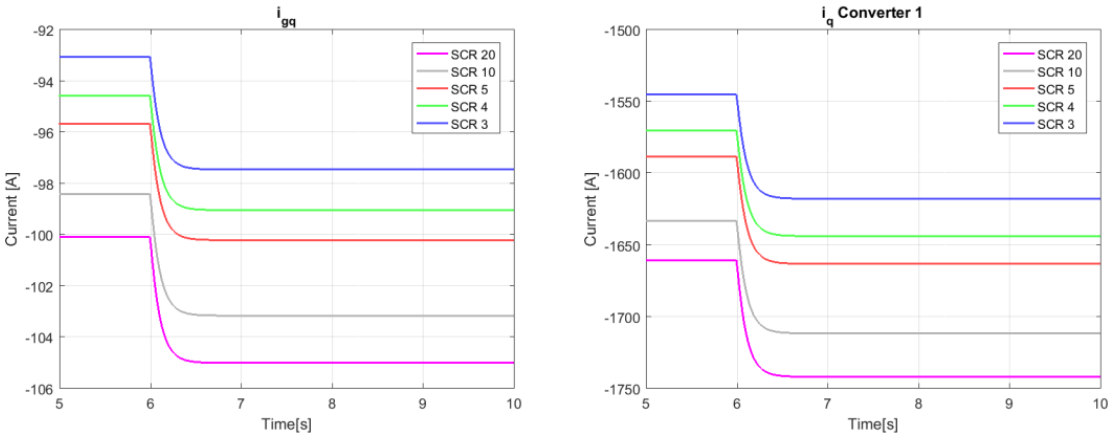

Figure 5.26 Time-domain results comparison for the q current components at the PCC and converter 1 impedance for different SCRs.

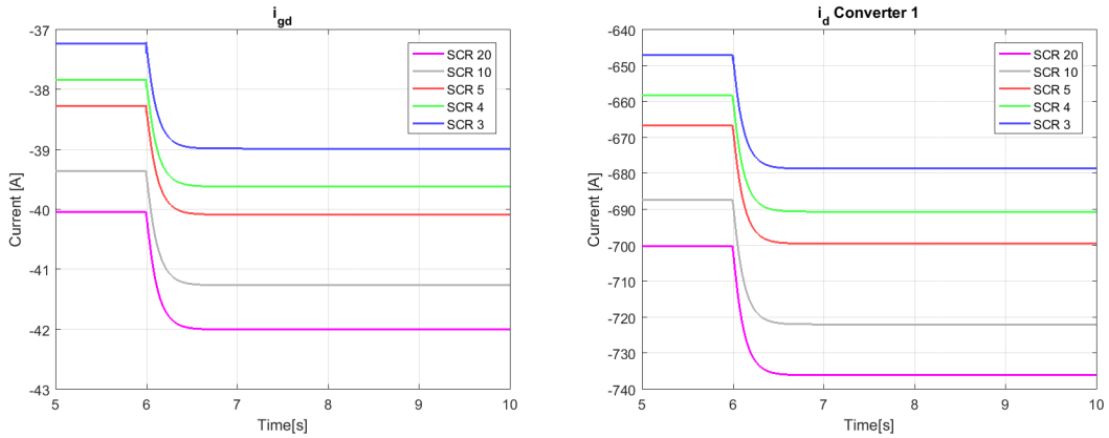

Figure 5.27 Time-domain results comparison for the d current components at the PCC and converter 1 impedance for different SCRs.

No big oscillations are observed in the current signals in either of the $qd0$ components. Considering that these signals are mainly used in the current loop and that the oscillations associated to it have very high dampening ratio, the obtained results seem coherent with the participation factor study.

5.5 Different Cable lengths

The effect of increasing inverter branch impedances can have on the dynamic behaviour of the system has been studied in this system. In this section the critical Eigen values of the system are plotted. Additionally, the results of the participation factor study are included showing the predominant oscillatory behaviour of the system as well as the internal states which participate in said oscillations. Finally, time domain simulations are used to compare the dynamic behaviour for different cable impedances for the most relevant variables.

5.5.1 Eigen Values

Upon increasing the cable impedance values for each of the converter branches, the system does not enter the unstable operation area as can be seen in Figure 5.28. The Eigen values of the system's A matrix have no positive real components for any of the studied cable lengths.

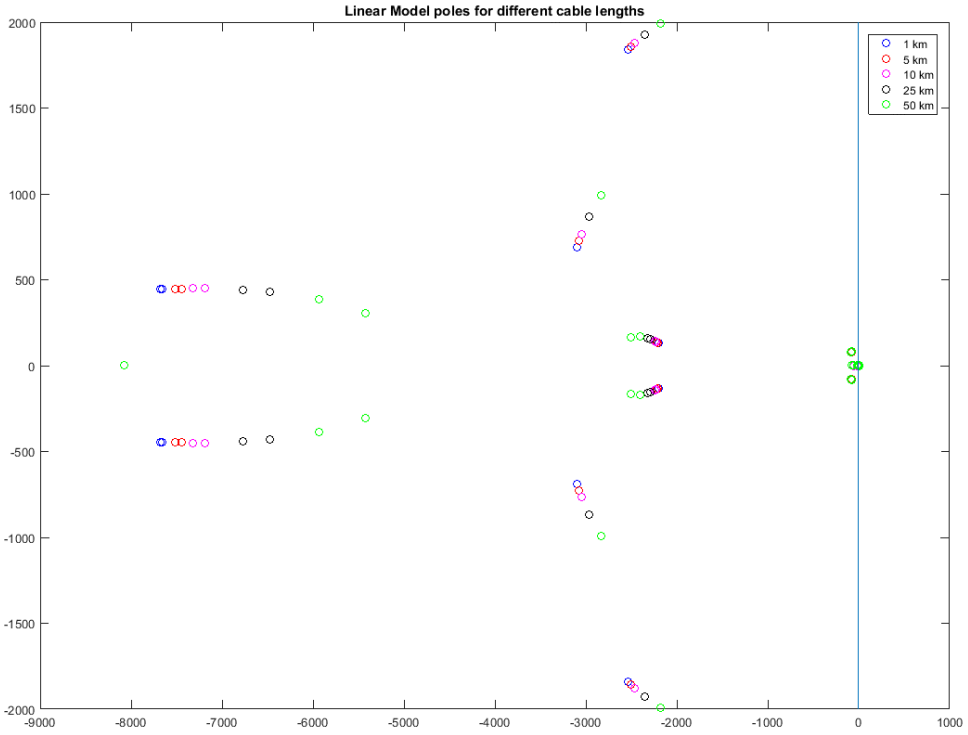

Figure 5.28 Eigenvalue plot for the different studied km values.

As can be seen, upon increasing the inverter branch impedances, the system's poles get closer to the stability limit, increasing the oscillatory behaviour of the system dynamics.

5.5.2 Participation factory analysis

The participation factor study has been performed for different cable lengths in the system. The objective of this study is to comprehend which oscillations are caused by increasing the grids internal impedances. The results of the participation factor studies for different cable lengths (50 km, 25 km, 10 km 5 km and 1 km) are presented in this section.

The results of the participation factor for 50 km cables can be seen in Figure 5.29:

Km=50	M1	M2	M3	M4	M5	M6	M7	M8	M9	M10	M11	M12	M13	M14	M15	M16	M17	M18
'f (Hz)'	61,688	61,688	48,806	48,806	316,801	316,801	158,075	158,075	26,606	26,606	27,004	27,004	12,949	12,949	12,791	12,791	12,811	12,811
'damp'	0,998	0,998	0,998	0,998	0,738	0,738	0,944	0,944	0,998	0,998	0,998	0,998	0,708	0,708	0,714	0,714	0,714	0,714
'Suc1_d '	0,00	0,00	0,00	0,00	0,00	0,00	0,00	0,00	0,00	0,00	0,00	0,00	0,98	0,98	1,00	1,00	0,24	0,24
'e_theta'	0,00	0,00	0,00	0,00	0,01	0,01	0,00	0,00	0,00	0,00	0,00	0,00	1,00	1,00	1,00	1,00	0,24	0,24
'SPinv1'	0,00	0,00	0,00	0,00	0,00	0,00	0,00	0,00	0,00	0,00	0,00	0,00	0,00	0,00	0,00	0,00	0,00	0,00
'SPc1 '	0,00	0,00	0,00	0,00	0,00	0,00	0,01	0,01	0,01	0,01	0,02	0,02	0,01	0,01	0,00	0,00	0,00	0,00
'SQinv1'	0,00	0,00	0,00	0,00	0,00	0,00	0,00	0,00	0,00	0,00	0,00	0,00	0,00	0,00	0,00	0,00	0,00	0,00
'SQc1 '	0,00	0,00	0,00	0,00	0,02	0,02	0,00	0,00	0,01	0,01	0,03	0,03	0,01	0,01	0,00	0,00	0,00	0,00
'Sic1_q_ref'	0,00	0,00	0,00	0,00	0,00	0,00	0,00	0,00	0,00	0,00	0,00	0,00	0,00	0,00	0,00	0,00	0,00	0,00
'Sic1_d_ref'	0,00	0,00	0,00	0,00	0,00	0,00	0,00	0,00	0,00	0,00	0,00	0,00	0,00	0,00	0,00	0,00	0,00	0,00
'Sic1_q'	0,00	0,00	0,00	0,00	0,00	0,00	0,00	0,00	0,00	0,00	0,00	0,00	0,00	0,00	0,00	0,00	0,00	0,00
'Sic1_d'	0,00	0,00	0,00	0,00	0,00	0,00	0,00	0,00	0,00	0,00	0,00	0,00	0,00	0,00	0,00	0,00	0,00	0,00
'Rmem1q'	1,00	1,00	0,33	0,33	0,04	0,04	0,75	0,75	0,15	0,15	0,41	0,41	0,00	0,00	0,00	0,00	0,00	0,00
'Rmem1d'	0,92	0,92	0,29	0,29	0,73	0,73	0,01	0,01	0,13	0,13	0,36	0,36	0,00	0,00	0,00	0,00	0,00	0,00
'Suc2_d '	0,00	0,00	0,00	0,00	0,00	0,00	0,00	0,00	0,00	0,00	0,00	0,00	0,94	0,94	0,00	0,00	0,99	0,99
'e_theta2'	0,00	0,00	0,00	0,00	0,01	0,01	0,00	0,00	0,00	0,00	0,00	0,00	0,96	0,96	0,00	0,00	1,00	1,00
'SPinv2'	0,00	0,00	0,00	0,00	0,00	0,00	0,00	0,00	0,00	0,00	0,00	0,00	0,00	0,00	0,00	0,00	0,00	0,00
'SPc2 '	0,00	0,00	0,00	0,00	0,00	0,00	0,01	0,01	0,02	0,02	0,00	0,00	0,01	0,01	0,00	0,00	0,00	0,00
'SQinv2'	0,00	0,00	0,00	0,00	0,00	0,00	0,00	0,00	0,00	0,00	0,00	0,00	0,00	0,00	0,00	0,00	0,00	0,00
'SQc2 '	0,00	0,00	0,01	0,01	0,03	0,03	0,00	0,00	0,03	0,03	0,00	0,00	0,01	0,01	0,00	0,00	0,00	0,00
'Sic2_q_ref'	0,00	0,00	0,00	0,00	0,00	0,00	0,00	0,00	0,00	0,00	0,00	0,00	0,00	0,00	0,00	0,00	0,00	0,00
'Sic2_d_ref'	0,00	0,00	0,00	0,00	0,00	0,00	0,00	0,00	0,00	0,00	0,00	0,00	0,00	0,00	0,00	0,00	0,00	0,00
'Sic2_q'	0,00	0,00	0,00	0,00	0,00	0,00	0,00	0,00	0,00	0,00	0,00	0,00	0,00	0,00	0,00	0,00	0,00	0,00
'Sic2_d'	0,00	0,00	0,00	0,00	0,00	0,00	0,00	0,00	0,00	0,00	0,00	0,00	0,00	0,00	0,00	0,00	0,00	0,00
'Rmem2q'	0,00	0,00	1,00	1,00	0,06	0,06	0,97	0,97	0,47	0,47	0,00	0,00	0,00	0,00	0,00	0,00	0,00	0,00
'Rmem2d'	0,00	0,00	0,90	0,90	0,93	0,93	0,01	0,01	0,40	0,40	0,00	0,00	0,00	0,00	0,00	0,00	0,00	0,00
'Suc3_d '	0,00	0,00	0,00	0,00	0,00	0,00	0,00	0,00	0,00	0,00	0,00	0,00	0,98	0,98	1,00	1,00	0,24	0,24
'e_theta3'	0,00	0,00	0,00	0,00	0,01	0,01	0,00	0,00	0,00	0,00	0,00	0,00	1,00	1,00	1,00	1,00	0,24	0,24
'SPinv3'	0,00	0,00	0,00	0,00	0,00	0,00	0,00	0,00	0,00	0,00	0,00	0,00	0,00	0,00	0,00	0,00	0,00	0,00
'SPc3 '	0,00	0,00	0,00	0,00	0,00	0,00	0,01	0,01	0,01	0,01	0,02	0,02	0,01	0,01	0,00	0,00	0,00	0,00
'SQinv3'	0,00	0,00	0,00	0,00	0,00	0,00	0,00	0,00	0,00	0,00	0,00	0,00	0,00	0,00	0,00	0,00	0,00	0,00
'SQc3 '	0,00	0,00	0,00	0,00	0,02	0,02	0,00	0,00	0,01	0,01	0,03	0,03	0,01	0,01	0,00	0,00	0,00	0,00
'Sic3_q_ref'	0,00	0,00	0,00	0,00	0,00	0,00	0,00	0,00	0,00	0,00	0,00	0,00	0,00	0,00	0,00	0,00	0,00	0,00
'Sic3_d_ref'	0,00	0,00	0,00	0,00	0,00	0,00	0,00	0,00	0,00	0,00	0,00	0,00	0,00	0,00	0,00	0,00	0,00	0,00
'Sic3_q'	0,00	0,00	0,00	0,00	0,00	0,00	0,00	0,00	0,00	0,00	0,00	0,00	0,00	0,00	0,00	0,00	0,00	0,00
'Sic3_d'	0,00	0,00	0,00	0,00	0,00	0,00	0,00	0,00	0,00	0,00	0,00	0,00	0,00	0,00	0,00	0,00	0,00	0,00
'Rmem3q'	1,00	1,00	0,33	0,33	0,04	0,04	0,75	0,75	0,15	0,15	0,41	0,41	0,00	0,00	0,00	0,00	0,00	0,00
'Rmem3d'	0,92	0,92	0,29	0,29	0,73	0,73	0,01	0,01	0,13	0,13	0,36	0,36	0,00	0,00	0,00	0,00	0,00	0,00
'SP '	0,00	0,00	0,00	0,00	0,00	0,00	0,00	0,00	0,00	0,00	0,00	0,00	0,00	0,00	0,00	0,00	0,00	0,00
'SQ '	0,00	0,00	0,00	0,00	0,00	0,00	0,00	0,00	0,00	0,00	0,00	0,00	0,00	0,00	0,00	0,00	0,00	0,00
'ic1_q'	0,45	0,45	0,17	0,17	0,06	0,06	0,78	0,78	0,33	0,33	1,00	1,00	0,00	0,00	0,00	0,00	0,00	0,00
'ic1_d'	0,37	0,37	0,13	0,13	0,79	0,79	0,03	0,03	0,30	0,30	0,95	0,95	0,01	0,01	0,00	0,00	0,00	0,00
'ic2_q'	0,00	0,00	0,52	0,52	0,08	0,08	1,00	1,00	1,00	1,00	0,00	0,00	0,00	0,00	0,00	0,00	0,00	0,00
'ic2_d'	0,00	0,00	0,41	0,41	1,00	1,00	0,03	0,03	0,94	0,94	0,00	0,00	0,02	0,02	0,00	0,00	0,00	0,00
'ic3_q'	0,45	0,45	0,17	0,17	0,06	0,06	0,78	0,78	0,33	0,33	1,00	1,00	0,00	0,00	0,00	0,00	0,00	0,00
'ic3_d'	0,37	0,37	0,13	0,13	0,79	0,79	0,03	0,03	0,30	0,30	0,95	0,95	0,01	0,01	0,00	0,00	0,00	0,00

Figure 5.29 Participation factor study results for 50 km cable length.

The results of the participation factor for 25 km cables can be seen in Figure 5.30:

Km=25	M1	M2	M3	M4	M5	M6	M7	M8	M9	M10	M11	M12	M13	M14	M15	M16	M17	M18
'f (Hz)'	70,458	70,458	68,617	68,617	307,043	307,043	138,281	138,281	24,565	24,565	25,622	25,622	12,927	12,927	12,764	12,764	12,773	12,773
'damp'	0,998	0,998	0,998	0,998	0,773	0,773	0,960	0,960	0,998	0,998	0,998	0,998	0,707	0,707	0,714	0,714	0,714	0,714
'Suc1_d '	0,00	0,00	0,00	0,00	0,00	0,00	0,00	0,00	0,00	0,00	0,00	0,00	0,98	0,98	1,00	1,00	0,25	0,25
'e_theta'	0,00	0,00	0,00	0,00	0,01	0,01	0,00	0,00	0,00	0,00	0,00	0,00	1,00	1,00	1,00	1,00	0,25	0,25
'SPinv1'	0,00	0,00	0,00	0,00	0,00	0,00	0,00	0,00	0,00	0,00	0,00	0,00	0,00	0,00	0,00	0,00	0,00	0,00
'SPc1 '	0,00	0,00	0,00	0,00	0,00	0,00	0,01	0,01	0,02	0,02	0,01	0,01	0,01	0,01	0,00	0,00	0,00	0,00
'SQinv1'	0,00	0,00	0,00	0,00	0,00	0,00	0,00	0,00	0,00	0,00	0,00	0,00	0,00	0,00	0,00	0,00	0,00	0,00
'SQc1 '	0,00	0,00	0,00	0,00	0,02	0,02	0,00	0,00	0,03	0,03	0,01	0,01	0,01	0,01	0,00	0,00	0,00	0,00
'Sic1_q_ref'	0,00	0,00	0,00	0,00	0,00	0,00	0,00	0,00	0,00	0,00	0,00	0,00	0,00	0,00	0,00	0,00	0,00	0,00
'Sic1_d_ref'	0,00	0,00	0,00	0,00	0,00	0,00	0,00	0,00	0,00	0,00	0,00	0,00	0,00	0,00	0,00	0,00	0,00	0,00
'Sic1_q'	0,00	0,00	0,00	0,00	0,00	0,00	0,00	0,00	0,00	0,00	0,00	0,00	0,00	0,00	0,00	0,00	0,00	0,00
'Sic1_d'	0,00	0,00	0,00	0,00	0,00	0,00	0,00	0,00	0,00	0,00	0,00	0,00	0,00	0,00	0,00	0,00	0,00	0,00
'Rmem1q'	1,00	1,00	0,29	0,29	0,06	0,06	0,85	0,85	0,35	0,35	0,10	0,10	0,00	0,00	0,00	0,00	0,00	0,00
'Rmem1d'	0,96	0,96	0,27	0,27	0,82	0,82	0,02	0,02	0,32	0,32	0,09	0,09	0,00	0,00	0,00	0,00	0,00	0,00
'Suc2_d '	0,00	0,00	0,00	0,00	0,00	0,00	0,00	0,00	0,00	0,00	0,00	0,00	0,99	0,99	0,00	0,00	1,00	1,00
'e_theta2'	0,00	0,00	0,00	0,00	0,01	0,01	0,00	0,00	0,00	0,00	0,00	0,00	1,00	1,00	0,00	0,00	1,00	1,00
'SPinv2'	0,00	0,00	0,00	0,00	0,00	0,00	0,00	0,00	0,00	0,00	0,00	0,00	0,00	0,00	0,00	0,00	0,00	0,00
'SPc2 '	0,00	0,00	0,00	0,00	0,00	0,00	0,01	0,01	0,00	0,00	0,02	0,02	0,01	0,01	0,00	0,00	0,00	0,00
'SQinv2'	0,00	0,00	0,00	0,00	0,00	0,00	0,00	0,00	0,00	0,00	0,00	0,00	0,00	0,00	0,00	0,00	0,00	0,00
'SQc2 '	0,00	0,00	0,00	0,00	0,03	0,03	0,00	0,00	0,00	0,00	0,03	0,03	0,01	0,01	0,00	0,00	0,00	0,00
'Sic2_q_ref'	0,00	0,00	0,00	0,00	0,00	0,00	0,00	0,00	0,00	0,00	0,00	0,00	0,00	0,00	0,00	0,00	0,00	0,00
'Sic2_d_ref'	0,00	0,00	0,00	0,00	0,00	0,00	0,00	0,00	0,00	0,00	0,00	0,00	0,00	0,00	0,00	0,00	0,00	0,00
'Sic2_q'	0,00	0,00	0,00	0,00	0,00	0,00	0,00	0,00	0,00	0,00	0,00	0,00	0,00	0,00	0,00	0,00	0,00	0,00
'Sic2_d'	0,00	0,00	0,00	0,00	0,00	0,00	0,00	0,00	0,00	0,00	0,00	0,00	0,00	0,00	0,00	0,00	0,00	0,00
'Rmem2q'	0,00	0,00	1,00	1,00	0,06	0,06	0,97	0,97	0,00	0,00	0,37	0,37	0,00	0,00	0,00	0,00	0,00	0,00
'Rmem2d'	0,00	0,00	0,95	0,95	0,93	0,93	0,02	0,02	0,00	0,00	0,33	0,33	0,00	0,00	0,00	0,00	0,00	0,00
'Suc3_d '	0,00	0,00	0,00	0,00	0,00	0,00	0,00	0,00	0,00	0,00	0,00	0,00	0,98	0,98	1,00	1,00	0,25	0,25
'e_theta3'	0,00	0,00	0,00	0,00	0,01	0,01	0,00	0,00	0,00	0,00	0,00	0,00	1,00	1,00	1,00	1,00	0,25	0,25
'SPinv3'	0,00	0,00	0,00	0,00	0,00	0,00	0,00	0,00	0,00	0,00	0,00	0,00	0,00	0,00	0,00	0,00	0,00	0,00
'SPc3 '	0,00	0,00	0,00	0,00	0,00	0,00	0,01	0,01	0,02	0,02	0,01	0,01	0,01	0,01	0,00	0,00	0,00	0,00
'SQinv3'	0,00	0,00	0,00	0,00	0,00	0,00	0,00	0,00	0,00	0,00	0,00	0,00	0,00	0,00	0,00	0,00	0,00	0,00
'SQc3 '	0,00	0,00	0,00	0,00	0,02	0,02	0,00	0,00	0,03	0,03	0,01	0,01	0,01	0,01	0,00	0,00	0,00	0,00
'Sic3_q_ref'	0,00	0,00	0,00	0,00	0,00	0,00	0,00	0,00	0,00	0,00	0,00	0,00	0,00	0,00	0,00	0,00	0,00	0,00
'Sic3_d_ref'	0,00	0,00	0,00	0,00	0,00	0,00	0,00	0,00	0,00	0,00	0,00	0,00	0,00	0,00	0,00	0,00	0,00	0,00
'Sic3_q'	0,00	0,00	0,00	0,00	0,00	0,00	0,00	0,00	0,00	0,00	0,00	0,00	0,00	0,00	0,00	0,00	0,00	0,00
'Sic3_d'	0,00	0,00	0,00	0,00	0,00	0,00	0,00	0,00	0,00	0,00	0,00	0,00	0,00	0,00	0,00	0,00	0,00	0,00
'Rmem3q'	1,00	1,00	0,29	0,29	0,06	0,06	0,85	0,85	0,35	0,35	0,10	0,10	0,00	0,00	0,00	0,00	0,00	0,00
'Rmem3d'	0,96	0,96	0,27	0,27	0,82	0,82	0,02	0,02	0,32	0,32	0,09	0,09	0,00	0,00	0,00	0,00	0,00	0,00
'SP '	0,00	0,00	0,00	0,00	0,00	0,00	0,00	0,00	0,00	0,00	0,00	0,00	0,00	0,00	0,00	0,00	0,00	0,00
'SQ '	0,00	0,00	0,00	0,00	0,01	0,01	0,00	0,00	0,00	0,00	0,00	0,00	0,00	0,00	0,00	0,00	0,00	0,00
'ic1_q'	0,37	0,37	0,11	0,11	0,08	0,08	0,88	0,88	1,00	1,00	0,28	0,28	0,00	0,00	0,00	0,00	0,00	0,00
'ic1_d'	0,33	0,33	0,10	0,10	0,89	0,89	0,04	0,04	0,98	0,98	0,27	0,27	0,01	0,01	0,00	0,00	0,00	0,00
'ic2_q'	0,00	0,00	0,39	0,39	0,09	0,09	1,00	1,00	0,00	0,00	1,00	1,00	0,00	0,00	0,00	0,00	0,00	0,00
'ic2_d'	0,00	0,00	0,34	0,34	1,00	1,00	0,04	0,04	0,00	0,00	0,97	0,97	0,01	0,01	0,00	0,00	0,00	0,00
'ic3_q'	0,37	0,37	0,11	0,11	0,08	0,08	0,88	0,88	1,00	1,00	0,28	0,28	0,00	0,00	0,00	0,00	0,00	0,00
'ic3_d'	0,33	0,33	0,10	0,10	0,89	0,89	0,04	0,04	0,98	0,98	0,27	0,27	0,01	0,01	0,00	0,00	0,00	0,00

Figure 5.30 Participation factor study results for 25 km cable length.

The results of the participation factor for 10 km cables can be seen in Figure 5.31:

Km=10	M1	M2	M3	M4	M5	M6	M7	M8	M9	M10	M11	M12	M13	M14	M15	M16	M17	M18
'f (Hz)'	71,539	71,539	71,553	71,553	299,043	299,043	121,913	121,913	22,300	22,300	22,867	22,867	12,912	12,912	12,746	12,746	12,750	12,750
'damp'	0,998	0,998	0,998	0,998	0,795	0,795	0,970	0,970	0,998	0,998	0,998	0,998	0,707	0,707	0,714	0,714	0,714	0,714
'Suc1_d '	0,00	0,00	0,00	0,00	0,00	0,00	0,00	0,00	0,00	0,00	0,00	0,00	0,98	0,98	1,00	1,00	0,25	0,25
'e_theta'	0,00	0,00	0,00	0,00	0,01	0,01	0,00	0,00	0,00	0,00	0,00	0,00	0,99	0,99	1,00	1,00	0,25	0,25
'SPinv1'	0,00	0,00	0,00	0,00	0,00	0,00	0,00	0,00	0,00	0,00	0,00	0,00	0,00	0,00	0,00	0,00	0,00	0,00
'SPc1 '	0,00	0,00	0,00	0,00	0,00	0,00	0,01	0,01	0,03	0,03	0,01	0,01	0,01	0,01	0,00	0,00	0,00	0,00
'SQinv1'	0,00	0,00	0,00	0,00	0,00	0,00	0,00	0,00	0,00	0,00	0,00	0,00	0,00	0,00	0,00	0,00	0,00	0,00
'SQc1 '	0,00	0,00	0,00	0,00	0,02	0,02	0,00	0,00	0,03	0,03	0,01	0,01	0,01	0,01	0,00	0,00	0,00	0,00
'Sic1_q_ref'	0,00	0,00	0,00	0,00	0,00	0,00	0,00	0,00	0,00	0,00	0,00	0,00	0,00	0,00	0,00	0,00	0,00	0,00
'Sic1_d_ref'	0,00	0,00	0,00	0,00	0,00	0,00	0,00	0,00	0,00	0,00	0,00	0,00	0,00	0,00	0,00	0,00	0,00	0,00
'Sic1_q'	0,00	0,00	0,00	0,00	0,00	0,00	0,00	0,00	0,00	0,00	0,00	0,00	0,00	0,00	0,00	0,00	0,00	0,00
'Sic1_d'	0,00	0,00	0,00	0,00	0,00	0,00	0,00	0,00	0,00	0,00	0,00	0,00	0,00	0,00	0,00	0,00	0,00	0,00
'Rmem1q'	1,00	1,00	0,26	0,26	0,07	0,07	0,92	0,92	0,31	0,31	0,08	0,08	0,00	0,00	0,00	0,00	0,00	0,00
'Rmem1d'	0,99	0,99	0,26	0,26	0,89	0,89	0,02	0,02	0,30	0,30	0,08	0,08	0,00	0,00	0,00	0,00	0,00	0,00
'Suc2_d '	0,00	0,00	0,00	0,00	0,00	0,00	0,00	0,00	0,00	0,00	0,00	0,00	0,99	0,99	0,00	0,00	1,00	1,00
'e_theta2'	0,00	0,00	0,00	0,00	0,01	0,01	0,00	0,00	0,00	0,00	0,00	0,00	1,00	1,00	0,00	0,00	1,00	1,00
'SPinv2'	0,00	0,00	0,00	0,00	0,00	0,00	0,00	0,00	0,00	0,00	0,00	0,00	0,00	0,00	0,00	0,00	0,00	0,00
'SPc2 '	0,00	0,00	0,00	0,00	0,00	0,00	0,01	0,01	0,00	0,00	0,03	0,03	0,01	0,01	0,00	0,00	0,00	0,00
'SQinv2'	0,00	0,00	0,00	0,00	0,00	0,00	0,00	0,00	0,00	0,00	0,00	0,00	0,00	0,00	0,00	0,00	0,00	0,00
'SQc2 '	0,00	0,00	0,00	0,00	0,03	0,03	0,00	0,00	0,00	0,00	0,03	0,03	0,01	0,01	0,00	0,00	0,00	0,00
'Sic2_q_ref'	0,00	0,00	0,00	0,00	0,00	0,00	0,00	0,00	0,00	0,00	0,00	0,00	0,00	0,00	0,00	0,00	0,00	0,00
'Sic2_d_ref'	0,00	0,00	0,00	0,00	0,00	0,00	0,00	0,00	0,00	0,00	0,00	0,00	0,00	0,00	0,00	0,00	0,00	0,00
'Sic2_q'	0,00	0,00	0,00	0,00	0,00	0,00	0,00	0,00	0,00	0,00	0,00	0,00	0,00	0,00	0,00	0,00	0,00	0,00
'Sic2_d'	0,00	0,00	0,00	0,00	0,00	0,00	0,00	0,00	0,00	0,00	0,00	0,00	0,00	0,00	0,00	0,00	0,00	0,00
'Rmem2q'	0,00	0,00	1,00	1,00	0,07	0,07	0,96	0,96	0,00	0,00	0,32	0,32	0,00	0,00	0,00	0,00	0,00	0,00
'Rmem2d'	0,00	0,00	0,98	0,98	0,93	0,93	0,02	0,02	0,00	0,00	0,30	0,30	0,00	0,00	0,00	0,00	0,00	0,00
'Suc3_d '	0,00	0,00	0,00	0,00	0,00	0,00	0,00	0,00	0,00	0,00	0,00	0,00	0,98	0,98	1,00	1,00	0,25	0,25
'e_theta3'	0,00	0,00	0,00	0,00	0,01	0,01	0,00	0,00	0,00	0,00	0,00	0,00	0,99	0,99	1,00	1,00	0,25	0,25
'SPinv3'	0,00	0,00	0,00	0,00	0,00	0,00	0,00	0,00	0,00	0,00	0,00	0,00	0,00	0,00	0,00	0,00	0,00	0,00
'SPc3 '	0,00	0,00	0,00	0,00	0,00	0,00	0,01	0,01	0,03	0,03	0,01	0,01	0,01	0,01	0,00	0,00	0,00	0,00
'SQinv3'	0,00	0,00	0,00	0,00	0,00	0,00	0,00	0,00	0,00	0,00	0,00	0,00	0,00	0,00	0,00	0,00	0,00	0,00
'SQc3 '	0,00	0,00	0,00	0,00	0,02	0,02	0,00	0,00	0,03	0,03	0,01	0,01	0,01	0,01	0,00	0,00	0,00	0,00
'Sic3_q_ref'	0,00	0,00	0,00	0,00	0,00	0,00	0,00	0,00	0,00	0,00	0,00	0,00	0,00	0,00	0,00	0,00	0,00	0,00
'Sic3_d_ref'	0,00	0,00	0,00	0,00	0,00	0,00	0,00	0,00	0,00	0,00	0,00	0,00	0,00	0,00	0,00	0,00	0,00	0,00
'Sic3_q'	0,00	0,00	0,00	0,00	0,00	0,00	0,00	0,00	0,00	0,00	0,00	0,00	0,00	0,00	0,00	0,00	0,00	0,00
'Sic3_d'	0,00	0,00	0,00	0,00	0,00	0,00	0,00	0,00	0,00	0,00	0,00	0,00	0,00	0,00	0,00	0,00	0,00	0,00
'Rmem3q'	1,00	1,00	0,26	0,26	0,07	0,07	0,92	0,92	0,31	0,31	0,08	0,08	0,00	0,00	0,00	0,00	0,00	0,00
'Rmem3d'	0,99	0,99	0,26	0,26	0,89	0,89	0,02	0,02	0,30	0,30	0,08	0,08	0,00	0,00	0,00	0,00	0,00	0,00
'SP '	0,00	0,00	0,00	0,00	0,00	0,00	0,00	0,00	0,00	0,00	0,00	0,00	0,00	0,00	0,00	0,00	0,00	0,00
'SQ '	0,00	0,00	0,00	0,00	0,01	0,01	0,00	0,00	0,00	0,00	0,00	0,00	0,00	0,00	0,00	0,00	0,00	0,00
'ic1_q'	0,32	0,32	0,09	0,09	0,09	0,09	0,95	0,95	1,00	1,00	0,26	0,26	0,00	0,00	0,00	0,00	0,00	0,00
'ic1_d'	0,31	0,31	0,08	0,08	0,95	0,95	0,05	0,05	0,99	0,99	0,26	0,26	0,01	0,01	0,00	0,00	0,00	0,00
'ic2_q'	0,00	0,00	0,33	0,33	0,10	0,10	1,00	1,00	0,00	0,00	1,00	1,00	0,00	0,00	0,00	0,00	0,00	0,00
'ic2_d'	0,00	0,00	0,31	0,31	1,00	1,00	0,05	0,05	0,00	0,00	0,99	0,99	0,01	0,01	0,00	0,00	0,00	0,00
'ic3_q'	0,32	0,32	0,09	0,09	0,09	0,09	0,95	0,95	1,00	1,00	0,26	0,26	0,00	0,00	0,00	0,00	0,00	0,00
'ic3_d'	0,31	0,31	0,08	0,08	0,95	0,95	0,05	0,05	0,99	0,99	0,26	0,26	0,01	0,01	0,00	0,00	0,00	0,00

Figure 5.31 Participation factor study results for 10 km cable length.

The results of the participation factor for 5 km cables can be seen in Figure 5.32:

Km=5	M1	M2	M3	M4	M5	M6	M7	M8	M9	M10	M11	M12	M13	M14	M15	M16	M17	M18
'f (Hz)'	71,539	71,539	71,553	71,553	299,043	299,043	121,913	121,913	22,300	22,300	22,867	22,867	12,912	12,912	12,746	12,746	12,750	12,750
'damp'	0,998	0,998	0,998	0,998	0,795	0,795	0,970	0,970	0,998	0,998	0,998	0,998	0,707	0,707	0,714	0,714	0,714	0,714
'Suc1_d '	0,00	0,00	0,00	0,00	0,00	0,00	0,00	0,00	0,00	0,00	0,00	0,00	0,98	0,98	1,00	1,00	0,25	0,25
'e_theta'	0,00	0,00	0,00	0,00	0,01	0,01	0,00	0,00	0,00	0,00	0,00	0,00	0,99	0,99	1,00	1,00	0,25	0,25
'SPinv1'	0,00	0,00	0,00	0,00	0,00	0,00	0,00	0,00	0,00	0,00	0,00	0,00	0,00	0,00	0,00	0,00	0,00	0,00
'SPc1 '	0,00	0,00	0,00	0,00	0,00	0,00	0,01	0,01	0,03	0,03	0,01	0,01	0,01	0,01	0,00	0,00	0,00	0,00
'SQinv1'	0,00	0,00	0,00	0,00	0,00	0,00	0,00	0,00	0,00	0,00	0,00	0,00	0,00	0,00	0,00	0,00	0,00	0,00
'SQc1 '	0,00	0,00	0,00	0,00	0,02	0,02	0,00	0,00	0,03	0,03	0,01	0,01	0,01	0,01	0,00	0,00	0,00	0,00
'Sic1_q_ref'	0,00	0,00	0,00	0,00	0,00	0,00	0,00	0,00	0,00	0,00	0,00	0,00	0,00	0,00	0,00	0,00	0,00	0,00
'Sic1_d_ref'	0,00	0,00	0,00	0,00	0,00	0,00	0,00	0,00	0,00	0,00	0,00	0,00	0,00	0,00	0,00	0,00	0,00	0,00
'Sic1_q'	0,00	0,00	0,00	0,00	0,00	0,00	0,00	0,00	0,00	0,00	0,00	0,00	0,00	0,00	0,00	0,00	0,00	0,00
'Sic1_d'	0,00	0,00	0,00	0,00	0,00	0,00	0,00	0,00	0,00	0,00	0,00	0,00	0,00	0,00	0,00	0,00	0,00	0,00
'Rmem1q'	1,00	1,00	0,26	0,26	0,07	0,07	0,92	0,92	0,31	0,31	0,08	0,08	0,00	0,00	0,00	0,00	0,00	0,00
'Rmem1d'	0,99	0,99	0,26	0,26	0,89	0,89	0,02	0,02	0,30	0,30	0,08	0,08	0,00	0,00	0,00	0,00	0,00	0,00
'Suc2_d '	0,00	0,00	0,00	0,00	0,00	0,00	0,00	0,00	0,00	0,00	0,00	0,00	0,99	0,99	0,00	0,00	1,00	1,00
'e_theta2'	0,00	0,00	0,00	0,00	0,01	0,01	0,00	0,00	0,00	0,00	0,00	0,00	1,00	1,00	0,00	0,00	1,00	1,00
'SPinv2'	0,00	0,00	0,00	0,00	0,00	0,00	0,00	0,00	0,00	0,00	0,00	0,00	0,00	0,00	0,00	0,00	0,00	0,00
'SPc2 '	0,00	0,00	0,00	0,00	0,00	0,00	0,01	0,01	0,00	0,00	0,03	0,03	0,01	0,01	0,00	0,00	0,00	0,00
'SQinv2'	0,00	0,00	0,00	0,00	0,00	0,00	0,00	0,00	0,00	0,00	0,00	0,00	0,00	0,00	0,00	0,00	0,00	0,00
'SQc2 '	0,00	0,00	0,00	0,00	0,03	0,03	0,00	0,00	0,00	0,00	0,03	0,03	0,01	0,01	0,00	0,00	0,00	0,00
'Sic2_q_ref'	0,00	0,00	0,00	0,00	0,00	0,00	0,00	0,00	0,00	0,00	0,00	0,00	0,00	0,00	0,00	0,00	0,00	0,00
'Sic2_d_ref'	0,00	0,00	0,00	0,00	0,00	0,00	0,00	0,00	0,00	0,00	0,00	0,00	0,00	0,00	0,00	0,00	0,00	0,00
'Sic2_q'	0,00	0,00	0,00	0,00	0,00	0,00	0,00	0,00	0,00	0,00	0,00	0,00	0,00	0,00	0,00	0,00	0,00	0,00
'Sic2_d'	0,00	0,00	0,00	0,00	0,00	0,00	0,00	0,00	0,00	0,00	0,00	0,00	0,00	0,00	0,00	0,00	0,00	0,00
'Rmem2q'	0,00	0,00	1,00	1,00	0,07	0,07	0,96	0,96	0,00	0,00	0,32	0,32	0,00	0,00	0,00	0,00	0,00	0,00
'Rmem2d'	0,00	0,00	0,98	0,98	0,93	0,93	0,02	0,02	0,00	0,00	0,30	0,30	0,00	0,00	0,00	0,00	0,00	0,00
'Suc3_d '	0,00	0,00	0,00	0,00	0,00	0,00	0,00	0,00	0,00	0,00	0,00	0,00	0,98	0,98	1,00	1,00	0,25	0,25
'e_theta3'	0,00	0,00	0,00	0,00	0,01	0,01	0,00	0,00	0,00	0,00	0,00	0,00	0,99	0,99	1,00	1,00	0,25	0,25
'SPinv3'	0,00	0,00	0,00	0,00	0,00	0,00	0,00	0,00	0,00	0,00	0,00	0,00	0,00	0,00	0,00	0,00	0,00	0,00
'SPc3 '	0,00	0,00	0,00	0,00	0,00	0,00	0,01	0,01	0,03	0,03	0,01	0,01	0,01	0,01	0,00	0,00	0,00	0,00
'SQinv3'	0,00	0,00	0,00	0,00	0,00	0,00	0,00	0,00	0,00	0,00	0,00	0,00	0,00	0,00	0,00	0,00	0,00	0,00
'SQc3 '	0,00	0,00	0,00	0,00	0,02	0,02	0,00	0,00	0,03	0,03	0,01	0,01	0,01	0,01	0,00	0,00	0,00	0,00
'Sic3_q_ref'	0,00	0,00	0,00	0,00	0,00	0,00	0,00	0,00	0,00	0,00	0,00	0,00	0,00	0,00	0,00	0,00	0,00	0,00
'Sic3_d_ref'	0,00	0,00	0,00	0,00	0,00	0,00	0,00	0,00	0,00	0,00	0,00	0,00	0,00	0,00	0,00	0,00	0,00	0,00
'Sic3_q'	0,00	0,00	0,00	0,00	0,00	0,00	0,00	0,00	0,00	0,00	0,00	0,00	0,00	0,00	0,00	0,00	0,00	0,00
'Sic3_d'	0,00	0,00	0,00	0,00	0,00	0,00	0,00	0,00	0,00	0,00	0,00	0,00	0,00	0,00	0,00	0,00	0,00	0,00
'Rmem3q'	1,00	1,00	0,26	0,26	0,07	0,07	0,92	0,92	0,31	0,31	0,08	0,08	0,00	0,00	0,00	0,00	0,00	0,00
'Rmem3d'	0,99	0,99	0,26	0,26	0,89	0,89	0,02	0,02	0,30	0,30	0,08	0,08	0,00	0,00	0,00	0,00	0,00	0,00
'SP '	0,00	0,00	0,00	0,00	0,00	0,00	0,00	0,00	0,00	0,00	0,00	0,00	0,00	0,00	0,00	0,00	0,00	0,00
'SQ '	0,00	0,00	0,00	0,00	0,01	0,01	0,00	0,00	0,00	0,00	0,00	0,00	0,00	0,00	0,00	0,00	0,00	0,00
'ic1_q'	0,32	0,32	0,09	0,09	0,09	0,09	0,95	0,95	1,00	1,00	0,26	0,26	0,00	0,00	0,00	0,00	0,00	0,00
'ic1_d'	0,31	0,31	0,08	0,08	0,95	0,95	0,05	0,05	0,99	0,99	0,26	0,26	0,01	0,01	0,00	0,00	0,00	0,00
'ic2_q'	0,00	0,00	0,33	0,33	0,10	0,10	1,00	1,00	0,00	0,00	1,00	1,00	0,00	0,00	0,00	0,00	0,00	0,00
'ic2_d'	0,00	0,00	0,31	0,31	1,00	1,00	0,05	0,05	0,00	0,00	0,99	0,99	0,01	0,01	0,00	0,00	0,00	0,00
'ic3_q'	0,32	0,32	0,09	0,09	0,09	0,09	0,95	0,95	1,00	1,00	0,26	0,26	0,00	0,00	0,00	0,00	0,00	0,00
'ic3_d'	0,31	0,31	0,08	0,08	0,95	0,95	0,05	0,05	0,99	0,99	0,26	0,26	0,01	0,01	0,00	0,00	0,00	0,00

Figure 5.32 Participation factor study results for 5 km cable length.

The results of the participation factor for 1 km cables can be seen in Figure 5.33:

Km=1	M1	M2	M3	M4	M5	M6	M7	M8	M9	M10	M11	M12	M13	M14	M15	M16	M17	M18
'f (Hz)'	70,716	70,716	70,798	70,798	293,254	293,254	109,528	109,528	20,746	20,746	20,842	20,842	12,902	12,902	12,736	12,736	12,736	12,736
'damp'	0,998	0,998	0,998	0,998	0,809	0,809	0,976	0,976	0,998	0,998	0,998	0,998	0,707	0,707	0,714	0,714	0,714	0,714
'Suc1_d '	0,00	0,00	0,00	0,00	0,00	0,00	0,00	0,00	0,00	0,00	0,00	0,00	0,99	0,99	1,00	1,00	0,25	0,25
'e_theta'	0,00	0,00	0,00	0,00	0,01	0,01	0,00	0,00	0,00	0,00	0,00	0,00	1,00	1,00	1,00	1,00	0,25	0,25
'SPinv1'	0,00	0,00	0,00	0,00	0,00	0,00	0,00	0,00	0,00	0,00	0,00	0,00	0,00	0,00	0,00	0,00	0,00	0,00
'SPc1 '	0,00	0,00	0,00	0,00	0,00	0,00	0,01	0,01	0,03	0,03	0,01	0,01	0,01	0,01	0,00	0,00	0,00	0,00
'SQinv1'	0,00	0,00	0,00	0,00	0,00	0,00	0,00	0,00	0,00	0,00	0,00	0,00	0,00	0,00	0,00	0,00	0,00	0,00
'SQc1 '	0,00	0,00	0,00	0,00	0,03	0,03	0,00	0,00	0,03	0,03	0,01	0,01	0,01	0,01	0,00	0,00	0,00	0,00
'Sic1_q_ref'	0,00	0,00	0,00	0,00	0,00	0,00	0,00	0,00	0,00	0,00	0,00	0,00	0,00	0,00	0,00	0,00	0,00	0,00
'Sic1_d_ref'	0,00	0,00	0,00	0,00	0,00	0,00	0,00	0,00	0,00	0,00	0,00	0,00	0,00	0,00	0,00	0,00	0,00	0,00
'Sic1_q'	0,00	0,00	0,00	0,00	0,00	0,00	0,00	0,00	0,00	0,00	0,00	0,00	0,00	0,00	0,00	0,00	0,00	0,00
'Sic1_d'	0,00	0,00	0,00	0,00	0,00	0,00	0,00	0,00	0,00	0,00	0,00	0,00	0,00	0,00	0,00	0,00	0,00	0,00
'Rmem1q'	1,00	1,00	0,25	0,25	0,07	0,07	0,96	0,96	0,29	0,29	0,07	0,07	0,00	0,00	0,00	0,00	0,00	0,00
'Rmem1d'	1,00	1,00	0,25	0,25	0,93	0,93	0,03	0,03	0,29	0,29	0,07	0,07	0,00	0,00	0,00	0,00	0,00	0,00
'Suc2_d '	0,00	0,00	0,00	0,00	0,00	0,00	0,00	0,00	0,00	0,00	0,00	0,00	0,99	0,99	0,00	0,00	1,00	1,00
'e_theta2'	0,00	0,00	0,00	0,00	0,01	0,01	0,00	0,00	0,00	0,00	0,00	0,00	1,00	1,00	0,00	0,00	1,00	1,00
'SPinv2'	0,00	0,00	0,00	0,00	0,00	0,00	0,00	0,00	0,00	0,00	0,00	0,00	0,00	0,00	0,00	0,00	0,00	0,00
'SPc2 '	0,00	0,00	0,00	0,00	0,00	0,00	0,01	0,01	0,00	0,00	0,03	0,03	0,01	0,01	0,00	0,00	0,00	0,00
'SQinv2'	0,00	0,00	0,00	0,00	0,00	0,00	0,00	0,00	0,00	0,00	0,00	0,00	0,00	0,00	0,00	0,00	0,00	0,00
'SQc2 '	0,00	0,00	0,00	0,00	0,03	0,03	0,00	0,00	0,00	0,00	0,03	0,03	0,01	0,01	0,00	0,00	0,00	0,00
'Sic2_q_ref'	0,00	0,00	0,00	0,00	0,00	0,00	0,00	0,00	0,00	0,00	0,00	0,00	0,00	0,00	0,00	0,00	0,00	0,00
'Sic2_d_ref'	0,00	0,00	0,00	0,00	0,00	0,00	0,00	0,00	0,00	0,00	0,00	0,00	0,00	0,00	0,00	0,00	0,00	0,00
'Sic2_q'	0,00	0,00	0,00	0,00	0,00	0,00	0,00	0,00	0,00	0,00	0,00	0,00	0,00	0,00	0,00	0,00	0,00	0,00
'Sic2_d'	0,00	0,00	0,00	0,00	0,00	0,00	0,00	0,00	0,00	0,00	0,00	0,00	0,00	0,00	0,00	0,00	0,00	0,00
'Rmem2q'	0,00	0,00	1,00	1,00	0,08	0,08	0,96	0,96	0,00	0,00	0,29	0,29	0,00	0,00	0,00	0,00	0,00	0,00
'Rmem2d'	0,00	0,00	1,00	1,00	0,93	0,93	0,03	0,03	0,00	0,00	0,29	0,29	0,00	0,00	0,00	0,00	0,00	0,00
'Suc3_d '	0,00	0,00	0,00	0,00	0,00	0,00	0,00	0,00	0,00	0,00	0,00	0,00	0,99	0,99	1,00	1,00	0,25	0,25
'e_theta3'	0,00	0,00	0,00	0,00	0,01	0,01	0,00	0,00	0,00	0,00	0,00	0,00	1,00	1,00	1,00	1,00	0,25	0,25
'SPinv3'	0,00	0,00	0,00	0,00	0,00	0,00	0,00	0,00	0,00	0,00	0,00	0,00	0,00	0,00	0,00	0,00	0,00	0,00
'SPc3 '	0,00	0,00	0,00	0,00	0,00	0,00	0,01	0,01	0,03	0,03	0,01	0,01	0,01	0,01	0,00	0,00	0,00	0,00
'SQinv3'	0,00	0,00	0,00	0,00	0,00	0,00	0,00	0,00	0,00	0,00	0,00	0,00	0,00	0,00	0,00	0,00	0,00	0,00
'SQc3 '	0,00	0,00	0,00	0,00	0,03	0,03	0,00	0,00	0,03	0,03	0,01	0,01	0,01	0,01	0,00	0,00	0,00	0,00
'Sic3_q_ref'	0,00	0,00	0,00	0,00	0,00	0,00	0,00	0,00	0,00	0,00	0,00	0,00	0,00	0,00	0,00	0,00	0,00	0,00
'Sic3_d_ref'	0,00	0,00	0,00	0,00	0,00	0,00	0,00	0,00	0,00	0,00	0,00	0,00	0,00	0,00	0,00	0,00	0,00	0,00
'Sic3_q'	0,00	0,00	0,00	0,00	0,00	0,00	0,00	0,00	0,00	0,00	0,00	0,00	0,00	0,00	0,00	0,00	0,00	0,00
'Sic3_d'	0,00	0,00	0,00	0,00	0,00	0,00	0,00	0,00	0,00	0,00	0,00	0,00	0,00	0,00	0,00	0,00	0,00	0,00
'Rmem3q'	1,00	1,00	0,25	0,25	0,07	0,07	0,96	0,96	0,29	0,29	0,07	0,07	0,00	0,00	0,00	0,00	0,00	0,00
'Rmem3d'	1,00	1,00	0,25	0,25	0,93	0,93	0,03	0,03	0,29	0,29	0,07	0,07	0,00	0,00	0,00	0,00	0,00	0,00
'SP '	0,00	0,00	0,00	0,00	0,00	0,00	0,00	0,00	0,00	0,00	0,00	0,00	0,00	0,00	0,00	0,00	0,00	0,00
'SQ '	0,00	0,00	0,00	0,00	0,01	0,01	0,00	0,00	0,00	0,00	0,00	0,00	0,00	0,00	0,00	0,00	0,00	0,00
'ic1_q'	0,30	0,30	0,08	0,08	0,10	0,10	0,99	0,99	1,00	1,00	0,25	0,25	0,00	0,00	0,00	0,00	0,00	0,00
'ic1_d'	0,30	0,30	0,08	0,08	0,99	0,99	0,05	0,05	1,00	1,00	0,25	0,25	0,01	0,01	0,00	0,00	0,00	0,00
'ic2_q'	0,00	0,00	0,30	0,30	0,10	0,10	1,00	1,00	0,00	0,00	1,00	1,00	0,00	0,00	0,00	0,00	0,00	0,00
'ic2_d'	0,00	0,00	0,30	0,30	1,00	1,00	0,05	0,05	0,00	0,00	1,00	1,00	0,01	0,01	0,00	0,00	0,00	0,00
'ic3_q'	0,30	0,30	0,08	0,08	0,10	0,10	0,99	0,99	1,00	1,00	0,25	0,25	0,00	0,00	0,00	0,00	0,00	0,00
'ic3_d'	0,30	0,30	0,08	0,08	0,99	0,99	0,05	0,05	1,00	1,00	0,25	0,25	0,01	0,01	0,00	0,00	0,00	0,00

Figure 5.33 Participation factor study results for 1 km cable length.

Regarding the internal oscillation modes obtained from the modal analysis, there are 4 main types of oscillations depending on the participating factors:

- Modes (M1-M4): The first four modes that can be seen in the participation factor computation are related to the delay that was introduced to the system enabling a correct initialisation of the model. As can be seen, the dampening ratio of this oscillation is very high for all of the studied cable length values.

- Modes (M5-M8): These oscillation modes are associated to the interactions between the initialisation delay and the current loop variables (Modes 5 and 6 correspond to the q component and 7 and 8 to the d components). Considering that the cable for converter 2 is 1.5 times longer than the rest, when the total cable lengths are increased, the interaction of converter 1 and 3 are irrelevant for the 50 km study. The highest oscillations can be observed in these modes. However, in the most extreme case, the dampening ratio is still fairly high and therefore it looks like it won't compromise system stability.

- Modes (M9-M12): In comparison with the SCR variation study, the impact of changing cable lengths is very similar. The only difference is the oscillation frequency which varies about 6 Hz more.

- Modes (M13-M18): Just like in the SCR variation study, the internal oscillations of the different PLLs in this system are seen. The frequency stays around the 12 Hz mark and the dampening ratio is around 0.7 for all the studied cable lengths.

5.5.3 Time domain simulation comparing different cable length values

The effect that different cable impedances have on the internal oscillations of the model has been presented in the participation factor study contained within the previous section.

In this section, time domain simulations will be carried out on the non-linear model comparing different cable length values, validating the conclusions from the small signal analysis.

In Figure 5.34 and Figure 5.35 the simulation results for the active and reactive power measured at the PCC are shown:

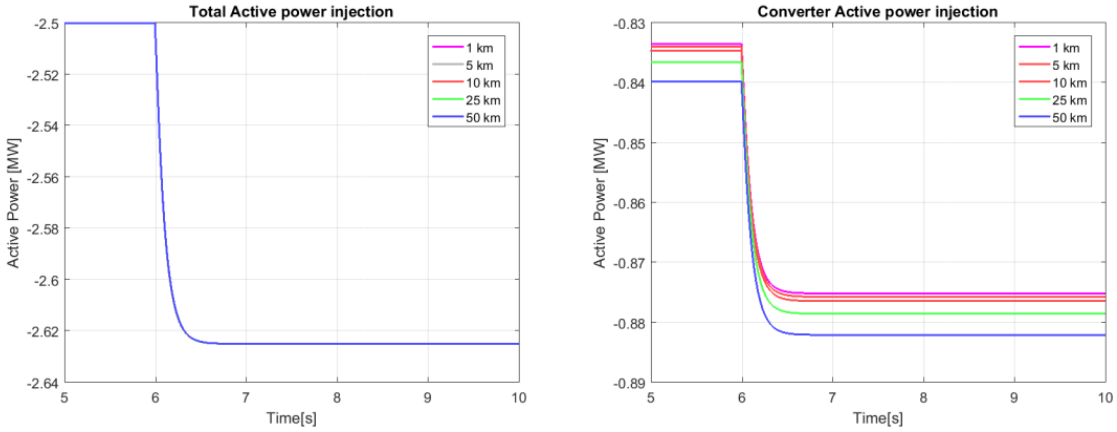

Figure 5.34 Time-domain results comparison for the PCC and converter 1 Active power for different cable impedance values.

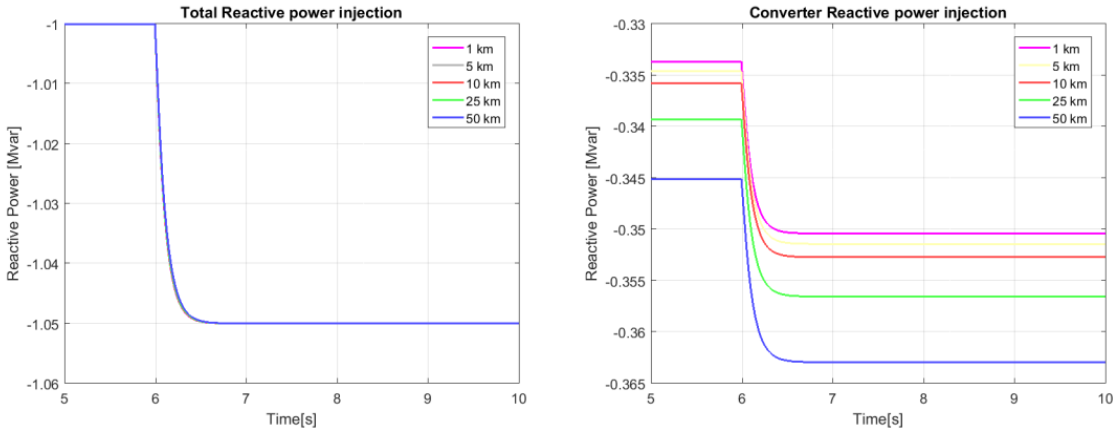

Figure 5.35 Time-domain results comparison for the PCC and converter 1 Reactive power for different cable impedance values.

As can be seen, changing the impedance value of each of the converter branches has an impact on the amount of power that must be injected into the system by each of the converters. An increase in impedance increases the active and reactive power losses of the cable. Significant oscillations cannot be observed on these variables.

The following and compare the d and q voltage components of the voltage values at the PCC and at converter 1 for different cable impedance values.

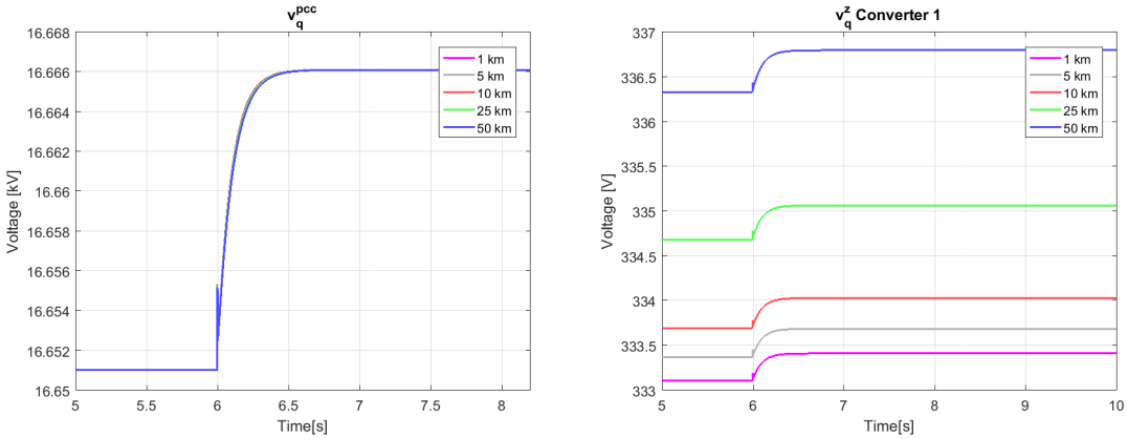

Figure 5.36 Time-domain results comparison for the q voltage components (PCC and grid-side impedance voltage for different cable impedance values.

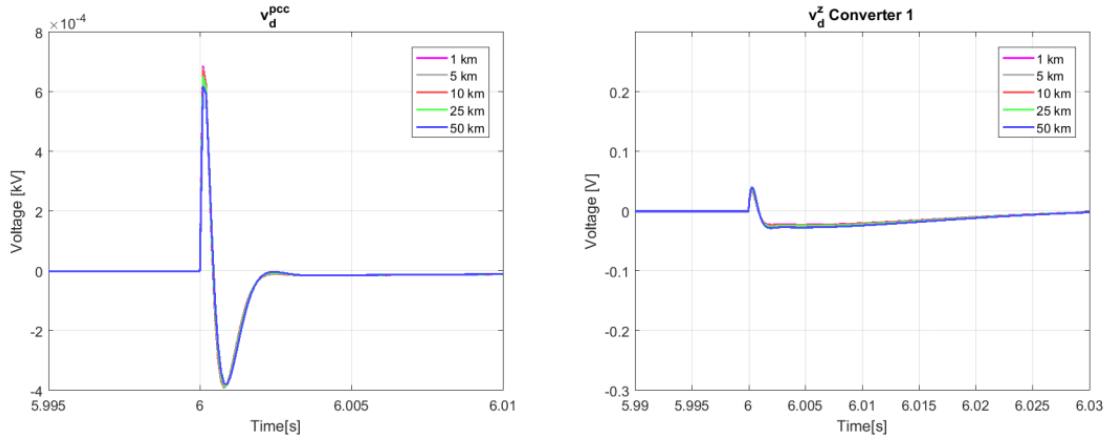

Figure 5.37 Time-domain results comparison for the d voltage components (PCC and grid-side impedance voltage) for different cable impedance values.

Regarding the q components, considering with cable length the impedance of each of the branches increases, the voltage needed at the different points of the circuit must also change in proportion to enable correct power reference satisfaction.

Regarding the d components of the voltage, the different PLLs connected throughout the system impose that the d component of the voltage must be 0. The dynamic response includes a higher overshoot of the voltage and a longer establishment time. This is a direct consequence of the increased impedance, since the dampening ratios of the oscillations lowers. In comparison with the SCR test presented earlier in this chapter, varying cable lengths does not have as big an impact on the system and therefore the time domain simulations show subtler differences.

The following figure shows the controllable voltage source voltage of converter 1:

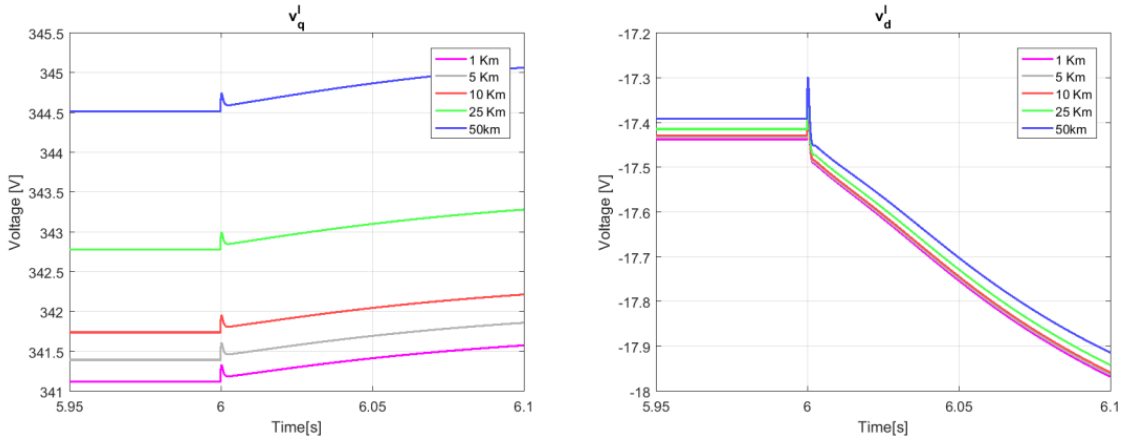

Figure 5.38 Time-domain results comparison for the d and q voltage components at converter 1 converter side for different cable impedance values.

As can be seen, the cable impedance increase results in a higher overshoot. However, the oscillations can barely be seen due its high dampening ratio.

Finally, regarding the current flowing through the PCC and the converter branches, they can be seen in:

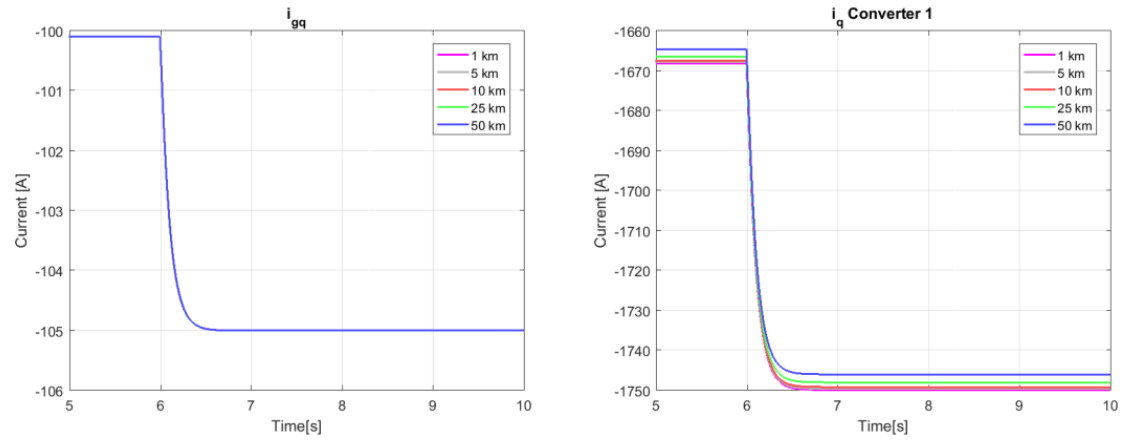

Figure 5.39 Time-domain results comparison for the q current components at the PCC and converter 1 impedance for different cable impedance values.

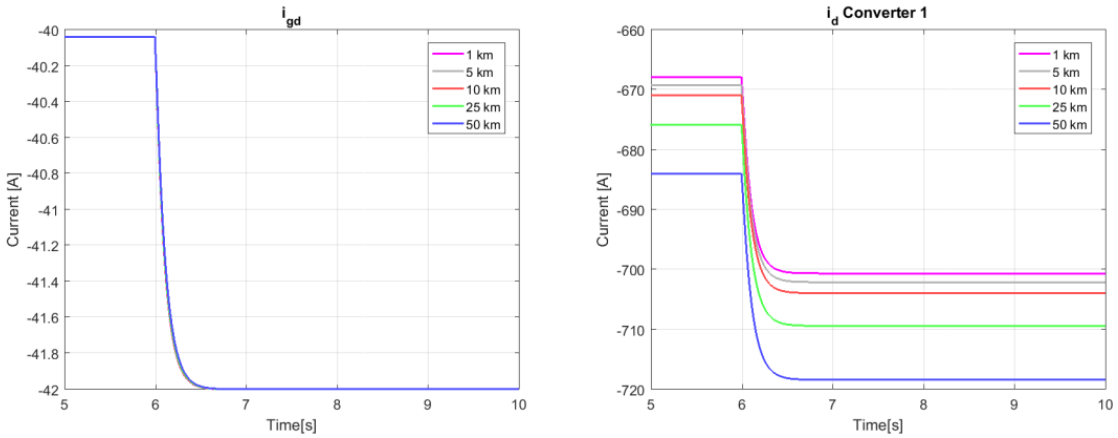

Figure 5.40 Time-domain results comparison for the d current components at the PCC and converter 1 impedance for different cable impedance values.

No big oscillations are observed in the current signals in either of the $qd0$ components. Considering that these signals are mainly used in the current loop and that the oscillations associated to it have very high dampening ratio, the obtained results are coherent with the participation factor study.

6 Conclusions

This thesis has introduced the basic principles of the VSC converter topology, its control and its application in a PV solar plant as well as the general structure of a photovoltaic power controller (PPC). Said principles enabled the construction of a series of models and simulations sets which enabled a fair degree of completion of the objectives proposed in this thesis:

- The integration of the VSC converter and its control in a PV plant internal grid has been comprehended. In consequence, a non-linear model reproducing its operation was produced. Application of linearization techniques and the state-space control theory enabled linearization of the PV plant model for further analysis of its dynamic behaviour.

- The linear model has been validated by comparing the dynamic behaviour it produced with its non-linear counterpart. The small signal model was simulated using different grid impedance values enabling comprehension of the effect of the grid strength on the stability of the system.

- Consequently, internal oscillation modes that could compromise the system stability were identified, quantified and its causes were discovered.

Upon completion of this thesis, several future lines of work related to this project come to mind. Firstly, a more complete electrical model can be implemented, including the cable's capacitive behaviour and a full transformer model. Secondly, the DC side of the converters can be modelled including the PV panel strings and even a DC/DC converter. Finally, aside from changing the grid strength, other variables can be changed in order to understand the oscillations it can produce. These variables, such as the cable impedances and the PPC power loop time constant can probably produce considerable oscillation in the system.

In conclusion, the techniques applied in this project enable comprehension of the oscillatory behaviour of a dynamic system. The linearized small-signal model produced will be used in further studies in the fields of renewable integration and control stability.

Appendix A: Environmental Impact

This section exposes the environmental impact derived from grand scale PV power plants and other related issues such as the implications projects like the one presented in this thesis has in the energy sector.

Environmental impact of Photovoltaic systems

Even though PV systems are always included into the renewable energy systems that can enable sustainable development in the future, certain environmental issues are derived from their use.

Firstly, the vast surface areas occupied by PV installations can cause land degradation, loss of habitat of autochthonous species and loss of cultivatable land. Considering that large scale PV power plants can occupy up to 46 square kilometres (the Tengger desert solar plant in China), the allocation of these plants must be well thought of in advance. Countries with large desert areas are currently installing very large scale PV power plants in areas where land surface area is not an issue with the afore mentioned problems [24]. Other solutions which are more related to lower power PV applications consist on installing PV panels on roofs and highway protections where the surface upon which they are installed would otherwise be useless.

Secondly, the raw materials used to manufacture PV panels and other hardware associated to the PV power plants include iron, copper, aluminium and other similar materials. In comparison, thermal plants do not require as many of these materials as the PV power sector and therefore the mineral depletion associated to this technology must be taken into account in its environmental impact.

Finally, there are a series of hazardous by-products associated to the manufacturing of inverters and PV Panels which include nitric acid, sulphuric acid and acetone.

However, in comparison with the currently deployed technologies used in the generation sector, the impact of large-scale PV power plants is clearly lower. Thermal plants produce a very high amount of nitrogen oxides and sulphates which directly harm the population living in the vicinity of these plants.

Appendix B: Budget

In this section, the budget of this project is presented. The different types of costs associated to its development are separated into labour costs and research infrastructure.

Labour costs

This project was developed over an 8 month time-lapse in which the different phases of the project were carried out. The hours and costs associated to each phase are presented in Table 3:

Table 3 Labour Costs

CONCEPT	QUANTITY	PRICE	TOTAL
RESEARCH HOURS	250 hr	40 €/h	10000 €
DEVELOPMENT HOURS	400 hr	40 €/h	16000 €
WRITING HOURS	200 hr	40 €/h	8000 €
TOTAL	850 hr		34000 €

Research infrastructure

The research infrastructure costs englobe all the software licensing, the hardware used for the simulations and all of the associated electrical bill. Thankfully, the project was developed at the CITCEA-UPC lab and therefore all of the afore mentioned concepts are provided by the university. Therefore, these costs are not directly included in the project's budget.

Total cost

Taking into account all of the previously detailed concepts, the total cost of the project is of 34000 €.

Appendix C: The synchronous reference frame

The equations of said control system are based on the $qd0$ synchronous reference frame as opposed to the usual abc reference used in many electrical engineering problems. Therefore, in the process of explaining how the control system of the VSC works, an introduction to the synchronous reference frame seems adequate.

The following expression illustrates the definition of a balanced three-phase voltage signal:

$$\begin{bmatrix} \underline{v_a} \\ \underline{v_b} \\ \underline{v_c} \end{bmatrix} = \underline{v_{abc}} = \begin{bmatrix} 230\angle 0º \\ 230\angle -120º \\ 230\angle 120º \end{bmatrix}$$

The phasors represent the voltage vector modulus and the initial phase. The angular position (phase) increases with time in relation to its frequency. Therefore, the phasor diagram can in fact be understood as an initial state series of complex vectors. These complex vectors represent the modulus and the actual phase as a function of time. Hence, the vectors would rotate on a real-complex plane like shown in Figure 6.1:

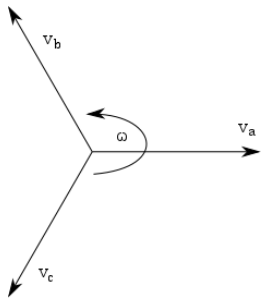

Figure 6.1 Complex plane rotation of the three-phase voltage vectors.

Since mathematical operations with three out of phase sine waves is not trivial and the afore mentioned sine waves can be plotted in a phasor diagram, the Clarke transform proposes the use of a geometrical solution to simplify the signal analysis.

Upon inspection of the previously included balanced three phase diagram, three phasors with a 120-degree angle between them can be seen. Such phasor diagram represents the three AC voltage oscillations in canonical form.

The Clarke transform proposes a basis change in which the phasors no longer form 120-degree angles between them. Instead, two phasors form a 90-degree angle between them and the third is perpendicular to the x-y axes like so:

$$\begin{bmatrix} v_\alpha \\ v_\beta \\ 0 \end{bmatrix} = \begin{bmatrix} 1 & -\frac{1}{2} & -\frac{1}{2} \\ 0 & \frac{\sqrt{3}}{2} & -\frac{\sqrt{3}}{2} \\ \frac{1}{2} & \frac{1}{2} & \frac{1}{2} \end{bmatrix} \frac{2}{3} \begin{bmatrix} v_a \\ v_b \\ v_c \end{bmatrix}$$

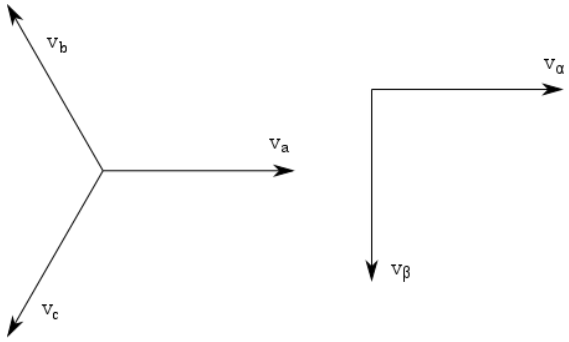

Figure 6.2 Phasor diagram of the abc reference and its equivalent alpha-beta reference

The Clarke transform greatly simplifies operations on the voltage signals. However, it is with the Park rotation that simplification is hugely increased. The rotation essentially consists on rotating the basis of the phasor diagram in sync with the pulsing frequency of the voltage phasors. By doing so, instead of working with sine waves the voltage waves are linearized thus enabling easier analysis.

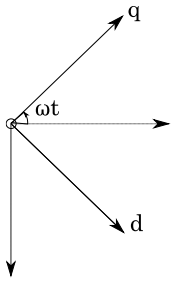

Figure 6.3 Rotation of the alpha beta reference at 50 Hz produces the $qd0$ synchronous reference frame

As can be seen in Figure 6.3, the $qd0$ frame rotates in synchrony with the voltage vectors outputting constant values in the steady state [25]. Working with constant values is ideal in order to ease control of any given system. The Park rotation is a central part in most phase locked loop architectures due to its advantages.

In order to apply the rotation, the output vector from the Clarke transform is multiplied by a simple rotation matrix. Naturally, the angle of the voltage signal must correspond to the angle within the matrix.

$$\begin{bmatrix} v_q \\ v_d \end{bmatrix} = \begin{bmatrix} \cos\theta & -\sin\theta \\ \sin\theta & \cos\theta \end{bmatrix} \begin{bmatrix} v_\alpha \\ v_\beta \end{bmatrix}$$

Bibliography

[1] Y. Liu, M. Huang, L. Qu, and X. Zha, “Interaction of voltage and current control loop in three-phase voltage source converter,” in *IECON 2017 - 43rd Annual Conference of the IEEE Industrial Electronics Society*, 2017, pp. 6847–6852.

[2] E. Sánchez-Sánchez, E. Prieto-Araujo, and O. Gomis-Bellmunt, “Multi-terminal HVDC Voltage Droop Control Design Considering DC Grid, AC Grid and MMC Dynamics,” *13th IET Int. Conf. AC DC Power Transm. (ACDC 2017)*, p. 52 (6 .)-52 (6 .), 2017.

[3] T. Bruckner, I. A. Bashmakov, Y. Mulugetta, H. Chum, A. de la Vega Navarro, J. Edmonds, A. Faaij, B. Fungtammasan, A. Garg, E. Hertwich, D. Honnery, D. Infield, M. Kainuma, S. Khennas, S. Kim, H. B. Nimir, K. Riahi, N. Strachan, R. Wiser, and X. Zhang, “Climate Change 2014: Mitigation of Climate Change. Contribution of Working Group III to the Fifth Assessment Report of the Intergovernmental Panel on Climate Change,” Cambridge University Press, Cambridge, United Kingdom and New York, NY, USA., Camrbdige and New York, 2014.

[4] BP, “BP Energy Outlook 2017.”

[5] “2050 Energy Strategy - European Commission.” [Online]. Available: https://ec.europa.eu/energy/en/topics/energy-strategy-and-energy-union/2050-energy-strategy. [Accessed: 19-Sep-2018].

[6] “2016 SNAPSHOT OF GLOBAL PHOTOVOLTAIC MARKETS.”

[7] D.-L. Popa, M.-S. Nicolae, P.-M. Nicolae, and M. Popescu, “Design and simulation of a 10 MW photovoltaic power plant using MATLAB and Simulink,” in *2016 IEEE International Power Electronics and Motion Control Conference (PEMC)*, 2016, pp. 378–383.

[8] A. Cabrera-Tobar, E. Bullich-Massagué, M. Aragüés-Peñalba, and O. Gomis-Bellmunt, “Topologies for large scale photovoltaic power plants,” *Renew. Sustain. Energy Rev.*, vol. 59, pp. 309–319, Jun. 2016.

[9] M. A. Green, A. Ho-Baillie, and H. J. Snaith, “The emergence of perovskite solar cells,” *Nat. Photonics*, vol. 8, no. 7, pp. 506–514, Jul. 2014.

[10] N. H. Zaini, M. Z. A. Kadir, M. Izadi, N. I. Ahmad, M. A. . Radzi, and N. Azis, “The effect of temperature on a mono-crystalline solar PV panel,” in *2015 IEEE Conference on Energy Conversion (CENCON)*, 2015, pp. 249–253.

[11] M. S. Ashhab and O. Akash, “Experiment on PV panels tilt angle and dust,” in *2016 5th International Conference on Electronic Devices, Systems and Applications (ICEDSA)*, 2016, pp. 1–3.

[12] S. H. Shehadeh, H. H. H. Aly, and M. E. El-Hawary, “An overview of inverter topologies for photovoltaic electrical energy,” in *2013 IEEE Electrical Power & Energy Conference*, 2013, pp. 1–8.

[13] M. S. Agamy, M. Harfman-Todorovic, A. Elasser, R. L. Steigerwald, J. A. Sabate, S. Chi, A. J. McCann, L. Zhang, and F. Mueller, “A high efficiency DC-DC converter topology suitable for distributed large commercial and utility scale PV systems,” in

2012 15th International Power Electronics and Motion Control Conference (EPE/PEMC), 2012, p. LS2d.3-1-LS2d.3-6.

[14] Wei Feng, Bojin Qi, Yipeng Wang, and Haolin Liu, “High power DC-DC converter for renewable energy power system,” in *2014 IEEE Conference and Expo Transportation Electrification Asia-Pacific (ITEC Asia-Pacific)*, 2014, pp. 1–4.

[15] M. Orkisz, “Estimating effects of individual PV panel failures on PV array output,” in *2016 IEEE 16th International Conference on Environment and Electrical Engineering (EEEIC)*, 2016, pp. 1–5.

[16] A. K. Koshti and M. N. Rao, “A brief review on multilevel inverter topologies,” in *2017 International Conference on Data Management, Analytics and Innovation (ICDMAI)*, 2017, pp. 187–193.

[17] A. Egea-Alvarez, A. Junyent-Ferré, and O. Gomis-Bellmunt, “Active and Reactive Power Control of Grid Connected Distributed Generation Systems,” 2012, pp. 47–81.

[18] Fang Zheng Peng and Jih-Sheng Lai, “Generalized instantaneous reactive power theory for three-phase power systems,” *IEEE Trans. Instrum. Meas.*, vol. 45, no. 1, pp. 293–297, 1996.

[19] H. Akagi, E. H. Watanabe, and M. Aredes, *Instantaneous power theory and applications to power conditioning*. Wiley, 2007.

[20] Se-Kyo Chung, “A phase tracking system for three phase utility interface inverters,” *IEEE Trans. Power Electron.*, vol. 15, no. 3, pp. 431–438, May 2000.

[21] V. Konoval and R. Prytula, “PARTICIPATION FACTOR IN MODAL ANALYSIS OF POWER SYSTEMS STABILITY.”

[22] A. Yazdani and R. Iravani, *Voltage-sourced converters in power systems : modeling, control, and applications*. IEEE Press/John Wiley, 2010.

[23] O. Gomis-Bellmunt, L. Serrano-Salamanca, R. Ferrer-San-José, C. Pacheco-Navas, M. Aragüés-Peñalba, and E. Bullich-Massagué, “Power plant control in large-scale photovoltaic plants: design, implementation and validation in a 9.4 MW photovoltaic plant,” *IET Renew. Power Gener.*, vol. 10, no. 1, pp. 50–62, Jan. 2016.

[24] O. US EPA, “State Renewable Energy Resources.”

[25] R. H. Park, “Abridgment of two-reaction theory of synchronous machines generalized method of analysis — Part I,” *J. A.I.E.E.*, vol. 48, no. 3, pp. 194–194, Mar. 1929.